Carbon Molecular Sieve Membranes for Gas Separation:

Study, Preparation and Characterization

Marta Maria Cabral Campo dos Santos

Dissertation presented for the degree of

Doctor in Chemical and Biological Engineering

by

University of Porto

Supervisors

Adélio Miguel Magalhães Mendes

Fernão Domingos de Montenegro Baptista

Malheiro de Magalhães

Ciência.Inovação 2010   Programa Operacional Ciência e Inovação 2010

Acknowledgments

First of all, I thank God, who above all, is giving me strength to be who I am, for helping me living everyday, and for guiding me through the most difficult moments… Thank you for allowing me to finish my PhD.

I would like to thank Professor Adélio Mendes and Prof. Fernão Magalhães for inviting me to work with them and for their supervision. Thankful words are also directed to LEPAE for providing the necessary conditions to carry out my work, to DEQ and to FEUP.

I would also like to special thank Professor Matthias Wessling for having received me at MTG, University of Twente, The Netherlands, and to Dr. Ing. Kitty Nijmeijer for the attention and supervision during my 3 months internship.

My thankful words to Luís Carlos for performing mercury porosimetry and to Mr. Nelson Neves for giving life to my drawings.

I am grateful to Dr. Daniela Silva from CEMUP, University of Porto, for her expertise performing SEM/EDS analysis; to Dr. Rosário Soares from LCA, University of Aveiro, for performing XDR analysis.

I would like to express my gratitude to Miguel Jorge for his availability to discuss and clarify some doubts.
I would like to thank D. Fátima, D. Rosa, D. Maria José and Joana Azeredo for their kindness and help with paper and secretary work.

Thank you to my mother for translating the abstract to French. Thank you to my aunt Tatá for revising the abstract in English. Sorry for the headhake!!

I would like to acknowledge my lab mates for all their help. To my DEQ mates, thank you for all your support, friendship, patience, and for listening in my "despair" moments. Thank you for the relaxing coffee breaks, and for lunch time. Thank you to my colleagues in MTG, Twente, for kindly receiving me, especially to Tymen Visser who has helped to prepare my first carbon membranes.

To all my truly friends, in-and-outside FEUP, thank you for all the talks, advisements and mainly for trusting and believing me... for being there for me.

Thank you to my father- and mother-in-law, to my brothers-in-law and to Sara, for sharing my problems and helping dealing with it, for their trust and feelings.

A big kiss and hug to my dear grandparents...always in my heart...you're the sweetest!

To my father, my mother, my brother Nuno and my young sister Inês, thank you all for the amazing people you are, for being so present in my life, for having taught me the real values of life, for not letting me down, for trusting me, for the encouragements and kind words, for being severe when needed, for believing in me and helping me believe in myself.

Finally, thank you João, for the colleague you were since I started my PhD, for the assistance, knowledge and help you gave me while working together as teammates; thank you for all the exchanged ideas and for managing problems with me. Thank you for all the calm, serenity and balance you have transmitted me. Thank you my dear husband for all the patience, for the standing by my side in the most turbulent moments and for the love you express each and every single day of our lives.

To my dear husband…

To my parents…

Abstract

This thesis is focused on the study of carbon molecular sieve membranes (CMSM). These are inorganic membranes, capable of withstanding high temperatures and harsh chemical conditions due to their "inert" inorganic carbon matrix. Furthermore, CMSM combine high selectivities with high permeabilities, when compared to dense inorganic membranes. CMSM present a narrow pore size distribution with selective pores (constrictions) in the range of 0.3-0.5 nm, responsible for the molecular sieving properties of the membranes. These constrictions allow the passage of smaller permeants in detriment of bulkier permeants, which are retained. The preparation of such membranes involves several steps, the more important being the selection and preparation of the precursor and the pyrolysis step. However, there are reports that CMSM suffer from aging due to oxygen exposure, compromising the reliability of these membranes to be implemented in an industrial membrane separation unit. Therefore, in Chapter II, a comparative study between a CMSM and a CMS adsorbent suited for air separation was done. The purpose of this analysis was to better understand the mass transport mechanism in CMS membranes and show how it is related to the material's structure and the aging differences between the two materials. Contrarily to what was expected, no significant aging differences were observed in either material. The main differences found were related to the adsorption kinetics; the pressure dependences of the apparent time constants were obtained for CO_2, O_2, Ar and N_2, and different models were used to predict the experimental results, emphasizing the very important role of the ultramicroporosity on the properties of the materials. The CMS membrane exhibited a pore blockage effect when permeating O_2 and CO_2 and a physical explanation is provided. The vulnerability of these materials to water vapor exposure is compared and related to the surface chemistry of each material. The existence of hydrophilic groups responsible for the water vapor adsorption in such carbonaceous materials has been related to the surface chemistry by means of X-ray microanalysis and by thermogravimetry. A new model accounting for both adsorption and desorption of

water vapor is presented. The kinetics of water vapor adsorption was determined for both materials, following the LDF model. The X-ray microanalyses showed that the membrane presents a lower C/O ratio than the adsorbent, suggesting a higher susceptibility towards water vapor. This was confirmed by the significant adsorption of water vapor for very low relative pressures and by the higher rate constants on the membranes.

In Chapter III, the preparation of carbon hollow fiber membranes based on a co-polyimide P84/S-PEEK blend is described. The influence of the pyrolysis parameters on the properties of the membranes was studied and the resultant carbon membranes were characterized by permeation experiments and scanning electron microscopy (SEM). The highest permeabilities and ideal selectivities were obtained for the membranes submitted to an end temperature of 750 $^\circ$C, prior to quenching. It was also concluded that the existence of a final soaking time at the end temperature, just before quenching, did not improve the performance of the carbon membranes. The permeabilities in this case were lower than the ones obtained without soaking time. Furthermore, it was observed that the membranes revealed higher permeabilities when quenched at the end temperature than the ones naturally cooled down to room temperature. This chapter also reports on the preparation of CMSM from a commercial film of cellophane paper employing one single heating step; this was the first time such precursor was used. The influence of pyrolysis parameters on the structure, morphology and performance of the membranes, was examined through SEM, X-ray microanalysis, X-ray diffraction and single component permeation experiments towards He, H_2, Ar, N_2, CO_2, O_2, CH_4 and water vapor at 29.5 °C. The membranes revealed good ideal selectivities, with separation performances above the recently revised Robeson's upper bound for polymeric membranes.

Finally, Chapter IV focuses on the simulation of nitrogen production from water-vapor saturated air using a membrane module set with CMSMs at 29.5 °C. A model considering a pressure-dependent permeability was proposed and simulations were performed in counter-current mode, assessing the effect of the feed to permeate

pressure ratio and the increase in the feed pressure. The existence of pressure drop along the membranes was also accounted and studied. It was concluded to be possible of producing a stream of 99.9 % nitrogen from a four-component air mixture (N_2 – 78.7 %, O_2 – 22.9 %, CO_2 - 0.0003 %, water vapor - 100 % RH) with recoveries up to 65 %.

IV

Sumário

A presente tese foca o estudo de membranas de peneiro molecular de carbono (CMSM). Estas membranas são constituídas por uma matriz inorgânica de carbono com propriedades inertes, resistindo, assim, a altas temperaturas e a ambientes químicos agressivos. Para além disso, as CMSM apresentam, normalmente, elevadas permeabilidades, aliadas a selectividades também elevadas, quando comparadas com membranas poliméricas densas. As CMSM possuem uma distribuição de poros apertada, com poros selectivos (constrições), compreendidos entre os 0,3 e os 0,5 nm, responsáveis pelas propriedades de peneiro molecular das membranas. Estas constrições permitem a passagem de espécies mais pequenas, retendo, no entanto, as espécies de maior tamanho. A preparação destas membranas envolve diferentes etapas sendo as mais importantes a selecção do precursor e a etapa de pirólise. Contudo, há alguns estudos que apontam para o seu envelhecimento devido à sua exposição ao oxigénio, comprometendo assim, a fiabilidade destas membranas para aplicação industrial. Nesse sentido, efectuou-se um estudo comparativo, apresentado no Capitulo II, entre uma CMSM e um adsorvente comercial de peneiro molecular de carbono (CMS) desenvolvido para a separação do ar. Esta análise teve como objectivo compreender melhor o mecanismo de transporte de massa nas membranas de CMS, relacionando-o com a estrutura do material, e as diferenças de envelhecimento entre os dois materiais. Contrariamente ao esperado, os materiais não revelaram diferenças significativas relativamente ao seu envelhecimento. De facto, as principais diferenças obtidas dizem respeito à cinética de adsorção; as dependências das constantes de tempo aparentes com a pressão, foram obtidas para o CO_2, O_2, Ar e N_2, ajustando diferentes modelos da literatura aos dados experimentais, e enfatizando, deste modo, o papel importante da ultramicroporosidade nas propriedades dos materiais. A membrana de CMS apresentou um efeito de bloqueio à difusão das espécies O_2 e CO_2, propondo-se uma justificação para este facto. A vulnerabilidade destes materiais à exposição ao vapor de água foi comparada e relacionada com a superfície química de cada um. A existência de grupos hidrofílicos à superfície, responsáveis pela adsorção

de vapor de água neste tipo de materiais, foi relacionada com a química de superfície através de microanálise por raios-X e termogravimetria. Desenvolveu-se, ainda, um modelo capaz de prever os dois ramos de adsorção e dessorção do vapor de água. A cinética de adsorção do vapor de água foi também determinada em ambos os materiais, apresentando um comportamento de força directriz linear (LDF). Através da microanálise por raio-X concluiu-se que a razão C/O foi inferior no caso das membranas, sugerindo uma maior susceptibilidade ao vapor de água. Isto foi verificado pela adsorção significativa desta espécie a baixas pressões e pelos valores mais elevados das constantes cinéticas obtidas para as membranas.

O capítulo III descreve a preparação de membranas de peneiro molecular de fibra oca partindo de uma mistura de co-poliimida P84/S-PEEK. Estudou-se a influência dos parâmetros da pirólise nas propriedades das membranas de carbono, e caracterizaram-se as membranas através de experiências de permeação e por microscopia electrónica de varrimento (SEM). As permeabilidades e selectividades ideais mais elevadas foram obtidas para as membranas submetidas a uma temperatura final de pirólise de 750 ºC seguidas de arrefecimento brusco. Concluiu-se ainda que a existência de um patamar à temperatura final, precedendo um arrefecimento brusco, não contribuiu para a melhoria do desempenho das membranas. Neste caso, as permeabilidades foram inferiores às obtidas para as membranas pirolisadas sem patamar. Verificou-se ainda, que o arrefecimento brusco teve um efeito positivo nas permeabilidades das membranas, em detrimento de um arrefecimento natural lento até à temperatura ambiente. Ainda neste capítulo, reporta-se o uso do papel celofane comercial como filme precursor para a preparação de CMSM empregando um só passo de pirólise. Esta foi a primeira vez que este precursor foi usado. A influência dos parâmetros da pirólise na estrutura, morfologia e desempenho das membranas de carbono foi avaliada através de SEM, microanálise por raio-X, difracção por raio-X e permeação monocomponente das espécies He, H_2, Ar, N_2, CO_2, O_2, CH_4 e vapor de água a 29,5 °C. Estas membranas revelaram boas selectividades ideais, com desempenhos de separação posicionados acima do limite superior de Robeson para membranas poliméricas.

Finalmente, o capítulo IV apresenta a simulação de um módulo de membranas de carbono de fibra oca tendo em vista a produção de azoto a partir de uma corrente de ar saturado em vapor de água a 29,5 ºC. Propôs-se um modelo que considera a dependência da permeabilidade da membrana com a pressão e realizaram-se simulações em contra-corrente, analisando o efeito da razão entre as pressões da alimentação e permeado, e ainda, do aumento da pressão de alimentação. Estudou-se, também, o efeito da queda de pressão ao longo das membranas. Concluiu-se que é possível produzir azoto com uma pureza de 99,9 % a partir de uma corrente de ar (N_2-78,7 %, O_2-20,9 %, CO_2- 0,0003 %, vapor de água - 100 % RH) com recuperações até 65 %.

VIII

Sommaire

Cette thèse a pour objet l'étude de membranes de tamis moléculaire de carbone (CMSM). Ces membranes sont constituées par une matrice inorganique de carbone avec des propriétés inertes, résistant, de cette façon, à de hautes températures et à des ambiances chimiques agressives. En outres, les CMSM présentent, normalement des perméabilités élevées, alliées à des sélectivités aussi élevées, quand comparées avec des membranes polymériques (polymères) denses. Les CMSM possèdent une distribution de pores serrée avec des pores sélectifs (constrictions) contenus entre les 0,3 et les 0,5 nm, responsables par les propriétés de tamis moléculaire des membranes. Ces constrictions permettent le passage d'espèces plus petites, en retenant, pourtant, les espèces de taille plus grande. La préparation de celles-ci engage plusieurs étapes, en étant les plus importantes la sélection du précurseur et l'étape de pyrolyse. Cependant, il y a quelques études qui mentionnent un vieillissement de ces membranes dû à leur exposition à l'oxygène, en compromettant donc, la fiabilité de ces membranes pour l'application industrielle. Dans ce sens, on a effectué une étude comparative, présenté au Chapitre II, entre une CMSM et un adsorbant commercial de tamis moléculaire de carbone (CMS) développé pour la séparation de l'air. Cette analyse a eu comme objectif comprendre mieux le mécanisme de transport de masse dans les membranes de CMS, en montrant comment il se rapporte avec la structure du matériel, et encore les différences de vieillissement entre les deux matériaux. Contrairement à ce qu'on attendait, les matériaux n'ont pas révélé de différences significatives par rapport à leur vieillissement. Les principales différences obtenues se lient à la cinétique d'adsorption; les dépendances des constantes de temps apparentes avec la pression, ont été obtenues pour le CO_2, O_2, Ar et N_2, en ajustant les différents modèles de la littérature aux donnés expérimentaux, et en emphatisant, de cette façon, le rôle important de l'ultramicroporosité dans les propriétés des matériaux.

La membrane de CMS a présenté un effet de blocus à la diffusion des espèces O_2 et CO_2, et on propose une justification pour ce fait. La vulnérabilité de ces matériaux à

l'exposition à la vapeur d'eau a été comparée et mise en rapport avec la surface chimique de chacun d'eux. L'existence de groupes hydrophiles à la surface responsables par l'adsorption de vapeur d'eau dans ce type de matériaux, a été mise en rapport avec la chimie de surface à travers la microanalyse à rayon X et thermogravimétrie. On a développé encore un modèle capable de prévoir les deux branches d'adsorption et de désorption de la vapeur d'eau. La cinétique d'adsorption de la vapeur d'eau a aussi été déterminée dans les deux cas, en présentant un comportement de force motrice linéaire (LDF). À travers la microanalyse à rayon-X ont a conclu que le rapport C/O a été inférieur dans le cas des membranes, en suggérant une plus grande susceptibilité à la vapeur d'eau. Cela a été vérifié par l'adsorption significative de vapeur d'eau à pressions basses et par les valeurs plus élevés des constantes cinétiques obtenues pour les membranes.

Le chapitre III décrit la préparation de membranes de tamis moléculaire de fibre creuse à partir d'un alliage de co-poliimide P84/S-PEEK. On a étudié l'influence des paramètres de la pyrolyse dans les propriétés des membranes de carbone, et on a caractérisé les membranes à travers quelques expériences de perméation et par microscopie électronique à balayage (SEM). Les perméabilités et sélectivités idéales les plus élevées ont été obtenues pour les membranes soumises à une température finale de pyrolyse de 750 °C suivies d'un refroidissement brusque. On a conclu encore que l'existence d'un palier à la température finale, procédant d'un refroidissement brusque, n'a pas contribué à l'amélioration du dégagement des membranes. Dans ce cas, les perméabilités ont été inférieur que celles obtenues pour les membranes pyrolysées sans palier (à la température finale). On a vérifié, encore, que le refroidissement brusque a eu un effet positif dans les perméabilités des membranes, au détriment d'un refroidissement naturel et lent jusqu'à la température ambiant.

Dans ce chapitre encore, on se rapporte à l'utilisation du papier célophane commercial comme film précurseur pour la préparation de CMSM employant uniquement un pas de pyrolyse. (C'est la première fois qu'on a utilisé ce précurseur.) L'influence des paramètres de la pyrolyse dans la structure, morphologie et dégagement des membranes de carbone a été évaluée en travers SEM, microanalyse

rayon-X, diffraction à rayon-X et perméation monocomposante des espèces He, H_2, Ar, N_2, CO_2, O_2, CH_4 et vapeur d'eau à 29,5 °C. Ces membranes ont révélé de bonnes sélectivités idéales, avec des dégagements de séparation positionnés au-dessus de la limite supérieure de Robeson pour des membranes polymériques.

Finalement, le chapitre IV présente la simulation de membranes de carbone de fibre creuse ayant pour objet la production d'azote à partir d'une courante d'air saturé en vapeur d'eau à 29,5 °C. On a proposé un modèle qui considère la dépendance de la perméabilité de la membrane avec la pression et on a réalisé des simulations en contre-courant, en analysant l'effet du rapport entre les pressions de l'alimentation et du perméat, et, encore, l'augmentation de la pression de l'alimentation. On a, aussi, étudié l'effet de la chute de pression au long des membranes. On est arrivé à la conclusion qu'il est possible de produire de l'azote à 99,9 % de pureté à partir d'un courant d'air (N_2-78,7 %, O_2-20,9 %, CO_2- 0,0003 %, vapeur d'eau -100 % HR) avec des récupérations jusqu'à 65 %.

Table of Contents

List of Figure Captions

List of Table Captions

Chapter I

Chapter 1 - Introduction

1.1. Gas separation

1.1.1. Distillation, PSA and Membranes

The key for a sustainable industrial development is to seek new strategies and technologies for improving efficiency and minimizing environmental impact. Nowadays, the industry of gas separation requires the replacement of energy-demanding processes by simpler, low cost and cleaner technologies.

The separation or purification of gases was for a long time performed by distillation and cryogenic distillation processes; these allow for high recoveries and purities, and the possibility to operate at high pressures. Distillation, however, is known for its high energy consumption and cryogenic distillation is also known for being expensive [1-3]. Another technology for gas separation is absorption, a simple process, but with poor separations characteristics, reflected in low purities and recoveries [3].

Adsorption based processes are also an alternative technology. Pressure swing adsorption (PSA), preferentially operating at low pressures, leads to very high purity products, using a relatively simple process. However, both absorption and adsorption processes, require a regeneration step, i.e. the additional use of a solvent regeneration unit and a second adsorbent bed for the desorption step, respectively.

In the last 25 years, membrane processes have emerged as a new solution for separating gas mixtures. Since then, remarkable progress has been made in the development of new membranes [4, 5]. These processes are very promising for their versatility and simplicity; membrane processes are light weight, compact, and modular design, permitting an effortless expansion of the plants, easy maintenance and possibility to operate at partial capacity [5]. Globally, it is a low cost and energy saving technology.

These technologies compete with each other to better suit a certain application, where the final verdict is simply economics.

1.1.2. History of Membrane technology

The kick-off for the implementation of membrane technology in gas separation was done by polymeric membranes. Monsanto was the first company commercializing polymeric membranes for large scale gas separation, in 1980, and is today a division of Permea Inc. owned by Air products and Chemicals, Inc; their PRISM® membranes were developed for hydrogen separation [5, 6] and later used in other applications like nitrogen production, dehydration air drying, etc. Following, several other companies Grace, Separex, Cyanara [5, 7] and others, launched dry cellulose acetate membranes to the market of membrane technology for CO_2 removal from natural gas. Almost by the same time, 1983, Ube Industries, Ltd developed polyimide hollow fibers to separate H_2 from hydrocarbons, and two years later such membrane units were planted. The separation of nitrogen or oxygen from air using membranes was also rising in interest and Asahi Glass Company started the production of membrane systems to concentrate oxygen up to 40 %. A trade mark Spiragas® from Signal Company came out for ultrathin silicone film supported on a porous polysulfone shaped in a spiral wound membrane module. Dow Chemical also launched polyolefin made membranes by the trademark of GENERON® for producing a stream of 95 % nitrogen from air [4, 6]. Gas separation with membranes is becoming stronger with the development of new "spinnable" hollow fiber membranes [8]. Today the market of nitrogen production from air by membranes is the largest. Ube Industries become producing and commercializing polyimide membranes for air dehumidification and nitrogen production from air (www.ube-ind.co.jp). In the end of 2008, Air Products announced to increase in 50 %, their annual capacity of 40 000 PRISM hollow fiber membrane modules. Based on DuPont's polymeric fiber spinning technology, Air Liquide has recently launched hollow fiber membranes, (MEDAL™) for air separation/nitrogen generation, carbon dioxide removal and hydrogen purification [8].

1.1.3. Organic vs Inorganic Membranes

Porous polymeric membranes have high fluxes but low selectivities, while dense glassy polymeric membranes are extremely low permeable but with increased selectivities. However, polymers in general cannot withstand harsh conditions since they present chemical and thermal instability [8, 9]. Polymeric membranes can be irreversibly swollen or plasticized due to their exposition to CO_2 or hydrocarbons, even in small concentrations, compromising their performance and disabling the functionality of the membrane module. Therefore, modules assembled with organic membranes should often require a pre-treatment step to remove undesirable components [8]. Despite the large number of polymers studied and used at laboratory scale, only a few polymers are industrially implemented; the most important and used ones are cellulose acetate, polysulfone and polyimides [4]. To overcome the handicap of polymeric membranes, considerable attention started to be paid in recent years to the development of inorganic membranes as promising materials for gas separation [10]. These present a greater chemical and thermal stability than organic membranes and combine high permeances and selectivities, when compared to dense polymeric membranes. Still, these membranes also present some drawbacks which are their higher cost, modest reproducibility, and sealing difficulties when operated at high temperatures (>600 ℃) [8]. The industrial implementation of inorganic membranes is still very low; palladium dense membranes are one example for small-scale production of high purity hydrogen, by Johnson Matthey [4].

The available commercial porous membranes are ceramic ones, such as alumina, silica, titanium, porous glass and sintered metals. These membranes present very high permeabilities but very limited selectivities. Despite the very promising results obtained in lab-scale, microporous inorganic membranes, such as zeolite and carbon membranes, encounter their main obstacle in scale-up; they have reduced mechanical stability and are difficult to produce defect-free with reproducible performances. Furthermore, their large-scale production is very expensive when comparing to the manufacturing costs of polymeric membranes [11]. Nevertheless,

efforts to overcome these hindrances are being made as it is reflected by the research activity in this area (see Figure 1.1).
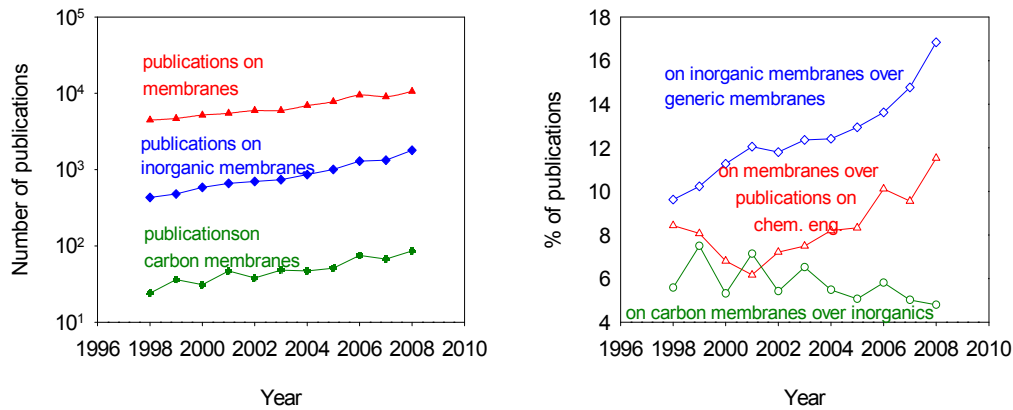
Figure 1.1 – Publications containing the keyword "membranes" (red triangles), "inorganic membranes" (blue diamonds) and "carbon membranes" (green circles) limited to the area of Chemical Engineering from 1998 until 2008 (data obtained from SCOPUS database) .

In the last decade, the number of publications on membranes has increased from 4 467 to 10 641. Among these, inorganic membranes present a rising rate of publication; they account for 10 % in 1998 and 17 % in 2008 over generic membranes. Within these statistics, the particular research on carbon membranes presents a volume of publications that increased from 24 up to 86 per year, in the same period of time, representing around 5 % of the remaining inorganic membranes (data obtained from scopus database: www.scopus.com). Despite the small amount of publications on carbon membranes, these are very promising materials, with several advantages over zeolitic and other inorganic membranes.

The subgroup of molecular sieving membranes (silica, zeolites and carbon) differs from the other microporous inorganic for presenting good permeability vs. selectivity relationships. In particular, carbon molecular sieve membranes, exhibit excellent resistance to heat and corrosion environments allied to great shape selectivities to planar molecules [10]. This is the category of membranes to be studied in the scope of this thesis.

1.2. Membrane Technology

1.2.1. Structure of inorganic membranes

Inorganic membranes can be classified, according to their structure, in dense (non-porous) or porous, and the last category can be divided in symmetric or asymmetric. Dense membranes comprise metallic membranes, metal alloys and solid electrolytes where the gas species permeates through their crystal lattices [12]. Porous membranes, in contrast, allow gas species to permeate through their free spaces, between lattices, the pores; these include oxides, sintered metal, carbon, glass, or zeolite membranes.

1.2.2. Porous membranes and their mass transport

The major difference between porous and non-porous membranes is mainly reflected on the comparable lower fluxes of non-porous membranes. However, within the porous categories there are different ranges of pore sizes that influence the regimes of mass transport, together with other aspects as the physical properties of the species and the pressure. For membranes with large pores, fluxes are expectedly high but selectivities are small. As pore sizes decrease, selectivity is enhanced while fluxes become smaller. When microporous membranes are composed by a selective layer over a porous support, the mass transport through the membrane is the overall contribution of both selective and support layers. The most usual transport mechanisms through porous membranes for gas separations (see Figure 1.2) are the following described ones:
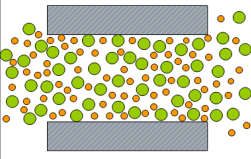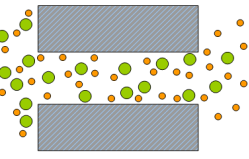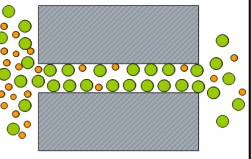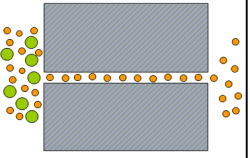
Figure 1.2 – Scheme of Transport mechanisms in pores.

Viscous flow (>50 nm) –Viscous flow characterizes the mass transfer through pores where intermolecular collisions are predominant. The interactions between species lead to collisions with the pore walls resulting in an overall pressure drop along the membrane. With practically no selectivity the permeation occurs due to the establishment of a pressure gradient between the two sides of the membrane. Usually, this type of flow occurs in the supports or enough large defects.

Molecular diffusion – Also called simply diffusion, happens when species move from a more concentrated side to a less concentrated one. Usually happens in large pores or defects.

Knudsen diffusion (2-500 nm) – This regime happens under low pressure conditions and when the pore size is smaller than the mean-free path; as a result, species start to collide more with the pore walls than with each other. The selectivity is not high and is determined by the square root of the reciprocal ratio between the molecular weights of the species

Surface diffusion (0.5-2 nm) – Surface diffusion takes place when species are adsorbed on the pore walls of the membrane; once in the adsorbed state, the adsorbates move through the pore network by jumping from site to site. The different rates of diffusion are based on the different rates of adsorption; the highly adsorbable species will preferentially cross the membrane rather than species with lower affinity to the surface walls.

Molecular sieving (0.3-0.5 nm) – As the name suggests, when pores have sizes very close to those of molecules or atoms diameters, the membrane acts as a molecular sieve; smaller species are allowed to pass through very narrow pores, whereas larger species are retained. This regime is characterized by its high selectivity and low or moderate flux. Zeolite membranes as well as carbon molecular sieve membranes exhibit this type of mass transport regime.

In molecular sieve membranes, species are confined to the space between two carbon walls and subjected to a potential energy field as illustrated in Figure 1.3. If the pores are wide enough, the potential minima occurs independently for each wall. As the pore gets narrower, the two contributions from opposite walls start becoming significant, resulting in one minimum. This happens until the potential becomes positive and the pore becomes impermeable to the species. However, there is still an intermediate pore size where the species cannot be adsorbed, but with enough energy they can pass constrictions by an activated process.
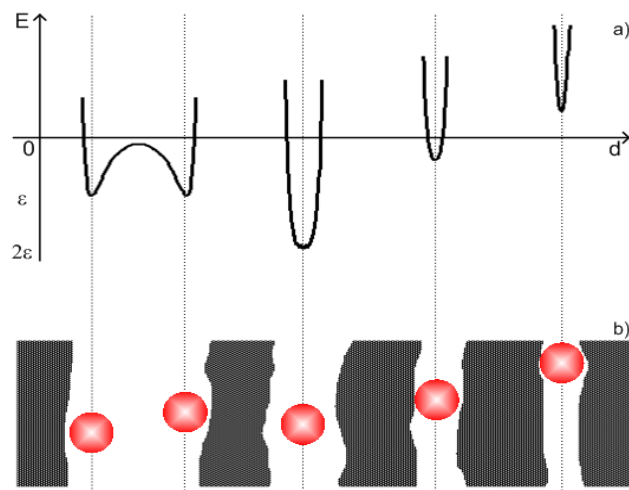
Figure 1.3 – Schematic representation of the species/wall interactions within a micropore or constriction. a) Potential energy E of a species within pores of different dimensions; b) sketch of the species in respective pores (adapted from [13]).

The previous mentioned regimes are a result of the existent pore sizes of the membrane, of the operating conditions, and of the size and shape of the permeating species. Usually, the selective layer of microporous membranes is characterized by a surface diffusion and molecular sieving. On the other hand, supports normally have larger pores, where viscous flow or Knudsen diffusion takes place.

1.3. Carbon molecular sieve membranes

1.3.1. Introduction

Carbon molecular sieve membranes (CMSM) result from a heat treatment under controlled atmosphere, or under vacuum, of a polymeric precursor. During the heat treatments, which can be diverse as will be explained next, the polymeric chains decompose originating an amorphous carbon skeleton, with interconnected pores. This pore network is responsible for the mechanism of separation, characteristic of these membranes. Interactions with the carbon walls are important, since adsorption phenomena do occur, but the carbon matrix itself is assumed to be impervious, in opposition to what happens with polymeric membranes [14]. Usually, CMSM present a narrow pore size distribution with pores within the range of 0.3-0.5 nm. These are the so called selective pores, which are responsible for the sieving properties of carbon membranes. However, there might be larger pores, from 0.5-0.8 nm, responsible for the surface diffusion. The pore network may, therefore, be a sequence of narrow and large pores [15]. The distinctive feature of CMSM is that, by employing different pyrolysis conditions, they can be tailored in order to yield different gas permeation properties [16]. The pore network can also be adjusted or tuned by combining several pre- or post-treatments leading to the desired pore size distribution. However, the control over all variables involved in the development of the membranes and their microstructure is very difficult to get; there are too many factors involved in the preparation of the final carbon membrane and these also differ from precursor to precursor.

1.3.2. Configurations

Carbon membranes are produced in a supported or unsupported (self-supported) form. The supports are usually used to provide extra mechanical strength to the selective membrane (reducing its fragility), introducing a negligible mass transfer resistance [12]. The unsupported membranes can be flat, hollow or capillary fibers, while supported membranes present a flat or tubular form, depending on the shape

of the support. The decision for making supported /unsupported, flat or tubular carbon membranes would be determined by the application in view. For fundamental studies at lab-scale, flat sheets are preferred. The use of supports is often required, though, to overcome the fragility or brittleness so characteristic of carbon membranes. At an industrial scale, costs are always a very important factor and, hence, the future should involve the production of hollow fiber like modules; these have a greater surface to volume ratio when compared to modules assembled with flat sheet membranes [5]. Moreover, the only sold CMSM modules were set with hollow fibers.
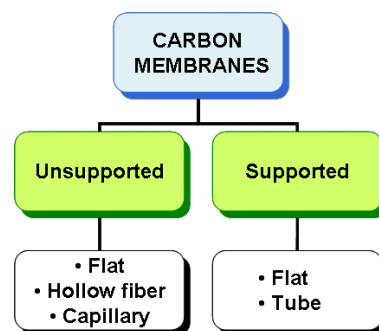
Figure 1.4 – Configurations for carbon membranes.

1.3.3. Preparation

Recently, Saufi and Ismail [10] have published a review on the fabrication of carbon membranes for gas separation. The preparation of carbon membranes for gas separation involves the optimization of six different steps by the following sequential order provided in Figure 1.5:
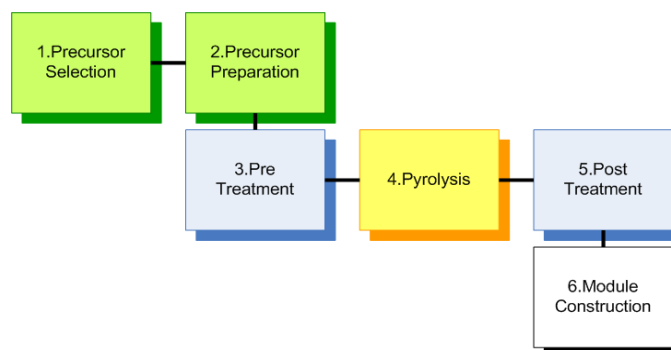
Figure 1.5 – Process for preparing carbon membranes.

Among these steps, the one that influences the most the final success of the membrane is the pyrolysis step. During this stage the polymeric matrix is decomposed, giving place to the carbon structure and the pore network, dictating this way, the ability of the carbon membrane to separate gases.

1.3.3.1. Precursors

The selection of the polymeric precursor to be used as the carbon source for the resultant carbon membrane is one of the most important steps. Different membrane precursors, submitted to the same heat treatment lead to carbon membranes with different properties. Several carbon-containing precursors have been tested to form carbon membranes, such as resin, pitch, coal [17], graphite, plants and polymers. The polymeric materials are usually preferred falling the following main requirements: the membrane precursor should have a high yield of fixed carbon and should be thermosetting. The polymeric precursor should not melt or soften during pyrolysis, but rather decompose without causing defects in the carbon structure, such as, cracks or pinhole pore-holes, that could compromise the selectivity of the carbon membrane [18].

A summary of these materials is shown in Table 1.1. However, some authors have also tried to prepare blends of thermally stable polymers with thermally labile ones [19-22]. In order to further improve the membrane properties, the precursor was often loaded with metals such as silver [23, 24], copper [25], platinum [26, 27] , etc, and other alkali metals [28, 29], for enhancing the affinity of the final carbon membrane towards certain permeants.

Table 1.1 – Polymeric precursors for carbon membranes.

Precursor	Reference
Polyacrilonitrile (PAN)	[30-32]
Cellulose	[25, 33-37]
Polyimides and derivatives	[38-68]
Phenolic resin	[69-85]
Polyfurfuryl alcohol (PFA)	[86-93]
Polyetherimide (PEI)	[94-100]
Poly(vinylidene chloride)	[101-103]
Polyphenylene oxide (PPO)	[21, 28, 104-109]
Condensed polynuclear aromatic (COPNA) resins	[110]
Lignin	[111-114]
Heteropolyacid	[115]
Poly(phthalazinone ether sulfone ketone)(PPESK)	[116, 117]

From Table 1.1 it is possible to see that polyimides are the most used precursor for carbon membranes. These are high carbon-containing polymers withstanding elevated temperatures, such as 300 ºC, without losing their shape. They are very stable, with a high glass transition temperature, decomposing before achieving their melting point, assuring this way a resultant defect-free carbon structure. The most commercially used (co-)polyimides referred in literature are: Kapton, Matrimid, P84, etc. However, the big disadvantage of using polyimides is their high cost, what can eventually compromise the economical viability of the resultant carbon membranes.

Phenolic resins are also acceptable precursors employed by several authors to prepare carbon molecular sieve membranes. These polymers present the advantage of being inexpensive, contrarily to polyimides, due to their large applicability in several sectors, such as, commodity construction, high technology materials, etc.

Polyfurfuryl alcohol (PFA) has been initially prepared as a thin film on a rigid support revealing some problems related with mechanical and elastic properties. Therefore, other techniques were developed to succeed in the preparation of CMSM based on

PFA. A spray coating technique has been reported [86], but it was an ultrasonic deposition technique developed by Shiflett and Foley [87, 89] that led to the best results.

Another thermally stable polymer is polyacrilonitrile (PAN), largely used in the production of high performance carbon fibers. PAN has a high melting point, decomposing below this temperature, yielding greater carbon contents. Due to its ordered molecular orientation, the unsupported derived carbon membranes are mechanically stronger.

Cellulose is a natural and renewable polymer, abundant in the planet. The applications of cellulosic materials are vast and widespread. Cellulose presents a sufficient yield of carbon resulting in a good alternative for preparing carbon molecular sieve membranes with enough mechanical stability. In addition, cellulosic precursors have a low cost enhancing the economical viability of carbon molecular sieve membranes. More information concerning other precursors can be found elsewhere, as indicated in Table 1.1.

Independently on the polymer selected to originate carbon membranes, the preparation of this precursor will determine part of the success of the process. Thus, the conditions should be optimized to assure a good quality precursor. An imperfection on the polymeric film, fiber or supported layer, will definitely compromise the quality of the resultant carbon membranes. Small defects in the polymeric precursor can be amplified in the final carbon membrane, resulting in small cracks or pinholes destroying their molecular sieving properties. Heterogeneity in the selective layer thickness is another undesirable factor that should be avoided and prevented during the polymer deposition on supports, casting of unsupported flat sheets, or spinning fibers. It should also be kept in mind that during carbonization the polymeric material shrinks, which can also cause defects or cracks.

1.3.3.2. Pre-treatment

Before submitting the polymeric membrane precursor to the pyrolysis step there are some treatments that might be employed in order to provide additional dimensional stability to the polymeric matrix. This is used to guarantee that the polymeric structure is preserved. The pre-treatments are split into physical and chemical. As expected, the use of a given precursor demands a proper pre-treatment. Stretching (physical) is commonly employed to spun hollow fibers in order to attenuate non uniformities in diameter formed during extrusion, conferring a greater dimensional stability to these fibers. Oxidation is a treatment under an oxidative agent, i.e. oxygen or air, with the objective of avoiding an undesirable release of volatiles during pyrolysis, ensuring a final carbon membrane with maximized carbon content and minimized pinholes. There are also chemical treatments obtained through immersion of the precursor into aqueous solutions, or obtained with catalysts [10]. An example of a pre-treatment very important to successful preparation of carbon membranes is the removal of residual solvents or humidity from the polymer to prevent its undesirable decomposition at lower temperatures. This care, however, can be included in the pyrolysis step, by employing a heat treatment with dwells or extremely lower heating rates; this will allow undesirable matter to be released at lower temperatures preventing the polymeric matrix from being damaged.

1.3.3.3. Pyrolysis /carbonization

The core of the whole process is the stage where the polymeric matrix is turned into carbon through a pyrolysis step. During this step the precursor is submitted to a specific heating protocol under a controlled inert or vacuum atmosphere. The product of this pyrolysis will be an amorphous carbon membrane with a pore network characteristic for the specific used polymer. At this stage the decomposition of the polymeric matrix takes place in a controlled way, where a significant loss of weight occurs; it is associated to the release of diverse volatile matter. These byproducts are typically H_2, H_2O, CO, CO_2, and residual HCN, CH_4, and NH_3 depending on the precursor's nature [44]. As volatiles are set free, the resulting carbon matrix cross-

links, forming disordered non homogeneous graphene layers, typical of non graphitizable carbons. The interconnected spaces among chaotic graphene layers are the pores of the membrane; narrower ultramicropores, called constrictions are responsible for the molecular sieving properties of these membranes (selectivity), while larger interconnected pores allow for larger productivities (permeability). The size and shape of the pores, and their interconnectivity depend on the structure and morphology of the polymeric precursor and on the pyrolysis procedure employed. The pyrolysis parameters such as, heating rate, soaking or dwell times, end temperature, or gas atmosphere, are all important variables that can be adjusted in order to achieve a certain pore network. The influence of these parameters on the performance of carbon membranes is of great importance. The ideal carbon molecular sieve membrane should have a high micropore volume, with a narrow pore size distribution allowing high permeances and selectivities. The pore network should have a very low tortuosity, and an effective porosity, in a sequence of larger pores interconnected with narrower selective pores. The membrane should be as thin as possible but with enough mechanical strength. Moreover, the carbon surface should be chemically stable.

1.3.3.4. Post-treatment

After pyrolysis the carbon membrane is already created and the pore network is formed. However, sometimes there is the need to repair some eventual defects and a post-treatment can often solve the problem. Coating the membranes with another polymers followed by recarbonization is often used to correct the defects. On the other hand, the desire to better suit for a certain application demands a more precise pore tuning, narrowing the pore size distribution or simply reducing or enlarging the pore widths, as intended. Post-oxidation, to reopen or enlarge pores, chemical vapor deposition (CVD), by means of carbon deposition in order to close or reduce pore widths are post-pyrolysis treatments. Carbon membranes are normally hydrophobic but present some oxygenated functional groups, or unstable carbon atoms at the pore walls prone to chemisorb oxygen in the form of functional groups. To avoid this

phenomena, passivation treatments with hydrogen at around 600 °C have been reported [118]. It is stated that this passivation procedure under reducing atmosphere removes some of the functional groups, or chemisorbed oxygen, stabilizing the surface of the membrane and weakening its hydrophilic character.

1.3.3.5. Module construction

The geometry of the membranes and the mode they should be packed together in a suitable device – membrane module – are very important aspects for the industrial implementation of a membrane separation system. The cost of the module, the type of application and the functionality of the module, all have influence on the modules' final configuration.

In the particular case of carbon membranes, their brittleness will *a priori* limit the possible configurations. The continuity of CMSM as alternative membrane technology should involve the assembly of hollow fiber like modules, rather than spiral-wound geometry, flat or honeycomb like modules. In fact, this is the only way to assemble a carbon membrane module capable of being commercialized. The hollow fiber membrane modules present very good surface to volume ratios, (>1000 $m^2 m^{-3}$) superior to any other configuration. Investment and operating costs, as well as the maintenance costs are also important considerations to take into account. The main advantages of using an inorganic membrane, such a CMSM, are its ability to withstand harsh thermal and chemical conditions. However, to assemble the carbon membranes into a membrane module there is the need to find an appropriate sealant. The reliability of the sealing materials and procedures, especially for high temperature applications, may be a problem.

1.3.4. State of the art on CMSM

The first concept of compacted carbon molecular sieve membranes has been introduced by Barrer and Strachan in 1955, when these authors compressed a high specific surface carbon powder yielding a microporous plug. They have seen the importance of surface flow for the most polarisable gases and recognized the

importance of such membranes for gas separation applications [119]. A few years later, Bird et al. [120] tried to prepare supported and unsupported carbon molecular sieve membranes by using polyfurfuryl alcohol as the carbon source. The authors failed their attempt since they could not prepare a defect-free membrane with controllable pore size.

However, it was by the hands of Koresh and Soffer in the 80's [13, 15, 121, 122], that carbon molecular sieve membranes for gas separation were successfully crack-free developed. For a decade, several patents were filed by these authors [123-125] and by the end of the 1990's the Israeli company Carbon Membranes Inc. began commercializing CMSM. These authors have used cellulose and phenolic resin precursors to prepare membranes with good permeabilities and selectivities [126]. These membranes present a very narrow pore size distribution, with pore sizes within the range of 0.3-0.5 nm, making possible the separation of molecules with similar diameters, such as nitrogen and oxygen. However, the company closed in 2001. Back to 1993, Rao and Sircar [127, 128] from the company Air Products have prepared nanoporous carbon membranes from the carbonization of poly(vinylidene chloride) supported on macroporous alumina to provide mechanical stability. The pore sizes of the selective carbon layer were between the diameter of the more adsorbable species and about four times the diameter of the largest species; strongly adsorbable species, as hydrocarbons, could be effectively separated from hydrogen due to selective adsorption and surface diffusion; selectivities of C_4H_{10} and C_3H_8 over H_2 of respectively, 94.4 and 21.3, were obtained. Air Products Inc. has kept this research on selective surface flow (SSF) carbon membranes for more than one decade trying to industrially implement them [101, 102, 127, 128]. Unfortunately, they did not succeed. These were the only two attempts, up to now, to implement carbon membranes in the industry of gas separation. However, several academic researches have carried on trying to improve and develop successful carbon membranes and solving problems associated to this kind of material. In 1994, Jones and Koros [40, 129] used a polyimide hollow fiber as a precursor for CMSM to air separation. The result was a membrane with a selectivity of oxygen over nitrogen of 14. Besides that, the carbon membranes also revealed good performances to other important

18

separations such as CO_2/N_2, CO_2/CH_4 and H_2/CH_4. However, these same authors [130, 131] verified that these carbonaceous materials suffer from a kind of deactivation due to adsorption of water vapor present in humidified streams leading to a decrease of performance. The same problem was also later reported by Menendez et al. [132] in 2001 and by Lagorsse et al. [133] in 2008 for respectively, phenolic resin and cellulose derived carbon membranes. They verified that the existence of oxygen based functional groups on the surface of the membrane could enhance the adsorption of water vapor blocking the pore network, reducing the performance of the membrane. In 1998, Fuertes et al. [134] prepared asymmetric carbon membranes from polyamic acid. These authors [99] also coated a macroporous support with a thin layer of a commercial polyimide (polyetherimide) and carbonized; the derived carbon membranes exhibited high ideal selectivity for permanent gas pairs (O_2/N_2, N_2/He and CO_2/CH_4). After these reported studies, several works were performed concerning the preparation and characterization of carbon membranes for gas separation, as reviewed in literature [10, 14, 135]. In 2003, Barsema et al. [23, 24, 136] incorporated silver in the polyimide precursor's matrix in order to achieve even higher selectivities for separations involving O_2. Still by that time, Sanderson and Saduki [26] prepared polyacrilonitrile derived carbon hollow fibers coated with platinum to be used in a catalytic membrane reactor for the separation of hydrogen from hydrocarbons with equilibrium-limited reactions. Some other studies report the use of palladium nanoparticles to improve H_2/N_2 selectivies of carbon molecular sieve membranes [137]. In 2006 Hagg et al. [33] selected cellulose treated with trifluoroacetic acid as a promising precursor for carbon molecular sieve membranes. These authors [25] have also loaded the precursor with metals to improve the characteristics of the resultant carbon membranes. They aimed at the development of cheap carbon membranes for CO_2 recovery from various gas mixtures [33] and for hydrogen recovery [34]. Dong et al. [93] prepared H_2-selective carbon membrane by polymerizing furfuryl alcohol on α-alumina supports and carbonizing up to 200-1000 °C. The carbon membrane showed high separation factors at 150 °C for binary gas mixtures: α (H_2/CO_2) >22 900, α (H_2/N_2)>2 480 and α (H_2/CO) >2 510. Supported carbon membranes were prepared by a novel approach using Novolac phenol-formaldehyde resin containing a

little hexamine as a precursor coated on a porous resin support from the same material. With one step, both selective film and support were carbonized at 800 °C originating good ideal selectivity for H_2/N_2 and H_2/CH_4 [85]. The use of Novolac phenol-formaldehyde resin blended with a thermolabile polymer such as poly(ethylene glycol) was also carried out with the intuit of inducing pore formation [72]. Hosseini et al. [138] developed carbon membranes derived from PBI-polyimide blends obtaining very good results targeting the separations of CO_2/CH_4, H_2/CO_2 showing selectivities of, respectively, 204.0 and 33.4; the separation of N_2/CH_4 exhibited a great nitrogen permeability of 7.99 barrer and a selectivity of 2.78. Very recently, the use of a new polymeric precursor, poly(phthalazinone ether sulfone) (PPES) has been tried to prepare carbon membranes. The membranes were prepared up to 700 °C and tested at 30 °C exhibiting permeabilities towards H_2, CO_2, O_2 and N_2 of respectively, 610.1, 439.9, 147.0, and 27.0 barrer; the selectivities for the pairs H_2/N_2, CO_2/N_2, and O_2/N_2 were 22.6, 16.3, and 5.5, respectively. Effects of sulfone/ketone in poly(phthalazinone ether sulfone ketone) (PPESK) have also been studied [117].

1.4. Motivation and outline

The present thesis was driven by the need of deeper understanding and studies on the properties of carbon molecular sieve membranes, which was still lacking in literature. The morphology and structure of the pore network influence the properties of the membranes. This part of the research work started within a European project entitled "Development of New Materials and Processes to Enhance Specialty Gas Separations", which has stimulated the start up of a new research project funded by FCT, designated "Systematic optimization of Carbon Molecular Sieve Membranes Synthesis - Development of Oxygen Stable Membranes". In addition to the study of membrane properties and their influence on performance, seeking for inexpensive precursors capable of yielding stable CMSM in a single heating step, suitable for certain applications, was also a goal of this research work.

The present thesis is divided in three main chapters as follows:

In Chapter II, "Comparative study between a CMS membrane and a CMS adsorbent", the adsorption equilibrium and kinetics of permanent gases was determined and related to the intrinsic properties for each material. The behavior towards exposure of water vapor is also studied and related to the surface chemistry of each material.

Chapter III, "Preparation and characterization of carbon molecular sieve membranes", reports the pyrolysis and characterization of carbon membranes derived from a blend of P84/SPEEK hollow fiber precursor foreseeing the possibility for metal impregnation. This work was mostly performed at MTG in the University of Twente, the Netherlands. The study of a commercial cellophane paper, a cellulose based precursor, as an alternative for preparing carbon membranes is also presented. The preparation and characterization of these last membranes was carried at LEPAE.

The Chapter IV, "Carbon molecular sieve membranes for air separation", presents a simulation study for the separation of nitrogen from air in a hollow fiber membrane module. The mass transfer through the membranes was described using the characteristics determined for cellophane derived carbon membranes.

Finally, Chapter V, "General Conclusions and Future Work", summarizes the main conclusions of this thesis. Further ideas and framed suggestions for future research directions are presented, together with brief description of some preliminary performed work.

Appendix A shows extra results obtained during the internship at MTG. Further details on the experimental set-ups used along this work are presented in Appendix B. Appendix C presents some preliminary work to be continued in the future.

1.5. References

[1]   R.T. Yang, Gas separation by adsorption processes, Imperial College Press, London, 1997.

[2]   D.M. Ruthven, Principles of adsorption and adsorption processes, Wiley & Sons, Inc, New York, 1984.

[3]   M.T. Ravanchi, T. Kaghazchi, A. Kargari, Application of membrane separation processes in petrochemical industry: a review, Desalination 235 (2009) 199-244.

[4]   S.P. Nunes, K.V. Peinemann, Gas Separation with Membranes, in: S.P. Nunes, K.V. Peinemann (Eds.), Membrane Technology in the Chemical Industry, Wiley, Weinheim, 2006, pp. 53-75.

[5]   R.W. Baker, Membrane Technology and Applications, 2nd ed., John Wiley & Sons Ltd, California, 2004.

[6]   A.K. Fritzsche, J.E. Kurz, The Separation of Gases by Membranes, in: M.C. Porter (Ed.), Handbook of Industrial Membrane Technology, Noyes Publications, Westwood, New Jersey, U.S.A., 1990, pp. 559-593.

[7]   R.W. Baker, E.L. Cussler, W. Eykamp, W.J. Koros, R.L. Riley, H. Strathmann, Membrane Separation systems: Recent Developments and Future Directions, Noyes Data Corporation, New Jersey, 1991.

[8]   P. Bernardo, E. Drioli, G. Golemme, Membrane Gas Separation: A Review/State of the Art, Ind. Eng. Chem. Res. 48 (2009) 4638-4663.

[9]   A. Basu, J. Akhtar, M.H. Rahman, M.R. Islam, A review of separation of gases using membrane systems, Pet. Sci. Technol. 22 (2004) 1343-1368.

[10]   S.M. Saufi, A.F. Ismail, Fabrication of carbon membranes for gas separation - a review, Carbon 42 (2004) 241-259.

[11]   A.M. Mendes, F.D. Magalhães, C.A.V. Costa, New trends on membrane science, Fluid Transport in Nanoporous Materials 219 (2006) 439-479.

[12]   Y.S. Lin, Microporous and dense inorganic membranes: current status and prospective, Sep. Purif. Technol. 25 (2001) 39-55.

[13]   J. Koresh, A. Soffer, Study of Molecular-Sieve Carbons. 2. Estimation of Cross-Sectional Diameters of Non-Spherical Molecules, J Chem Soc Farad T 1 76 (1980) 2472-2485.

[14]   A.F. Ismail, L.I.B. David, A review on the latest development of carbon membranes for gas separation, J. Membr. Sci. 193 (2001) 1-18.

[15]   J. Koresh, A. Soffer, Study of Molecular-Sieve Carbons. 1. Pore Structure, Gradual Pore Opening and Mechanism of Molecular-Sieving, J Chem Soc Farad T 1 76 (1980) 2457-2471.

[16]   H. Suda, A. Wenzel, H. Yanagishita, K. Haraya, Gas permeation properties of carbon molecular sieve membranes prepared in alkali metal-organic solvent systems, Mol Cryst Liq Cryst 341 (2000) 1371-1376.

[17]   C.H. Liang, G.Y. Sha, S.C. Guo, Carbon membrane for gas separation derived from coal tar pitch, Carbon 37 (1999) 1391-1397.

[18]   A. Soffer, D. Rosen, S. Saguee, J. Koresh, Carbon membranes, GB patent 2207666, 1989.

[19]   Y.K. Kim, H.B. Park, Y.M. Lee, Gas separation properties of carbon molecular sieve membranes derived from polyimide/polyvinylpyrrolidone blends: effect of the molecular weight of polyvinylpyrrolidone, J. Membr. Sci. 251 (2005) 159-167.

[20]   Y.K. Kim, H.B. Park, Y.M. Lee, Carbon molecular sieve membranes derived from thermally labile polymer containing blend polymers and their gas separation properties, J. Membr. Sci. 243 (2004) 9-17.

[21]   H.J. Lee, H. Suda, K. Haraya, S.H. Moon, Gas permeation properties of carbon molecular sieving membranes derived from the polymer blend of polyphenylene oxide (PPO)/polyvinylpyrrolidone (PVP), J. Membr. Sci. 296 (2007) 139-146.

[22]   H. Hatori, T. Kobayashi, Y. Hanzawa, Y. Yamada, Y. Limura, T. Kimura, M. Shiraishi, Mesoporous carbon membranes from polyimide blended with poly(ethylene glycol), J. Appl. Polym. Sci. 79 (2001) 836-841.

[23]   J.N. Barsema, J. Balster, V. Jordan, N.F.A. van der Vegt, M. Wessling, Functionalized Carbon Molecular Sieve membranes containing Ag-nanoclusters, J. Membr. Sci. 219 (2003) 47-57.

[24]   J.N. Barsema, J. Balster, N.F.A. Van der Vegt, G.H. Koops, V. Jordan, M. Wessling, Ag functionalized Carbon Molecular Sieves membranes for separating O2 and N2, Membranes-Preparation, Properties and Applications 752 (2003) 207-212.

[25]   J.A. Lie, M.B. Hagg, Carbon membranes from cellulose and metal loaded cellulose, Carbon 43 (2005) 2600-2607.

[26]   R.D. Sanderson, E.R. Sadiku, Synthesis and morphology of platinum-coated hollow-fiber carbon membranes, J. Appl. Polym. Sci. 87 (2003) 1051-1058.

[27]   A. Berenguer-Murcia, E. Morallon, D. Cazorla-Amoros, A. Linares-Solano, Preparation of silicalite-1 layers on Pt-coated carbon materials: a possible electrochemical approach towards membrane reactors, Microporous Mesoporous Mater. 78 (2005) 159-167.

[28]   M. Yoshimune, I. Fujiwara, H. Suda, K. Haraya, Gas transport properties of carbon molecular sieve membranes derived from metal containing sulfonated poly(phenylene oxide), Desalination 193 (2006) 66-72.

[29] Y.K. Kim, H.B. Park, Y.M. Lee, Carbon molecular sieve membranes derived from metal-substituted sulfonated polyimide and their gas separation properties, J. Membr. Sci. 226 (2003) 145-158.

[30] C.W. Song, T.H. Wang, Y.H. Qiu, J.S. Qiu, H.M. Cheng, Effect of carbonization atmosphere on the structure changes of PAN carbon membranes, J. Porous Mater. 16 (2009) 197-203.

[31] L.I.B. David, A.F. Ismail, Influence of the thermastabilization process and soak time during pyrolysis process on the polyacrylonitrile carbon membranes for O2/N2 separation, J. Membr. Sci. 213 (2003) 285-291.

[32] J.F. Sun, C.J. He, S.J. Zhu, Q.G. Wang, Effects of oxidation time on the structure and properties of polyacrylonitrile-based activated carbon hollow fiber, J. Appl. Polym. Sci. 106 (2007) 470-474.

[33] J.A. Lie, M.B. Hagg, Carbon membranes from cellulose: Synthesis, performance and regeneration, J. Membr. Sci. 284 (2006) 79-86.

[34] D. Grainger, M.B. Hagg, Evaluation of cellulose-derived carbon molecular sieve membranes for hydrogen separation from light hydrocarbons, J. Membr. Sci. 306 (2007) 307-317.

[35] D. Grainger, M.B. Hagg, The recovery by carbon molecular sieve membranes of hydrogen transmitted in natural gas networks, Int. J. Hydrogen Energy 33 (2008) 2379-2388.

[36] C.H. Jung, G.W. Kim, S.H. Han, Y.M. Lee, Gas separation of pyrolyzed polymeric membranes: Effect of polymer precursor and pyrolysis conditions, Macromolecular Research 15 (2007) 565-574.

[37] S. Lagorsse, F.D. Magalhães, A. Mendes, Carbon molecular sieve membranes - Sorption, kinetic and structural characterization, J. Membr. Sci. 241 (2004) 275-287.

[38] M. Inagaki, T. Ibuki, T. Takeichi, Carbonization Behavior of Polyimide Films with Various Chemical Structures, J. Appl. Polym. Sci. 44 (1992) 521-525.

[39] Y.D. Chen, R.T. Yang, Preparation of Carbon Molecular-Sieve Membrane and Diffusion of Binary-Mixtures in the Membrane, Ind. Eng. Chem. Res. 33 (1994) 3146-3153.

[40] C.W. Jones, W.J. Koros, Carbon Molecular-Sieve Gas Separation Membranes .1. Preparation and Characterization Based on Polyimide Precursors, Carbon 32 (1994) 1419-1425.

[41] V.M. Linkov, R.D. Sanderson, B.A. Rychkov, Composite Carbon-Polyimide Membranes, Mater. Lett. 20 (1994) 43-46.

[42] K. Haraya, H. Suda, H. Yanagishita, S. Matsuda, Asymmetric Capillary Membrane of a Carbon Molecular-Sieve, J Chem Soc Chem Comm (1995) 1781-1782.

[43] H. Suda, K. Haraya, Molecular-Sieving Effect of Carbonized Kapton Polyimide Membrane, J Chem Soc Chem Comm (1995) 1179-1180.

[44] V.C. Geiszler, W.J. Koros, Effects of polyimide pyrolysis conditions on carbon molecular sieve membrane properties, Ind. Eng. Chem. Res. 35 (1996) 2999-3003.

[45] J. Hayashi, H. Mizuta, M. Yamamoto, K. Kusakabe, S. Morooka, Pore size control of carbonized BPDA-pp'ODA polyimide membrane by chemical vapor deposition of carbon, J. Membr. Sci. 124 (1997) 243-251.

[46] Y. Kusuki, H. Shimazaki, N. Tanihara, S. Nakanishi, T. Yoshinaga, Gas permeation properties and characterization of asymmetric carbon membranes prepared by pyrolyzing asymmetric polyimide hollow fiber membrane, J. Membr. Sci. 134 (1997) 245-253.

[47] J. Petersen, M. Matsuda, K. Haraya, Capillary carbon molecular sieve membranes derived from Kapton for high temperature gas separation, J. Membr. Sci. 131 (1997) 85-94.

[48] H. Suda, K. Haraya, Gas permeation through micropores of carbon molecular sieve membranes derived from Kapton polyimide, J. Phys. Chem. B 101 (1997) 3988-3994.

[49] M. Yamamoto, K. Kusakabe, J. Hayashi, S. Morooka, Carbon molecular sieve membrane formed by oxidative carbonization of a copolyimide film coated on a porous support tube, J. Membr. Sci. 133 (1997) 195-205.

[50] A.B. Fuertes, D.M. Nevskaia, T.A. Centeno, Carbon composite membranes from Matrimid (R) and Kapton (R) polyimides for gas separation, Microporous Mesoporous Mater. 33 (1999) 115-125.

[51] N. Tanihara, H. Shimazaki, Y. Hirayama, S. Nakanishi, T. Yoshinaga, Y. Kusuki, Gas permeation properties of asymmetric carbon hollow fiber membranes prepared from asymmetric polyimide hollow fiber, J. Membr. Sci. 160 (1999) 179-186.

[52] J.N. Barsema, N.F.A. van der Vegt, G.H. Koops, M. Wessling, Carbon molecular sieve membranes prepared from porous fiber precursor, J. Membr. Sci. 205 (2002) 239-246.

[53] D.Q. Vu, W.J. Koros, S.J. Miller, High pressure CO2/CH4 separation using carbon molecular sieve hollow fiber membranes, Ind. Eng. Chem. Res. 41 (2002) 367-380.

[54] J.N. Barsema, G.C. Kapantaidakis, N.F.A. van der Vegt, G.H. Koops, M. Wessling, Preparation and characterization of highly selective dense and hollow fiber asymmetric membranes based on BTDA-TDI/MDI co-polyimide, J. Membr. Sci. 216 (2003) 195-205.

[55]   J.N. Barsema, S.D. Klijnstra, J.H. Balster, N.F.A. van der Vegt, G.H. Koops, M. Wessling, Intermediate polymer to carbon gas separation membranes based on Matrimid PI, J. Membr. Sci. 238 (2004) 93-102.

[56]   Y.K. Kim, J.M. Lee, H.B. Park, Y.M. Lee, The gas separation properties of carbon molecular sieve membranes derived from polyimides having carboxylic acid groups, J. Membr. Sci. 235 (2004) 139-146.

[57]   H.B. Park, Y.K. Kim, J.M. Lee, S.Y. Lee, Y.M. Lee, Relationship between chemical structure of aromatic polyimides and gas permeation properties of their carbon molecular sieve membranes, J. Membr. Sci. 229 (2004) 117-127.

[58]   S.T. Pei, T.S. Chung, S. Kawi, M.D. Guiver, Novel approaches to fabricate carbon molecular sieve membranes based on chemical modified and solvent treated polyimides, Microporous Mesoporous Mater. 73 (2004) 151-160.

[59]   L. Shao, T.S. Chung, G. Wensley, S.H. Goh, K.P. Pramoda, Casting solvent effects on morphologies, gas transport properties of a novel 6FDA/PMDA-TMMDA copolyimide membrane and its derived carbon membranes, J. Membr. Sci. 244 (2004) 77-87.

[60]   M.N. Islam, W.L. Zhou, T. Honda, K. Tanaka, H. Kita, K. Okamoto, Preparation and gas separation performance of flexible pyrolytic membranes by low-temperature pyrolysis of sulfonated polyimides, J. Membr. Sci. 261 (2005) 17-26.

[61]   Y.K. Kim, H.B. Park, Y.M. Lee, Preparation and characterization of carbon molecular sieve membranes derived from BTDA-ODA polyimide and their gas separation properties, J. Membr. Sci. 255 (2005) 265-273.

[62]   Y.C. Xiao, Y. Dai, T.S. Chung, M.D. Guiver, Effects of brominating matrimid polyimide on the physical and gas transport properties of derived carbon membranes, Macromolecules 38 (2005) 10042-10049.

[63]   P.S. Tin, Y.C. Xiao, T.S. Chung, Polyimide-carbonized membranes for gas separation: Structural, composition, and morphological control of precursors, Separation and Purification Reviews 35 (2006) 285-318.

[64]   K. Wang, L.S. Loo, K. Haraya, CO2 permeation in carbon membranes with different degrees of carbonization, Ind. Eng. Chem. Res. 46 (2007) 1402-1407.

[65]   C.J. Anderson, S.J. Pas, G. Arora, S.E. Kentish, A.J. Hill, S.I. Sandler, G.W. Stevens, Effect of pyrolysis temperature and operating temperature on the performance of nanoporous carbon membranes, J. Membr. Sci. 322 (2008) 19-27.

[66]   E.P. Favvas, E.P. Kouvelos, G.E. Romanos, G.I. Pilatos, A.C. Mitropoulos, N.K. Kanellopoulos, Characterization of highly selective microporous carbon hollow fiber membranes prepared from a commercial co-polyimide precursor, J. Porous Mater. 15 (2008) 625-633.

[67]   A.C. Lua, J.C. Su, Structural Changes and Development of Transport Properties During the Conversion of a Polyimide Membrane to a Carbon Membrane, J. Appl. Polym. Sci. 113 (2009) 235-242.

[68]   Y.C. Xiao, T.S. Chung, M.L. Chng, S. Tarnai, A. Yamaguchi, Structure and properties relationships for aromatic polyimides and their derived carbon membranes: Experimental and simulation approaches, J. Phys. Chem. B 109 (2005) 18741-18748.

[69]   H. Kita, H. Maeda, K. Tanaka, K. Okamoto, Carbon molecular sieve membrane prepared from phenolic resin, Chem. Lett. (1997) 179-180.

[70]   W.L. Zhou, M. Yoshino, H. Kita, K. Okamoto, Preparation and gas permeation properties of carbon molecular sieve membranes based on sulfonated phenolic resin, J. Membr. Sci. 217 (2003) 55-67.

[71]   X.Y. Zhang, H.Q. Hu, Y.D. Zhu, S.W. Zhu, Effect of carbon molecular sieve on phenol formaldehyde novolac resin based carbon membranes, Sep. Purif. Technol. 52 (2006) 261-265.

[72]   X.Y. Zhang, H.Q. Hu, Y.D. Zhu, S.W. Zhu, Carbon molecular sieve membranes derived from phenol formaldehyde novolac resin blended with poly(ethylene glycol), J. Membr. Sci. 289 (2007) 86-91.

[73]   S.S. Wang, M.Y. Zeng, Z.Z. Wang, Carbon membranes for gas separation, Sep. Sci. Technol. 31 (1996) 2299-2306.

[74]   S.S. Wang, M.Y. Zeng, Z.H. Wang, Asymmetric molecular sieve carbon membranes, J. Membr. Sci. 109 (1996) 267-270.

[75]   T. Steriotis, K. Beltsios, A.C. Mitropoulos, N. Kanellopoulos, S. Tennison, A. Wiedenman, U. Keiderling, On the structure of an asymmetric carbon membrane with a novolac resin precursor, J. Appl. Polym. Sci. 64 (1997) 2323-2345.

[76]   T.A. Centeno, A.B. Fuertes, Supported carbon molecular sieve membranes based on a phenolic resin, J. Membr. Sci. 160 (1999) 201-211.

[77]   T.A. Centeno, A.B. Fuertes, Carbon molecular sieve membranes derived from a phenolic resin supported on porous ceramic tubes, Sep. Purif. Technol. 25 (2001) 379-384.

[78]   A.B. Fuertes, Preparation and characterization of adsorption-selective carbon membranes for gas separation, Adsorption 7 (2001) 117-129.

[79]   A.B. Fuertes, Effect of air oxidation on gas separation properties of adsorption-selective carbon membranes, Carbon 39 (2001) 697-706.

[80]   W.L. Zhou, M. Yoshino, H. Kita, K. Okamoto, Carbon molecular sieve membranes derived from phenolic resin with a pendant sulfonic acid group, Ind. Eng. Chem. Res. 40 (2001) 4801-4807.

[81]   A.B. Fuertes, I. Menendez, Separation of hydrocarbon gas mixtures using phenolic resin-based carbon membranes, Sep. Purif. Technol. 28 (2002) 29-41.

[82]   T.A. Centeno, A.B. Fuertes, Influence of separation temperature on the performance of adsorption-selective carbon membranes, Carbon 41 (2003) 2016-2019.

[83]   T.A. Centeno, J.L. Vilas, A.B. Fuertes, Effects of phenolic resin pyrolysis conditions on carbon membrane performance for gas separation, J. Membr. Sci. 228 (2004) 45-54.

[84]   F.K. Katsaros, T.A. Steriotis, G.E. Romanos, M. Konstantakou, A.K. Stubos, N.K. Kanellopoulos, Preparation and characterisation of gas selective microporous carbon membranes, Microporous Mesoporous Mater. 99 (2007) 181-189.

[85]   W. Wei, G.T. Qin, H.Q. Hu, L.B. You, G.H. Chen, Preparation of supported carbon molecular sieve membrane from novolac phenol-formaldehyde resin, J. Membr. Sci. 303 (2007) 80-85.

[86]   M. Acharya, H.C. Foley, Spray-coating of nanoporous carbon membranes for air separation, J. Membr. Sci. 161 (1999) 1-5.

[87]   M.B. Shiflett, H.C. Foley, Ultrasonic deposition of high-selectivity nanoporous carbon membranes, Science 285 (1999) 1902-1905.

[88]   M. Acharya, H.C. Foley, Transport in nanoporous carbon membranes: Experiments and analysis, AIChE J. 46 (2000) 911-922.

[89]   M.B. Shiflett, H.C. Foley, On the preparation of supported nanoporous carbon membranes, J. Membr. Sci. 179 (2000) 275-282.

[90]   M.B. Shiflett, J.F. Pedrick, S.R. McLean, S. Subramoney, H.C. Foley, Characterization of supported nanoporous carbon membranes, Adv. Mater. 12 (2000) 21-25.

[91]   H.T. Wang, L.X. Zhang, G.R. Gavalas, Preparation of supported carbon membranes from furfuryl alcohol by vapor deposition polymerization, J. Membr. Sci. 177 (2000) 25-31.

[92]   A. Merritt, R. Rajagopalan, H.C. Foley, High performance nanoporous carbon membranes for air separation, Carbon 45 (2007) 1267-1278.

[93]   Y.R. Dong, N. Nishiyama, Y. Egashira, K. Ueyama, H2-selective carbon membranes prepared from furfuryl alcohol by vapor-phase synthesis, Ind. Eng. Chem. Res. 46 (2007) 4040-4044.

[94]   E. Barbosa-Coutinho, V.M.M. Salim, C.P. Borges, Preparation of carbon hollow fiber membranes by pyrolysis of polyetherimide, Carbon 41 (2003) 1707-1714.

[95]   M.G. Sedigh, M. Jahangiri, P.K.T. Liu, M. Sahimi, T.T. Tsotsis, Structural characterization of polyetherimide-based carbon molecular sieve membranes, AIChE J. 46 (2000) 2245-2255.

[96]   M.G. Sedigh, P.K.T. Liu, R.J. Ciora, T.T. Tsotsis, M. Sahimi, Polyetherimide-based carbon molecular sieve membranes: Transport investigations and morphological characterization, Adv. Filtr. Sep. Technol. 13 (1999) 974-980.

[97]   M.G. Sedigh, L.F. Xu, T.T. Tsotsis, M. Sahimi, Transport and morphological characteristics of polyetherimide-based carbon molecular sieve membranes, Ind. Eng. Chem. Res. 38 (1999) 3367-3380.

[98]   H. Kumazawa, J.S. Wang, T. Fukuda, E. Sada, Permeation of Carbon-Dioxide in Glassy Poly(Ether Imide) and Poly(Ether Ether Ketone) Membranes, J. Membr. Sci. 93 (1994) 53-59.

[99]   A.B. Fuertes, T.A. Centeno, Carbon molecular sieve membranes from polyetherimide, Microporous Mesoporous Mater. 26 (1998) 23-26.

[100]   T.H. Wang, L.H. Hu, Q.L. Liu, S.L. Liu, Z. Wang, M.X. Ding, Effects of precursor preoxidization on the structure and gas separation properties of polyetherimide derived carbon membranes, New Carbon Materials 23 (2008) 264-268.

[101]   M.B. Rao, S. Sircar, Performance and pore characterization of nanoporous carbon membranes for gas separation, J. Membr. Sci. 110 (1996) 109-118.

[102]   S. Sircar, M.B. Rao, C.M.A. Thaeron, Selective surface flow membrane for gas separation, Sep. Sci. Technol. 34 (1999) 2081-2093.

[103]   T.A. Centeno, A.B. Fuertes, Carbon molecular sieve gas separation membranes based on poly(vinylidene chloride-co-vinyl chloride), Carbon 38 (2000) 1067-1073.

[104]   H.J. Lee, M. Yoshimune, H. Suda, K. Haraya, Gas permeation properties of poly (2,6-dimethyl-1,4-phenylene oxide) (PPO) derived carbon membranes prepared on a tubular ceramic support, J. Membr. Sci. 279 (2006) 372-379.

[105]   H.J. Lee, D.P. Kim, H. Suda, K. Haraya, Gas permeation properties for the post-oxidized polyphenylene oxide (PPO) derived carbon membranes: Effect of the oxidation temperature, J. Membr. Sci. 282 (2006) 82-88.

[106]   M. Yoshimune, I. Fujiwara, H. Suda, K. Haraya, Novel carbon molecular sieve membranes derived from poly(phenylene oxide) and its derivatives for gas separation, Chem. Lett. 34 (2005) 958-959.

[107]   H.J. Lee, H. Suda, K. Haraya, Characterization of the post-oxidized carbon membranes derived from poly(2,4-dimethyl-1,4-phenylene oxide) and their gas permeation properties, Sep. Purif. Technol. 59 (2008) 190-196.

[108]   H.J. Lee, H. Suda, K. Haraya, D.P. Kim, Influence of oxidation temperature on the gas permeation and separation properties in a microporous carbon membrane, Korean J. Chem. Eng. 23 (2006) 435-440.

[109]   M. Yoshimune, I. Fujiwara, K. Haraya, Carbon molecular sieve membranes derived from trimethylsilyl substituted poly(phenylene oxide) for gas separation, Carbon 45 (2007) 553-560.

[110] K. Kusakabe, S. Gohgi, S. Morooka, Carbon molecular sieving membranes derived from condensed polynuclear aromatic (COPNA) resins for gas separations, Ind. Eng. Chem. Res. 37 (1998) 4262-4266.

[111] T. Koga, H. Kita, K. Tanaka, M. Funaoka, Rapid pyrolysis of lignin-based materials for the synthesis of molecular sieve carbon membrane, Transactions of the Materials Research Society of Japan 31 (2006) 287-290.

[112] H. Kita, K. Nanbu, M. Yoshino, K. Okamoto, M. Funaoka, Preparation of carbon membranes from lignin-based materials and their permeation properties., Abstracts of Papers of the American Chemical Society 222 (2001) U368-U368.

[113] H. Kita, T. Hamano, M. Yoshino, K. Okamoto, M. Funaoka, Carbon membranes derived from lignin-based materials., Abstracts of Papers of the American Chemical Society 223 (2002) D94-D94.

[114] Q. Shen, L. Zhong, Lignin-based carbon films and controllable pore size and properties, Materials Science and Engineering a-Structural Materials Properties Microstructure and Processing 445 (2007) 731-735.

[115] M.S. Strano, H.C. Foley, Synthesis and characterization of heteropolyacid nanoporous carbon membranes, Catal. Lett. 74 (2001) 177-184.

[116] B. Zhang, T.H. Wang, S.H. Zhang, J.S. Qiu, X.G. Han, Preparation and characterization of carbon membranes made from poly(phthalazinone ether sulfone ketone), Carbon 44 (2006) 2764-2769.

[117] T.H. Wang, B. Zhang, J.S. Qiu, Y.H. Wu, S.H. Zhang, Y.M. Cao, Effects of sulfone/ketone in poly(phthalazinone ether sulfone ketone) on the gas permeation of their derived carbon membranes, J. Membr. Sci. 330 (2009) 319-325.

[118] S. Lagorsse, M.C. Campo, F.D. Magalhães, A. Mendes, Water adsorption on carbon molecular sieve membranes: Experimental data and isotherm model, Carbon 43 (2005) 2769-2779.

[119] L.A.G. Aylmore, R.M. Barrer, Surface and Volume Flow of Single Gases and of Binary Gas Mixtures in a Microporous Carbon Membrane, Proc R Soc Lon Ser-A 290 (1966) 477-489.

[120] A.J. Bird, D.L. Trimm, Carbon Molecular-Sieves Used in Gas Separation Membranes, Carbon 21 (1983) 177-180.

[121] J.E. Koresh, A. Soffer, Molecular-Sieve Carbon Permselective Membrane .1. Presentation of a New Device for Gas-Mixture Separation, Sep. Sci. Technol. 18 (1983) 723-734.

[122] J. Koresh, A. Soffer, Molecular-Sieve Carbons .3. Adsorption-Kinetics According to a Surface-Barrier Model, J Chem Soc Farad T 1 77 (1981) 3005-3018.

[123] A. Sofer, J. Koresh, S. Saggy, Separation device, US004685940, 1987.

[124] A. Soffer., J. Gilron., S. Saguee., R. Hed-Ofek., H. Cohen., Process for the production of hollow carbon fiber membranes, US005925591 1999.

[125] A. Soffer, M. Azariah, A. Amar, H. Cohen, D. Golub, S. Saguee, H. Tobias, Method for improving the selectivity of carbon membranes by carbon chemical vapor deposition, US005695818, 1997.

[126] J. Koresh, A. Soffer, A Molecular-Sieve Carbon Membrane for Continuous Process Gas Separation, Carbon 22 (1984) 225-225.

[127] M.B. Rao, S. Sircar, Nanoporous Carbon Membranes for Separation of Gas-Mixtures by Selective Surface Flow, J. Membr. Sci. 85 (1993) 253-264.

[128] S. Sircar, M.B. Rao, Nanoporous Carbon Membranes for Separation of Gas-Mixtures, Abstracts of Papers of the American Chemical Society 207 (1994) 81-IEC.

[129] C.W. Jones, W.J. Koros, Carbon Molecular-Sieve Gas Separation Membranes. 2. Regeneration Following Organic-Exposure, Carbon 32 (1994) 1427-1432.

[130] C.W. Jones, W.J. Koros, Characterization of Ultramicroporous Carbon Membranes with Humidified Feeds, Ind. Eng. Chem. Res. 34 (1995) 158-163.

[131] C.W. Jones, W.J. Koros, Carbon Composite Membranes - a Solution to Adverse Humidity Effects, Ind. Eng. Chem. Res. 34 (1995) 164-167.

[132] I. Menendez, A.B. Fuertes, Aging of carbon membranes under different environments, Carbon 39 (2001) 733-740.

[133] S. Lagorsse, F.D. Magalhães, A. Mendes, Aging study of carbon molecular sieve membranes, J. Membr. Sci. 310 (2008) 494-502.

[134] A.B. Fuertes, T.A. Centeno, Preparation of supported asymmetric carbon molecular sieve membranes, J. Membr. Sci. 144 (1998) 105-111.

[135] A.F. Ismail, L.I.B. David, Future direction of R&D in carbon membranes for gas separation, Membrane Technology (2003) 4-8.

[136] J.N. Barsema, N.F.A. van der Vegt, G.H. Koops, M. Wessling, Ag-functionalized carbon molecular-sieve membranes based on polyelectrolyte/polyimide blend precursors, Adv. Funct. Mater. 15 (2005) 69-75.

[137] H. Suda, S. Yoda, A. Hasegawa, T. Tsuji, K. Otake, K. Haraya, Gas permeation properties of carbon molecular sieve membranes dispersed with palladium nano particles via supercritical CO_2 impregnation, Desalination 193 (2006) 211-214.

[138] S.S. Hosseini, T.S. Chung, Carbon membranes from blends of PBI and polyimides for N_2/CH_4 and CO_2/CH_4 separation and hydrogen purification, J. Membr. Sci. 328 (2009) 174-185.

Chapter II

Chapter 2 - Comparative study between a CMS Membrane and a CMS Adsorbent

2.1. Morphology, adsorption equilibrium and kinetics[1]

2.1.1. Abstract

This section presents a comparative study between a carbon molecular sieve (CMS) membrane and a commercial CMS adsorbent; these materials are suited for selective gas permeation and adsorption-based gas separations, respectively. The purpose of this analysis is to better understand the mass transport mechanism in CMS membranes and how it is related to the material's structure. The structural characterization based on the adsorption of CO_2 at 0 °C revealed that the adsorbent has a greater micropore volume, a smaller mean pore width and a micropore size distribution shifted to the left, when compared to the membrane. This translates into a lower adsorption capacity of the membrane towards N_2, Ar, CO_2 and O_2 at 29.5 °C and 0-7 bar. The adsorption kinetics were also studied and the pressure-dependence of the apparent time constants established; different models were used to predict the experimental results, emphasizing the very important role of the ultramicroporosity on the properties of the materials. The CMS membrane exhibited a pore blockage effect when permeating O_2 and CO_2. Further morphologic characterization was performed by SEM, X-ray diffraction and mercury porosimetry.

---

[1] M.C. Campo, F.D. Magalhães, A. Mendes, Comparative study between a CMS Membrane and a CMS Adsorbent: Part I – Morphology, adsorption equilibrium and kinetics, J. Membr. Sci. 346 (2010) 15-25.

2.1.2. Introduction

Gas separation plays a very important role on several industrial applications. One of the most important is the separation of nitrogen from air. Nitrogen is used in several applications concerning blanketing, food and pharmaceutical industry, purging and is also used for metal treating and others. The production of nitrogen from air started at the beginning of the XXth century, by cryogenic processes [1]. This is a very efficient large scale technology but also relatively costly for small to median scale production [2]. By the middle of the XXth century, special attention started being given to adsorption processes: pressure swing adsorption (PSA) systems were invented and the industry opened its mind to the development of new materials to be used as adsorbents in such units. Zeolites were the first adsorbents that allowed operating at ambient temperature regarding the separation of nitrogen from air [2]. Some years later, 1972-1973, Bergbau-Forschung achieved the industrial production of carbon molecular sieve adsorbents. The porous structure of these carbonaceous materials is in the size range of atoms/molecules, exhibiting a narrow pore size distribution that allows for kinetic and steric separations [3]. CMS are used for the specific kinetic separation of nitrogen from air by a PSA system.

Another emergent process for gas separation is membrane technology. The main benefit of this technology is its simplicity and easy scale-up; it can be also easily combined with other processes such as PSA (PSA-M) [4, 5]. In 1980 membrane-based processes for gas separation found industrial large scale application by Permea (USA), for hydrogen separation [6]. The success of this company quickly led to the development of more membrane-based applications such as the recovery of nitrogen from air by Generon (USA). Up to this date, only organic membranes were used. However, the need for high permeation rates, combined with high selectivies and good thermal and chemical stability, directed researchers towards the development of inorganic membranes. By the beginning of the 80's, Koresh and Soffer have developed the first crack free carbon molecular sieve membranes [7-9]. During the following years, several patents were filled by these and other authors and by the end of 1990's the company Carbon Membranes was created in Israel [8-10]. This company

developed modules of hollow fiber carbon molecular sieve membranes for producing nitrogen from air. As in the carbon molecular sieve adsorbents used in PSA technology, these membranes also present a pore network with a narrow pore size distribution capable of separating species based on their differences in size. Unfortunately, the company bankrupted by the end of 2001. A major problem with the existing technology was related to loss of performance after a short period of time, due to oxygen exposure [11-13]. This aging effect is commonly recognized in CMS membrane materials. On the other hand, it is not observed in CMS adsorbents, which can be exposed to oxygen for long time periods, without any loss of performance.

Carbon molecular sieve adsorbents and carbon molecular sieve membranes might have similar structural characteristics, but are essentially different in shape. The adsorbents are usually granular or pelletized, with sizes in the order of 1-6 mm, while unsupported membranes, in flat sheet or hollow fiber form, preferentially have a thin selective layer in the range of 1-50 μm. As both materials are essentially made of a carbon skeleton, the preparation techniques are conditioned by the flexibility of the final material; this is not so relevant for carbon molecular sieve adsorbents, which are granular, but is a very important issue for carbon membranes, which are known for their brittleness.

The present work provides a comparison between structural properties of a carbon molecular sieve adsorbent and a carbon molecular sieve membrane, in order to assess their influence on the performance of each material. Several characterization techniques were employed, such as, scanning electron microscopy (SEM), X-ray diffraction (XRD). Mercury porosimetry was also used, to assess macroporosity, and carbon dioxide adsorption at $0\,^{\circ}C$, to determine ultramicroporosity. Adsorption measurements were conducted for several species, allowing for the determination of equilibrium isotherms and kinetic parameters.

Carbon molecular sieves for nitrogen separation from air may be prepared from coconut shell, coal tar, coal tar pitch, granulated carbon impregnated with phenolic or furan resins, among others. These are heat treated at 600-900 $^{\circ}C$ under inert atmospheres or carbon-sourced streams, or previously impregnated with gaseous or

even liquid hydrocarbons. These carbon depositions may occur in single or multiple steps [14-22]. The precise manufacturer procedure for the carbon molecular sieve adsorbent characterized in this chapter is unknown.

The carbon molecular sieve membranes studied were manufactured by Carbon Membranes, and are derived from cellulosic hollow fibers. According to the relevant patents and the information given by the producers, the carbon membranes were prepared according to the combination of several treatments: a) water removal from the precursor fibers by heating under vacuum or inert atmosphere; b) pyrolysis of the fibers within the range 500-800 °C by adding a catalyst, namely HCl diluted at 0-12 % in a nitrogen inert atmosphere; c) carbon vapor deposition (CVD) for partial pore closure, and d) activation using an oxidant gaseous agent for pore opening (air). The appropriate combination of CVD and activation allows for tuning the intended pore size within the range of 2.5-5.5 Å [8-10, 23].

2.1.3. Experimental

2.1.3.1. Materials

The hollow fiber carbon molecular sieve membranes, designated here as HF CM, were provided by the Israeli Company Carbon Membranes Ltd. The selected commercial carbon molecular sieve adsorbent is MSC3K-162, supplied by Takeda. This adsorbent is recommended for nitrogen production from air by PSA.

2.1.3.2. Morphological and structural analyses

Micrographs have been obtained by high vacuum SEM/EDS in a FEI Quanta 400FEG/EDAX Genesis X4M with a 1.2 nm resolution.

The X-ray diffraction analyses were performed in a Philips X'Pert MPD diffractometer with a CuKα radiation of 1.54056 Å wavelength (40 kV; 50 mA). The samples were milled prior to the analysis.

2.1.3.3. Pore size distribution

A Quantachrome mercury porosimeter, model POREMASTER 60, was used. This equipment allows determining the pore size distribution from 3.5 nm up to 200 μm.

The characterization of microporous material is essentially performed by physical adsorption of gases. The adsorption of N_2 at 77 K is the most used technique in the determination of microporosity. However, diffusional limitations occur when ultramicroporosity is involved (pores < 0.7 nm). For this reason, adsorption of CO_2 at 0 °C is a good alternative. At this higher temperature access to the smaller pores is facilitated [24]. The adsorption equilibrium isotherm of CO_2 was obtained by the gravimetric method in the suspension magnetic balance described below. From the adsorption isotherm it is possible to compute the surface area of micropores, micropore volume, mean pore width and pore size distribution [25].

2.1.3.4. Adsorption

The sorption studies on the CMS membrane and adsorbent were conducted using the gravimetric method, implemented in a magnetic suspension balance from Rubotherm® (metal version and 10^{-5} g precision). This system, illustrated in Figure 2.1, consists on the magnetic suspension balance, pressure sensors (Drück, range 0-7 bar and 0-350 mbar, 0.1 % FS), a vacuum pump (Edwards, model RV5) and a thermostatic bath (Huber, model CC1) for circulating water in the jacket of the system when operating at 29.5 °C and a commercial refrigeration liquid for CO_2 adsorption at 0 °C. The feeding system for permanent gases is made of a 5 L buffer tank, to minimize pressure variations during uptakes.

Adsorption equilibrium isotherms and uptakes for N_2, Ar, O_2 and CO_2 were determined at 29.5 °C. The increments in pressure taken for the uptake curves were small enough to ensure constant diffusivities within the transient range and to minimize thermal effects. For structural characterization, the adsorption equilibrium isotherm for CO_2 was obtained at 0 °C.
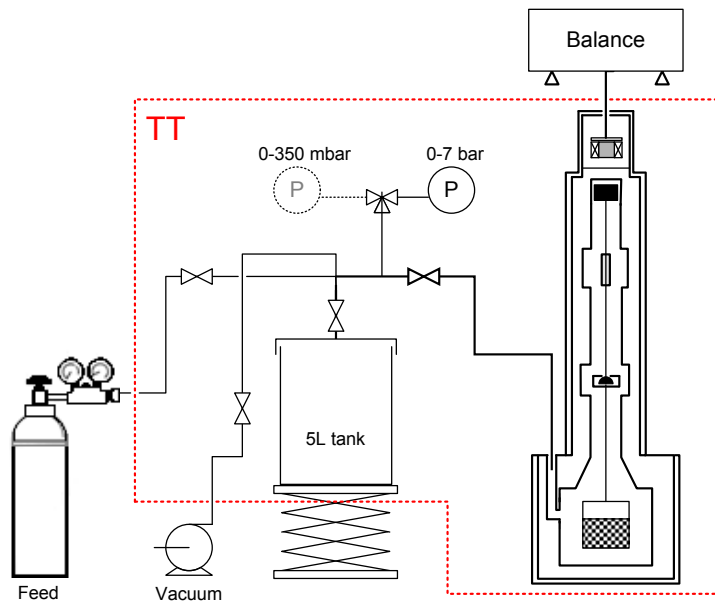
Figure 2.1 – Schematic representation of the gravimetric apparatus (adapted from [26]).

2.1.4. Results and discussion

2.1.4.1. SEM

MSC3K-162 and HF CM have been characterized by SEM in order to assess the surface and cross sectional topographies. For HF CM, the outer and inner (bore side) surfaces were analyzed.

Figure 2.2 presents several micrographs illustrating these views.

a$_1$) magnification x90	a$_2$) magnification x90	a$_3$) magnification x20 000
b$_1$) magnification x200	b$_2$) magnification x1000	b$_3$) magnification x20 000
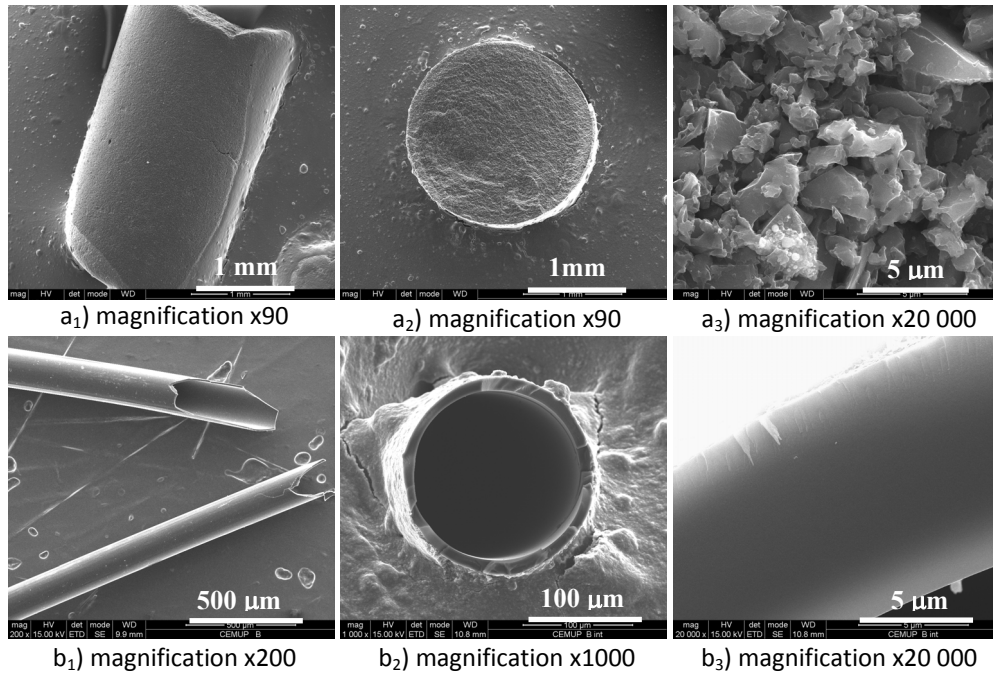
Figure 2.2 – SEM micrographs of MSC3K-162 from a$_1$ to a$_3$ and of HF CM from b$_1$ to b$_3$.

Sample MSC3K-162 exhibits similar textures from both in and outside surfaces. Micrograph a$_3$ confirms the existence of a macroporous structure in this material. Regarding sample HF CM it has apparently a very homogenous surface. Micrograph b$_3$ enhances the fact that a very dense carbon layer is present and macroporosity may not exist. SEM also allowed to obtain the diameter, d_e, of MSC3K-162 and the external diameter, d_e, of HF CM and membrane thickness, ℓ, shown in Table 2.1.

Table 2.1 – Characteristic dimensions.

	MSC3K-162	**HF CM**
d_e (μm)	1.85 x 10^3	157-181
ℓ (μm)	-	8.8-10.4

2.1.4.2. X-ray diffraction

X-ray diffraction allowed for a qualitative comparison between the structures of MSC3K 162 and HF CM and relating these to graphite. The distances between adjacent graphene layers were determined by employing Bragg's law and the results compared with the known values for graphite. Figure 2.3 presents the X-ray diffraction spectra.
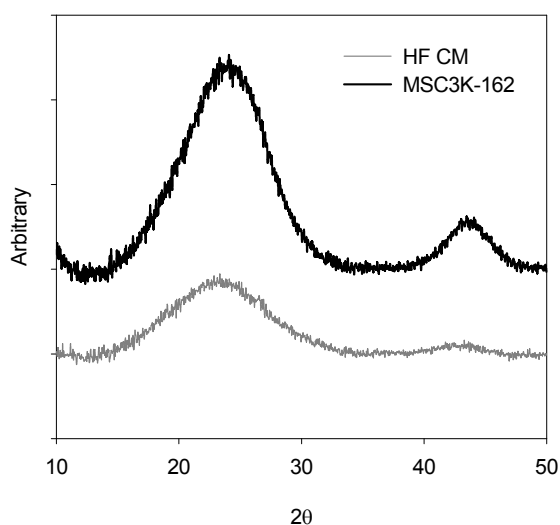
Figure 2.3 – X-ray diffraction patterns for HF CM and MSC3K-162.

The wide peaks are representative of the degree of amorphousness; this was expected for ungraphitizable porous carbons [27]. It is noted that MSC3K-162 presents more intense peaks, suggesting a more ordered structure than HF CM. Table 2.2 presents the angles of radiation for which the peaks occur, identifying the respective planes of diffraction, and the distance between lattices. As reference, corresponding values for graphite are also given. The results show that MSC3K-162 exhibits a behavior closer to graphite than HF CM. Concerning the plane 002, the diffraction peak appears for MSC3K-162 at 24.1° and for HF CM at 23.3°, corresponding, respectively, to an interlayer spacing of 0.369 and 0.381 nm. The same diffraction peak for graphite appears at 26.6°, corresponding to the known distance of 0.335 nm [28].

Table 2.2 – X-ray diffraction results obtained for MSC3K-162 and HF CM, and values for graphite.

	MSC3K-162		HF CM		Graphite [a]	
$h\ k\ l$	002	101	002	101	002	101
2θ	24.0709	43.4827	23.3489	43.2821	26.6106	43.4533
d (nm)	0.3694	0.2079	0.3807	0.2089	0.3347	0.2081

a) Data base of Philips X'Pert software

2.1.4.3. Mercury porosimetry

This technique of mercury intrusion allows for a macroscopic comprehension on the structure of the materials. Differences at this level may also help understand global differences between the carbon molecular sieve membrane and adsorbent.

Figure 2.4 shows the pore size distribution for MSC3K-162 in pellets and milled, respectively with a particle size of 1.8-2 mm and 0.5-0.74 mm. From Figure 2.4 it is seen that the macroporosity was not significantly affected by milling, even though a decrease on the total macropore volume is observed.
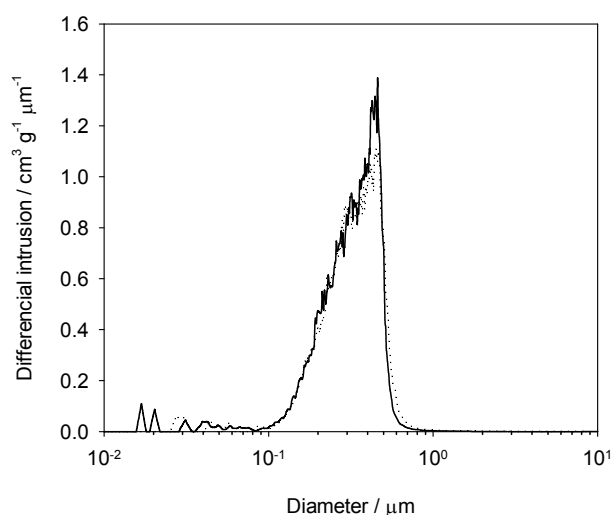
Figure 2.4 – Meso/macroporosity obtained from mercury porosimetry. The solid line represents the commercial adsorbent MSC3K-162 and the dashed line represents the same milled adsorbent.

In Figure 2.5 pore size distributions of MSC3K-162 and HF CM are compared. The average macropore size is 3.2×10^{-1} and 1.8×10^{-2} µm, respectively.
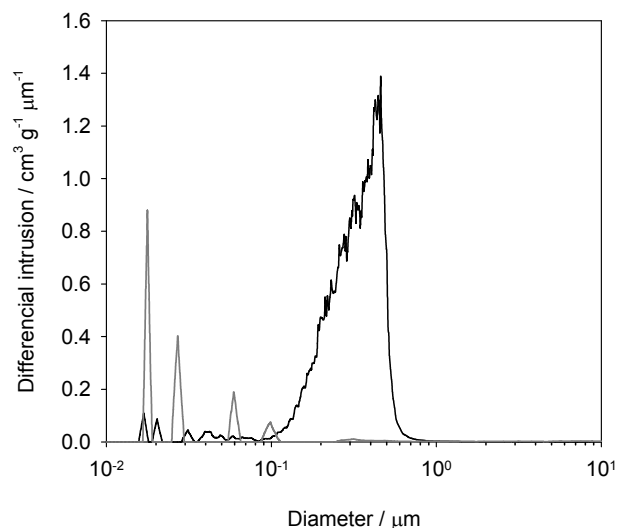
Figure 2.5 – Comparison of meso/macroporosity obtained from mercury porosimetry between the adsorbent MSC3K-162 (black line) and the HF CM (grey line).

Table 2.3 summarizes the physical properties obtained by mercury porosimetry and the skeleton density, ρ_{He} which was obtained by helium picnometry using the gravimetric method. It can be concluded that milling the adsorbent to half its size did not affect the physical properties of the material. This is in agreement with the pomegranate morphology observed for the CMS adsorbent, as seen in Figure 2.2.

From Figure 2.5 and Table 2.3 it can be seen that MSC3K-162 has higher macroporosity than HF CM. The total porosity for MSC3K-162 is 0.46. However, only the fraction of very small pores is relevant for molecular sieving. Therefore, $f_{<3.5\,nm}$, which is the fraction of overall porosity corresponding to pores smaller than 3.5 nm, is a good indicator of the kinetic separation characteristics of the CMS materials. The carbon membrane presents about 67 % of pores in this range, while adsorbent MSC3K-162 shows just 30 %. However, MSC3K-162 is still presenting the highest volume of pores with dimensions smaller than 3.5 nm ($\varepsilon_{<3.5\,nm}$ = 0.14) when compared to the membrane HF CM ($\varepsilon_{<3.5\,nm}$ = 0.11).

Table 2.3 – Physical properties of the samples.

	MSC3K-162	MSC3K-162 milled	HF CM
ρ_{He}^{*} / g cm^{-3}	1.98	1.98	2.07
ρ_{app} / g cm^{-3}	1.0702	1.0559	1.7423
ρ_{Hg} / g cm^{-3}	1.5747	1.5742	1.8383
ε_{total}	0.46	0.47	0.16
$\varepsilon_{<3.5\,nm}$	0.14	0.14	0.11
τ	1.8680	1.8579	2.1382
$f_{<3.5\,nm}$	0.30	0.29	0.67

2.1.4.4. CO_2 adsorption at 0 ^{o}C

Structural characterization

The adsorption equilibrium isotherms of CO_2 at 0 °C (see Figure 2.6) exhibit type I behavior in both MSC3K-162 and HF CM. As should be expected for carbon molecular sieves, the materials studied reach a plateau for the maximum adsorption capacity for relative pressures around 0.2, implying a significant volume fraction of micropores [29].
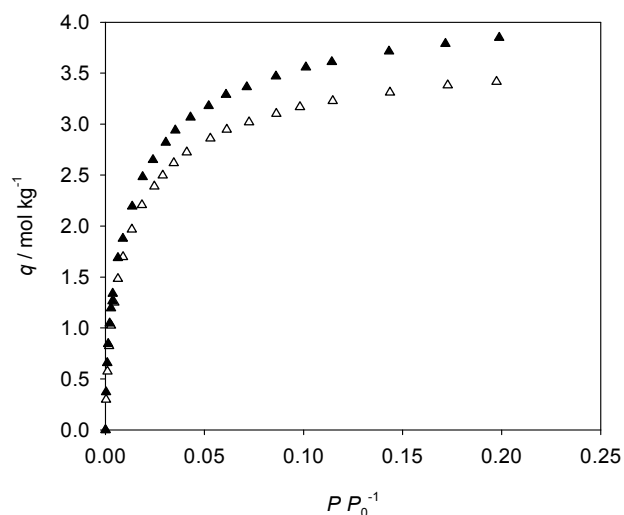
Figure 2.6 – Adsorption equilibrium isotherms for CO_2 at 0 °C: experimental data ▲ MSC3K-162 and △ HF CM.

Despite the existence of some mesoporosity, and even macroporosity, the adsorption capacity of a porous carbon material is mostly determined by its microporosity. For several years, the Dubinin-Radushkevich (DR) equation, based on the work previously carried by Polanyi, has been used for characterizing microporous materials. The inherent theory behind this equation is called the Theory for Volume Filling of Micropores (TVFM). Despite not following Henry law for very low pressures, DR equation, represented by eq. (2.1), is still commonly used mainly due to its simplicity and ability to provide relevant information on the pore network [30].

$$W = W_0 \; e^{-\left(A/\beta E_0\right)^2} \tag{2.1}$$

$W = q \cdot \upsilon_m$, is the volume filled at temperature, T, in this case 0 °C, at a certain relative pressure, P/P_0, that corresponds to a certain amount adsorbed, q. The molar volume, υ_m, used to translate the adsorbed amount of the probe CO_2 molecule into a corresponding volume in the adsorbed state, is 42.90 cm^3 mol^{-1} [31]. W_0 is the total micropore volume obtained by fitting the equation to experimental data, A is defined as $\Re T \ln\left(P_0/P\right)$, β is the affinity coefficient for carbon considered 0.35 and E_0 is the characteristic energy [24, 32]. For slit-like pores in carbons, the characteristic energy (E_0 between 40-42 kJ mol^{-1}) [24, 25] is related to the mean micropore width, L, through the relation of Stoeckli et al. [32] and consequently to the total surface area of micropores, S_{mic}, as follows [24, 33]:

$$L\left(\text{nm}\right) = \frac{10.8}{\left(E_0 - 11.4\right)} \tag{2.2}$$

$$S_{mic}\left(\text{m}^2\ \text{g}^{-1}\right) = \frac{2000\ W_0\left(\text{cm}^3\ \text{g}^{-1}\right)}{L\left(\text{nm}\right)} \tag{2.3}$$

The characteristic curves obtained for MSC3K-162 and HF CM are described by the DR approach, as presented in Figure 2.7. In both cases the fitting describes very well the experimental data.
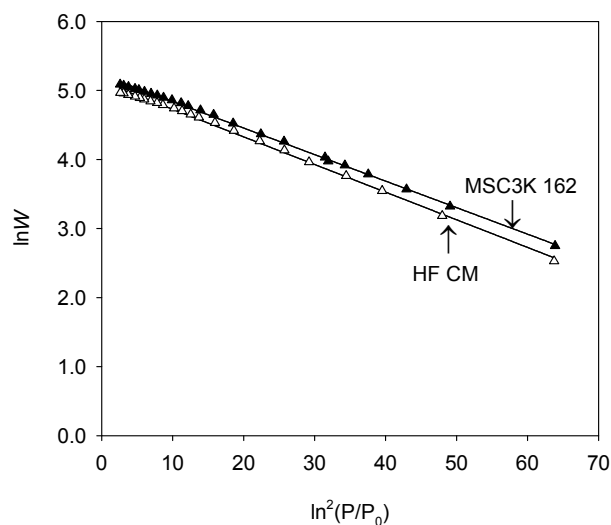
Figure 2.7 – Carbon dioxide characteristic curves at 0 °C for ▲ MSC3K-162 and △ HF CM. The solid lines represent DR fitting.

The structural parameters are listed in Table 2.4. Consistently with the conclusions taken from Hg porosimetry, MSC3K-162 has a higher micropore volume than the membrane HF CM. The characteristic energy is quite similar for both cases, indicating that the activated process of adsorption might happen with similar intensity. Thus, the resultant mean pore widths obtained from eq. (2.2) for MSC3K-162 and HF CM are also close, respectively, 0.498 and 0.514 nm. It is worth mentioning that these are just mean values. The pore size distribution provides more complete information about the differences between the two materials being studied.

Table 2.4 – Structural parameters for MSC3K-162 and HF CM.

	MSC3K-162	HF CM
W_0 (cm^3 kg^{-1})	185.7	168.7
E_0 (kJ mol^{-1})	33.1	32.4
L (nm)	0.498	0.514
S_{mic} (m^2 g^{-1})	746.1	656.9

2.1.4.5. Micropore size distribution

Carbon molecular sieves present a very complicated and heterogeneous microporous structure. Do et al. [34, 35] developed a structure-based method to account for the pore network heterogeneity by determining the micropore size distribution. Basically, the method consists in the use of the local Langmuir isotherm for all pores of size r while the heterogeneity of the system will be described by the distribution of micropores with different size, given by $f(r)$ [34]. The amount adsorbed is given by $q_{pore}(P,r)$, and q_{pore}^m is the maximum capacity for pores of size r.

$$q_{\text{pore}}(P,r) = q_{\text{pore}}^m(r) \frac{b_{\text{pore}}(r)P_{\text{pore}}(r)}{1+b_{\text{pore}}(r)P_{\text{pore}}(r)} \tag{2.4}$$

For each pore of size, r, the adsorption affinity constant, b_{pore}, is calculated as described in eq. (2.5), where, b_s, is the affinity factor related to adsorption on a flat surface.

$$b_{\text{pore}} = b_s \exp\left(\frac{E_{\text{pore}} - E_s}{\Re T}\right) \tag{2.5}$$

E_s is the potential energy when a molecule is adsorbed on a flat surface and E_{pore} is the potential energy when a molecule is adsorbed inside a pore. E_s and E_{pore} are calculated considering the heat of adsorption at zero loading, which corresponds to the minimum potential energy of adsorption. A slit like pore configuration is assumed here, as is often found for microporous carbonaceous materials [23, 35-37]. The potential energy of interaction between the graphite type walls and the probe gas molecule are described by the 10-4-3 potential of Steele [38, 39] shown in eq. (2.6) and corresponds to the symmetric of the heat of adsorption:

$$H(z) = 2\pi\rho_s\varepsilon_{sf}\sigma_{sf}^2\Delta\left[\frac{2}{5}\left(\frac{\sigma_{sf}}{z}\right)^{10} - \left(\frac{\sigma_{sf}}{z}\right)^4 - \frac{\sigma_{sf}^4}{3\Delta(0.61\Delta+z)^3}\right] \tag{2.6}$$

where z is the distance between the center of the probe molecule and the center of a carbon atom at the pore wall, Δ is the distance between graphene layers, ρ_s is the

density of carbon atoms in graphite, σ_{sf} and ε_{sf} are the solid-fluid interaction parameters estimated by the Lorentz-Berthelot mixture rules. The micropore potential energy is then calculated by the summation of contributions from both walls.

Furthermore, the local pore equilibrium isotherm also depends on the pressure and here this model distinguishes between the bulk, the gas confined in the pore and the adsorbed state. So, P_{pore}, which is the pressure of the gas confined in the pore is related to the bulk pressure, P_{bulk}, using an Arrhenius law dependency:

$$P_{\text{pore}} = P_{\text{bulk}} \exp\left(\frac{-E^g_{\text{pore}}}{\Re T}\right)$$
(2.7)

The E^g_{pore}, which is the mean potential energy of the gas state molecules confined in the pore, does not correspond to a minimum energy, but to a mean value, here approximated by the potential at the center of the pore, $z/2$.

The optimization is then performed using the experimental adsorption equilibrium isotherm for CO_2 at 0 °C. It has been used as a probe molecule due to its small size and ability to highly adsorb in porous carbons. The amount adsorbed at a given pressure, P, expressed as $q_{\text{exp}}(P)$, is the overall contribution of every single pore isotherm as stated in eq. (2.8):

$$q_{\text{exp}}(P) = \int_0^\infty q_{pore}(P,r) f(r)dr$$
(2.8)

Further details about this method are described elsewhere [34, 40]. The resulting pore size distributions for MSC3K-162 and HF CM were obtained and are presented in Figure 2.8.
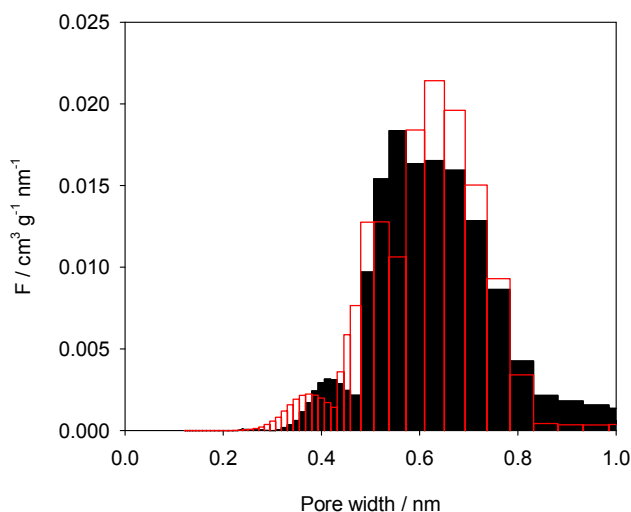
Figure 2.8 – Pore size distribution for MSC3K-162 (red line) and HF CM (black fill).

As reported in several works [23, 25, 29, 32, 41], subatmospheric CO_2 at 0 ºC is commonly used to assess very narrow microporosity (0.3-1 nm). Despite the existence of some larger pores, the resistance to mass transfer is caused by pores with sizes close to those of molecule dimensions. The experimental adsorption equilibrium isotherm for CO_2 at 0 ºC was determined in mol of adsorbed CO_2 per kg of adsorbent. To convert these units to volume of pores one used the molar volume already mentioned before. Once more, it is observed that the overall microporosity within the determined range is higher for MSC3K-162 than for the membranes HF CM, but both present pores in the range responsible for molecular sieving (0.3-0.6 nm). However, HF CM presents a micropore size distribution slightly shifted to the right, towards higher pore sizes when compared to MSC3K-162. Despite being small differences, they might be important and influence diffusion of molecules with closer sizes such as N_2, O_2, Ar and CO_2, cf. section 2.1.4.6.

Nevertheless, the micropore size distribution derived from adsorption equilibrium data may not be enough to explain the mass transport mechanism; the way pores are connected with each other should also play an important role [24, 35]. A carbon molecular sieve adsorbent might have dead end pores contributing for the separation capacity, but this is not true for membranes, where such pores do not contribute to the steady state permeation. The smallest pore sections existent all over the

50

membrane thickness are often called constrictions, and are responsible for the selectivity of such materials [42]. In the adsorbent, these smaller pores are eventually responsible for differences in the kinetics of adsorption.

Therefore, next section will provide complementary information about equilibrium and kinetics of adsorption for MSC3K-162 and HF CM.

2.1.4.6. Adsorption equilibrium

The adsorption equilibrium isotherms of N_2, O_2, Ar and CO_2 in MSC3K-162 and HF CM were determined at 29.5 °C. The Langmuir equation was used to fit the experimental adsorption equilibrium values of N_2, Ar and O_2 and the SIPS equation to fit the adsorption values of CO_2. In the case of CO_2, the Langmuir equation was not able to describe adsorption equilibrium values. The assumptions [43] behind this equation are not valid in this case; it assumes that the surface is homogeneous, what probably is not. Therefore, the SIPS equation, accounting for the heterogeneity of the system, has been used to fit CO_2 experimental data. The Langmuir and SIPS equations are as follows, respectively:

$$q = q_s \frac{bP}{1+bP} \tag{2.9}$$

$$q = q_s \frac{(bP)^{1/n}}{1+(bP)^{1/n}} \tag{2.10}$$

where q is the adsorbed solute concentration at pressure P, q_s is the adsorbed saturation capacity, b is the adsorption affinity constant, revealing the adsorption strength of a species onto the surface, and n is a parameter which accounts for the heterogeneity of the system. When n is equal to 1, then the SIPS equation turns to Langmuir equation. These parameters were obtained by fitting the equations to the experimental adsorption data, minimizing the sum of the squared residuals divided by the number of experimental points, np, for each gas.

Figure 2.9 represents the experimental adsorption equilibrium values and corresponding equation fits, and Table 2.5 lists the parameters obtained from these fits.
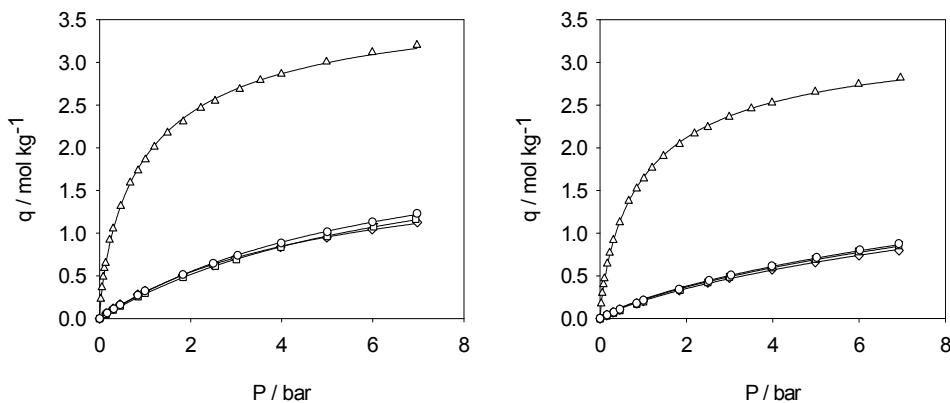
Figure 2.9 – Adsorption equilibrium isotherms on a) MSC3K-162 and b) HF carbon membranes at 29.5ºC: Experimental data ◇ N_2, □ Ar, △CO_2 and ○ O_2, — adsorption equilibrium equations.

Table 2.5 – Parameters of the Langmuir and SIPS equations for MSC3K-162 and HF-CM obtained from the adsorption equilibrium values determined by the gravimetric method at 29.5 ºC.

	Langmuir and SIPS parameters			
	q_s (mol kg^{-1})	b (bar^{-1})	n	$\Sigma\left(q-q^*\right)^2 \big/ np$
HF CM				
N_2	1.589	0.144	-	1.36×10^{-5}
Ar	1.994	0.108	-	2.82×10^{-6}
CO_2	3.618	0.773	1.334	3.01×10^{-5}
O_2	2.013	0.112	-	2.52×10^{-5}
MSC3K-162				
N_2	1.928	0.196		5.74×10^{-5}
Ar	2.325	0.142		2.88×10^{-5}
CO_2	4.221	0.718	1.407	9.54×10^{-5}
O_2	2.391	0.149		4.29×10^{-5}

In these carbonaceous materials the surface is mainly non-polar, and for that reason its interaction with non-polar or weakly polar species is attributed to Van der Walls forces. This is the case for N_2, Ar, O_2 and CO_2 adsorption onto carbon. Before

discussing the adsorption equilibrium results, it is important to remember the dimensions of each species: the molecular sizes of the sequence CO_2-O_2-Ar-N_2, are respectively, 3.30<3.47<3.54<3.64 Å [44].

As visualized in Figure 2.9, MSC3K-162 presents a higher adsorption capacity than HF CM towards all the tested gases, as also verified by the saturation capacity obtained from the fittings. This was already expected, since the DR analysis indicates a greater micropore volume for MSC3K-162. In both cases, the most adsorbable species is CO_2, due to its induced polarity and smaller size, followed by O_2, Ar and N_2, in this order. The Langmuir equation described well experimental data for N_2, Ar and O_2, but could not describe CO_2 adsorption. CO_2 has access to smaller pores that the other species do not; for that reason a model accounting for the heterogeneity of the system (SIPS) was a better choice. The fittings obtained for O_2, Ar and N_2 have very similar shapes, in both materials, but yielding slightly higher saturation capacities for O_2, followed by Ar, as shown by the parameters given in Table 2.5. Both materials showed reproducible nitrogen adsorption results after exposure to each of the other gases.

In order to assess the effect of the particle size of adsorbent on the adsorption capacity of the milled granules of MSC3K-162, the adsorption equilibrium isotherm of N_2 was also determined and equivalent equilibrium values were obtained.

2.1.4.7. Adsorption kinetics

Experimental uptakes

Experimental uptake curves have been determined at 29.5 °C for N_2, Ar, CO_2 and O_2 for both materials within the range of 0-7 bar. The rate of adsorption was quantitatively evaluated in terms of the apparent time constant, D/r^2, which is directly computed from the experimental uptakes. Concerning MSC3K-162, isothermal diffusion in a homogeneous spherical particle was considered [43]:

$$F = 1 - \frac{6}{\pi^2} \sum_{n=1}^{\infty} \frac{1}{n^2} \exp\left(-n^2 \pi^2 \frac{D}{r^2} t\right)$$
(2.11)

where F is the fractional uptake at instant t and D/r^2 is the apparent time constant.

However, for CO_2 and O_2, this model could not predict the uptakes due to thermal effects associated with a very fast diffusion. Thus, a non-isothermal model was applied to the uptake curves of CO_2 and O_2 in MSC3K-162 [45]. This model is as follows:

$$F = 1 - \sum_{n=1}^{\infty} \frac{9\left[\left(q_n \cot q_n - 1\right)/q_n^2\right]^2 \exp\left(-q_n^2 \frac{D}{r^2} t\right)}{\frac{1}{\beta} + \frac{3}{2}\left[q_n \cot q_n \left(q_n \cot q_n - 1\right)/q_n^2 + 1\right]} \qquad (2.12)$$

where q_n is evaluated by the roots of $3\beta\left(q_n \cot q_n - 1\right) = q_n^2 - \alpha$ with α and β being parameters of the model, as well as the apparent time constant D/r^2. In the limiting case when $\alpha \to \infty$ and $\beta \to 0$ the expression reverts to eq. (2.11). For the CO_2 uptakes, the values obtained for α and β were, respectively, within the range of 3.2-3.6 and 0.3-4.7; for O_2 uptakes, the ranges are, respectively, 0.6-0.7 and 0.2-0.9. The values of α, β and D/r^2 were obtained by fitting eq. (12) to experimental uptake curves.

For HF CM, the uptakes for the four gases were fit by the isothermal diffusion model for slab geometry [43] as represented in eq. (2.13):

$$F = 1 - \frac{2}{\pi^2} \sum_{n=1}^{\infty} \frac{1}{\left(n-1/2\right)^2} \exp\left[-\left(n-1/2\right)^2 \pi^2 \frac{D}{r^2} t\right] \qquad (2.13)$$

Other models assuming spherical or cylindrical configuration were tested but the fit of the experimental data was not as good. The amount of sample used in the experiments was lower than in the case of MSCK3-162 and therefore no significant thermal effects were observed. Figure 2.10 provides an example of the experimental uptakes obtained for the two materials, as well as the corresponding model fits.
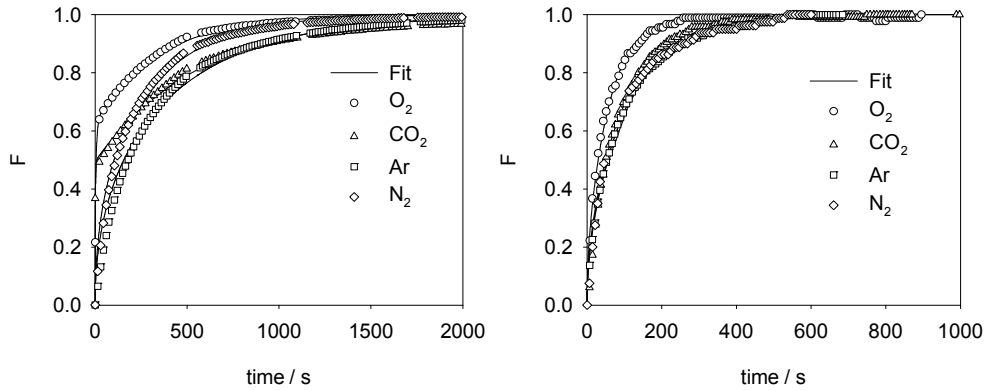
Figure 2.10 – Experimental uptake curves for N_2, Ar, CO_2 and O_2 in a) MSC3K-162 and b) HF CM at 29.5 ºC and 7 bar pressure and respective fitting models.

The models described experimental uptakes well and the apparent time constants were obtained for each pressure studied. Experimental uptake curves of N_2 were also performed in the milled adsorbent and coincident apparent time constants were obtained.

Next, in Figure 2.11, the apparent time constants of N_2, Ar, CO_2 and O_2 for a) MSC3K-162 and b) HF CM are presented.
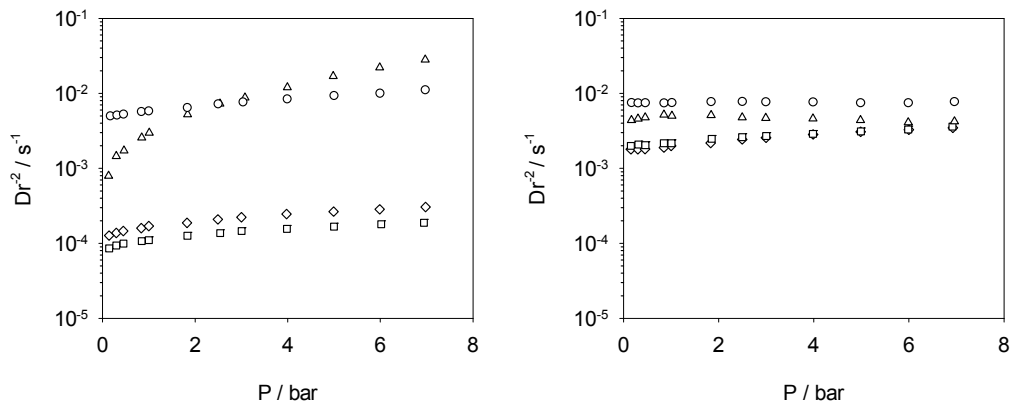
Figure 2.11 – Relationship between the apparent time constant and pressure at 29.5 ºC for ◇ N_2, □ Ar, △CO_2 and ○ O_2 on a) MSC3K-162 and b) HF carbon membranes.

In general, the apparent time constants revealed to be higher in HF CM than in MSC3K-162. Expectedly, adsorbent MSC3K-162, specially designed for the kinetic

separation of N_2 from air, presents higher kinetic selectivities for O_2/N_2, about 10 times higher than the ones found for HF CM. This fact should be related to the small differences in the mean pore width which is slightly smaller in the case of MSC3K-162, as seen before; however, due to the similar diameters of present species, this little difference in the pore width should be enough to slow down the diffusion rates by one hand, and to enhance kinetic selectivities on another.

The samples were regenerated with helium at 70 °C after uptake measurements of each gas. Analogously to what was done in the equilibrium determinations, N_2 uptakes, at low and high pressures, were performed after regeneration, in order to check the adsorption conditions uniformity along all determinations. Reproducible results were always obtained, even after exposure to oxygen. Additionally, the influence of macropore diffusion was assessed by employing the procedure outlined by Ruthven [46] and reported by Rutherford and Do on a CMS Takeda 3A [47]. It was indeed verified that macropore diffusion is negligible for the gases studied.

Pressure-dependence

Normally, the diffusivities and, hence, the apparent time constants, depend on pressure. The Darken relation is one of the most used models; it is derived considering that the driving force for mass transport is the chemical potential gradient and assuming ideal gas behavior. The commonly used simplified form of this relation is [43]:

$$D_{\mu} = D_{\mu 0} \frac{\partial \ln P}{\partial \ln q} \qquad (2.14)$$

where $D_{\mu 0}$ is the diffusivity at zero loading and is a parameter of the model. When the Langmuir or SIPS equation is used to describe the adsorption equilibrium, the Darken relation takes the following forms, respectively:

$$D_{\mu} = D_{\mu 0}^{'} \left(1 + bP\right) \qquad (2.15)$$

$$D_{\mu} = D_{\mu 0}^{'} \left(1 + \left(bP\right)^{1/n}\right) \qquad (2.16)$$

However, for some systems the Darken model fails to describe the relation of diffusivities with loading. Do et al. proposed a structural-diffusion model [48] which accounts for a stronger pressure-dependence:

$$D_\mu = \frac{A}{\partial q \Big/ \partial P} \qquad (2.17)$$

where A is a constant. The adsorbed concentration, q, is given by an adsorption isotherm equation. The SIPS equation was chosen in the present case:

$$D_\mu = D_{\mu 0}' \frac{\left(1+(bP)^{1/n}\right)^2}{(bP)^{\frac{1-n}{n}}} \qquad (2.18)$$

For adsorbent MSC3K-162, Figure 2.12 provides an overview on the pressure dependence of the apparent time constants obtained from the experimental uptakes.
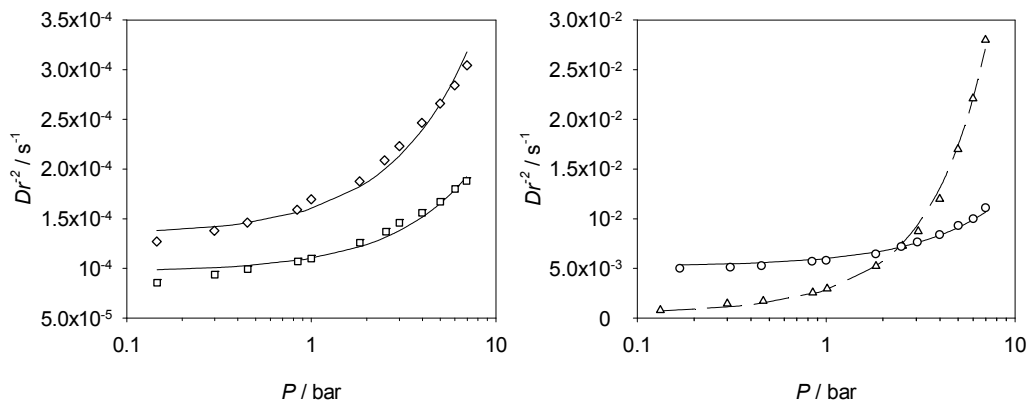
Figure 2.12 – Dependence of the apparent time constant with pressure at 29.5 ºC on MSC3K-162: experimental $\Diamond$ N$_2$, $\Box$ Ar, $\triangle$CO$_2$ and $\bigcirc$ O$_2$, —Darken model, eq. (2.15), – – Do model, eq. (2.18).

The apparent time constants exhibit increasing pressure dependence with loading, as also reported for other carbon molecular sieve adsorbents [40, 49]. The apparent time constants for Ar, N$_2$ and O$_2$ can be described by the Darken-Langmuir model. CO$_2$, on the other hand, showed a much stronger dependence, which is better fit by the Do-Sips relation. The species diffusion coefficients chase the following order: O$_2$>CO$_2$>N$_2$>Ar. However, this trend does not follow the suggested order based only on the kinetic diameters of the species. This tendency has been reported by other

authors [47, 49-52] and it has been questioned whether or not the atomic/molecular sizes are enough to explain differences in diffusivities. It has been more frequently accepted that other factors are important to justify these differences: shape, adsorption affinity, electronic properties, etc [49-52]. It was observed that CO_2, being smaller than O_2, presents a lower rate of adsorption up to ca. 2.5 bar. Similarly, O_2 and N_2, with close kinetic diameters, exhibit very different adsorption rates, hardly attributable to differences in size.

These models always predict an increase of diffusivity with loading when favorable isotherms are considered. However, most of the carbonaceous materials used to validate these models have been activated carbons, carbon blacks and some carbon molecular sieve adsorbents; very few information is available concerning carbon molecular sieve membranes [23, 53, 54].

Five decades ago, a work performed in molecular sieves revealed a decreasing loading-dependence for N_2 diffusivity [55]. On the other hand, CH_4 exhibited an increasing dependence in the same material [55]. Nevertheless, a physical interpretation was not provided. More recently, Chen and Yang [56] have also obtained experimental results for molecular sieve zeolites showing a decreasing pressure-dependence of diffusivities. Those authors suggested that this was caused by inter-molecular blockage effects occurring at higher pressures. Since Darken models or other structural models always predict an increase of diffusivities with loading, the need of a model which could explain either increasing or decreasing tendencies of experimental data was necessary. Chen and Yang developed a new model which includes an extra parameter, Λ, that accounts for the pore blockage effects as well as loading dependence [56]:

$$D_\mu = D'_{\mu 0} \frac{1-\theta+\frac{\Lambda}{2}\theta(2-\theta)+H(1-\Lambda)(1-\Lambda)\frac{\Lambda}{2}\theta^2}{\left(1-\theta+\frac{\Lambda}{2}\theta\right)^2} \qquad (2.19)$$

Here θ is the surface coverage and Λ the pore blockage parameter; when the parameter that measures the blockage extent is null (no blockage occurs) the expression becomes the Darken-Langmuir relation.

In 2007, Bhatia and Nicholson presented a molecular simulation study to validate a novel theory to predict the density dependence of diffusivities in molecularly sized nanopores, using CH_4 and CF_4 as probing species [57]. These are pore structures typical of activated carbons, silicas, zeolites and molecular sieves. These authors found that, for some adsorbate sizes, a concentration increase may lead to significant radial interactions between neighboring species, augmenting wall collisions and causing a decrease in apparent time constants.

In the present work, different behaviors were observed for the measured apparent time constants. Figure 2.13 presents both experimental data and model fits for the pressure-dependence of apparent time constants on HF CM.
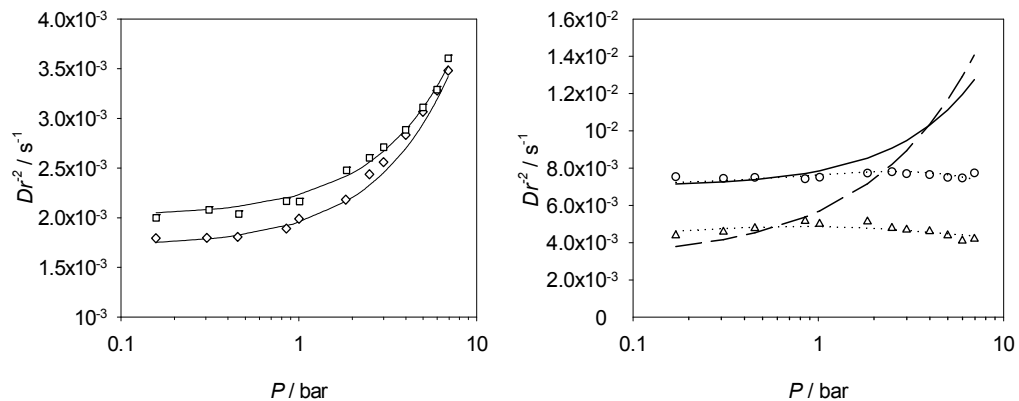
Figure 2.13 – Dependence of the apparent time constant with pressure at 29.5 ºC on HF carbon membranes: experimental ◇ N_2, □ Ar, △CO_2 and ○ O_2, —Darken-Langmuir models, – – Darken-SIPS model, ... Chen and Yang model.

Concerning HF CM, the species studied showed a different behavior than in MSC3K-162. Now, the faster diffusing species is O_2, followed by CO_2 and finally by Ar and N_2. Contrarily to adsorbent MSC3K-162, the membranes seem to lose some of their kinetic selectivity with increasing pressure. Also interesting, is that in opposition with what is verified to MSC3K-162, Ar diffuses faster than N_2, although they tend to become equally fast as loading increases; still in the case of membranes HF CM, both Ar and N_2 follow the Darken-Langmuir relation. However, for CO_2 or O_2, this relation only fits the diffusivities up to 1 bar and fails the prediction up to 7 bar, as the measured diffusivities actually decrease. The structural model developed by Do et al.

59

[48] also fails, since it predicts an even stronger pressure dependence. The model proposed by Chen and Yang was then used to fit O_2 and CO_2 apparent time constants as a function of the pressure and good results were achieved. It was also applied to results obtained with N_2 and Ar, where the fit value of Λ was zero, turning the model into the Darken-Langmuir relation.

Table 2.6 indicates the models used to describe the pressure-dependence of apparent time constants of each gas on each material and presents the parameters obtained for each model.

Table 2.6 – Pressure-dependent models and their parameters for MSC3K-162 and HF CM.

	MSC3K-162				HF CM			
	b (bar^{-1})	n	$D_{\mu 0}/r^2$ (s^{-1})	Model	b (bar^{-1})	Λ	$D_{\mu 0}/r^2$ (s^{-1})	Model
N_2	1.96×10^{-1}	-	1.34×10^{-4}	Darken-Langmuir	1.44×10^{-1}	-	1.71×10^{-3}	Darken-Langmuir
Ar	1.42×10^{-1}	-	9.67×10^{-5}	Darken-Langmuir	1.08×10^{-1}	-	2.02×10^{-3}	Darken-Langmuir
CO_2	7.18×10^{-1}	1.41	9.92×10^{-4}	Do-SIPS	-	2.2	4.06×10^{-3}	Diffusion+Block
O_2	1.49×10^{-1}	-	5.22×10^{-3}	Darken-Langmuir	-	3.1	7.09×10^{-3}	Diffusion+Block

As shown before, the pore size distribution of HF CM in the range responsible for molecular sieving (0.3-0.6 nm) is shifted to the right comparatively to MSC3K-162 (larger pores). This small difference may be responsible for the effect observed for the smaller species. The adsorbent should allow only a single layer of adsorbed species migrating through the constrictions, within the range of pressures studied. On the other hand, the membrane, with slightly larger pores, may accommodate, at higher pressures, two layers of the smaller species (CO_2 or O_2), but still only one layer of the larger species (Ar or N_2). According to the theory suggested by Bhatia and Nicholson [57], at low pressures only one layer for any gas should be formed and only axial interactions between adsorbates should occur; as loading increases, lateral (radial) adsorbate-adsorbate interactions should become relevant for the smaller species, CO_2

and O_2, and a superposition of the potentials from adsorbate-adsorbate and adsorbate-wall interactions should occur, leading to a deceleration of the molecules and hence, to a decrease in diffusivities. This explains why CO_2 and O_2 diffuse slower with increasing pressure, in opposition to Ar and N_2. These last species, being larger than O_2 and CO_2, behave according to Darken relation because they only form a line of adsorbed species due to the limitation of the pore width. To our knowledge, it is the first time that such behavior is evidenced for carbon molecular sieve membranes.

2.1.5. Conclusions

A carbon molecular sieve membrane (hollow fiber) and a carbon molecular sieve absorbent (spherical particle) have been compared. The morphology of these materials was analyzed by SEM showing that the adsorbent particle presents a macropore network structure in opposition to the hollow fiber, which is apparently dense. These structural differences were in agreement with the results found by Hg porosimetry; they revealed that the adsorbent particles present an overall macro/mesoporosity of 0.46 against 0.16 in the membranes. The adsorption of CO_2 at 0 °C was used to assess the ultramicroporosity: the micropore volume assessed by DR approach for MSC3K-162 and HF CM is, respectively, 185.7 and 168.7 cm^3 kg^{-1}. The mean pore widths determined using the relation of Stoeckli et al. are, respectively, 0.498 and 0.514 nm. Accordingly, the micropore size distribution of HF CM is slightly shifted towards larger values of pore width, in relation to MSC3K-162. This is probably the fundamental difference between these two carbonaceous materials.

The adsorption equilibrium isotherms of N_2, Ar, CO_2 and O_2 were determined at 29.5 °C in both materials and similar curves were obtained. The experimental equilibrium values of N_2, Ar, and O_2 were fit by the Langmuir equation while values of CO_2 were fit with the SIPS equation. MSC3K-162 presented slightly higher values than HF CM, which was expected due to its larger overall microporosity. Experimental uptakes of N_2, Ar, CO_2 and O_2 have been performed in both MSC3K-162 and HF CM at 29.5 °C and 0-7 bar. A diffusion model for a spherical homogenous particle was applied to fit experimental uptakes of N_2 and Ar. However, the fast diffusion of CO_2

and O_2 originates non-isothermal effects, implying the use of an appropriate model. On the other hand, experimental uptakes performed on HF CM were all properly fit with an isothermal diffusion model assuming slab geometry. The apparent time constants at different pressures were determined for each gas. The pressure dependence of the apparent time constants was then established; the adsorbent MSC3K-162 behaves according to Darken-Langmuir relation for the diffusion of species N_2, Ar and O_2. CO_2, on the other hand, exhibits a more pronounced pressure-dependence, following a Do-SIPS relation. HF CM presents a Darken-Langmuir behavior for the larger species, N_2 and Ar, while CO_2 and O_2 present a first increasing and then decreasing pressure-dependence. This last behavior was well described by a model developed by Chen and Yang. This model has an extra parameter which accounts for blockage effects that might occur inside the ultramicropores. The mass transport mechanism suggested by Bhatia and Nicholson [57] was found to provide a meaningful interpretation of these results; the pores in HF CM may allow lateral interactions (along the pore radial direction) of species CO_2 and O_2 rather than only axial interactions when two layers of adsorbed species happen. When pressure increases the adsorbed concentration also increases and repulsive interactions between neighboring adsorbates lead to an enhancement of wall collisions, causing a decrease in diffusivity. In MSC3K-162, which has slightly narrower micropores, only axial interactions should be relevant and diffusion follows an increasing pressure dependency.

2.1.6. Acknowledgements

2.2. Water vapor adsorption and surface chemistry[2]

2.2.1. Abstract

The adsorption/desorption equilibria of water vapor in a carbon molecular sieve (CMS) membrane and a commercial CMS adsorbent were determined, exhibiting S-shaped, type V isotherms. The fits of several models found in the literature to the experimental data were evaluated. The results obtained led to the development of a new model accounting for both adsorption and desorption and essentially based on the work of Lagorsse et al. (2005). Furthermore, the adsorption kinetics was also assessed for both materials and well described by a Linear Driving Force model. The existence of hydrophilic groups responsible for water vapor adsorption in such carbonaceous materials has been related to the surface chemistry by means of X-ray microanalysis and by thermogravimetry. It was concluded from X-ray microanalyses that the carbon membrane presents a lower C/O ratio and is thus more sensitive towards water vapor exposure, as evidenced by the measured water adsorption at lower relative pressures. It was also observed that the diffusion rates are higher for the CMS membrane than for the CMS adsorbent.

2.2.2. Introduction

The present section continues the comparative study between a carbon molecular sieve (CMS) membrane and a commercial CMS adsorbent suited for gas separation, reported previously, giving now emphasis to the surface chemistry of these materials.

It is widely known that many gaseous streams present water vapor to some extent [58]. In the particular case of the separation of nitrogen and oxygen from air using carbon molecular sieve materials, the influence of water vapor is of significant interest [59]. The presence of a small amount of water can sometimes disable or decrease the performance of the adsorbents [60].

---

[2] M.C. Campo, S. Lagorsse, F.D. Magalhães, A. Mendes, Comparative study between a CMS Membrane and a CMS Adsorbent: Part II –Water vapor adsorption and surface chemistry J. Membr. Sci. 346 (2010) 26–36.

These materials are mainly constituted of carbon atoms distributed as disordered graphene layers that work as hydrophobic sites for adsorption. However, some heteroatoms are also present, conferring a hydrophilic character to these carbon structures and allowing for the adsorption of water [31, 61, 62]. The heteroatom more often present in these structures is oxygen, which can assume different forms, as hydroxyl, carboxyl, quinone, peroxide or aldehyde functional groups [58, 60, 63]. Water molecules establish hydrogen bridges with the oxygen on the surface, known as primary adsorption sites [61, 64], and subsequent water molecules will then bond to the previously adsorbed water molecules [64]. When this molecular cluster becomes sufficiently large, dispersion forces become predominant and it leaves the primary site adsorbing thereafter into hydrophobic micropores [65]. The adsorption isotherm is therefore a function of the concentration and distribution of primary adsorption centers, pore structure and vapor pressure [60, 66].

According to IUPAC designation, the adsorption of water vapor in carbon materials having oxygen functional groups exhibits a type V isotherm also known as S-shape [65, 67-70]. It has been discussed in literature that hysteresis in such materials may be explained by differences between filling and emptying mechanisms, rather than by condensation in mesopores [64, 71].

In the previous section a carbon molecular sieve adsorbent from Takeda (MSC3K-162) and a carbon molecular sieve hollow fiber from Carbon Membranes, Inc. were studied. Their structural properties were compared and their influence on the performance of each material was assessed through several characterization techniques (scanning electron microscopy, X-ray diffraction, mercury porosimetry, micropore size distribution). The determination of equilibrium isotherms and kinetic parameters for N_2, Ar, CO_2 and O_2 was performed at 29.5 °C. In this section, both materials are characterized by thermogravimetric analyses, assessing the fixed carbon content and the volatile matter related to heteroatoms existent on the surface. The surface chemistry of each material is investigated by X-ray microanalysis and related to water vapor adsorption/desorption equilibrium and kinetics. The way different heat treatments influence the final hydrophilic group content [72] was also analyzed. The adsorption of water vapor on these groups provides meaningful information

about the structure of the carbonaceous materials. The experimental adsorption curves were fit by models described in the literature and a new model is also proposed.

2.2.3. Experimental

2.2.3.1. Materials studied

The carbon molecular sieve membranes designated here as HF CM were provided by Carbon Membranes Ltd., an Israeli company that bankrupted meanwhile. MSC3K-162 is a commercial carbon molecular sieve adsorbent supplied by Takeda and indicated for nitrogen production from air by PSA.

2.2.3.2. Thermogravimetric analysis (TGA)

The materials under study were submitted to a proximate analysis by thermogravimetry in order to determine their content in moisture, volatile matter, fixed carbon and ashes. The analyses were performed in a Netzsch TG 209 F1 Iris thermogravimetric balance, with 10^{-5} g precision; samples of 5 mg were used. The feed gases were N_2, up to the oxidation stage (950 °C), and O_2, afterwards. The temperature protocol used was mainly based on the work published by Ottaway [73] and is presented in Figure 2.14. The heating rate was 25 °C min^{-1}, with dwells at 50 °C, 110 °C and 950 °C. The long dwells used at 50 °C and 110 °C are mainly related to O_2 removal for preventing oxidation at higher temperatures. The dwell at 110 °C assures that all water is removed. The final dwell at 950 °C has a total extent of 20 min, divided in two subdwells; 9 min under N_2 for volatile matter release and 11 min under oxygen for assessing the ash content.
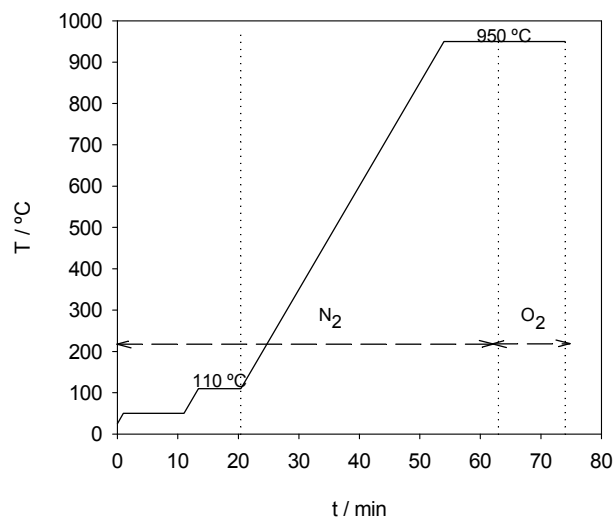
Figure 2.14 – Procedure for proximate analysis.

2.2.3.3. X-ray microanalysis

The surface chemistry of both MSC3K-162 and HF CM was assessed by X-ray microanalysis using a FEI Quanta 400FEG / EDAX Genesis X4M. These analyses were performed in simultaneous with SEM, already presented in the previous section.

2.2.3.4. Adsorption

The sorption studies in the CMS membrane and adsorbent were conducted using the gravimetric method, in the same magnetic suspension balance from Rubotherm® (metal version and 10^{-5} g precision) already presented in the previous section. However, the system has been adapted to allow sorption studies towards water vapor, as illustrated below: a small tank filled with liquid water was added for supplying vapor, up to the desired pressure, to the 5 L feeding tank. This system is represented in dashed lines in Figure 2.15. The samples were regenerated with helium at 70 °C before and after water vapor measurements. Nitrogen was used to check the adsorption stability of the materials by determining adsorption equilibrium values and uptake curves before and after vapor exposure.
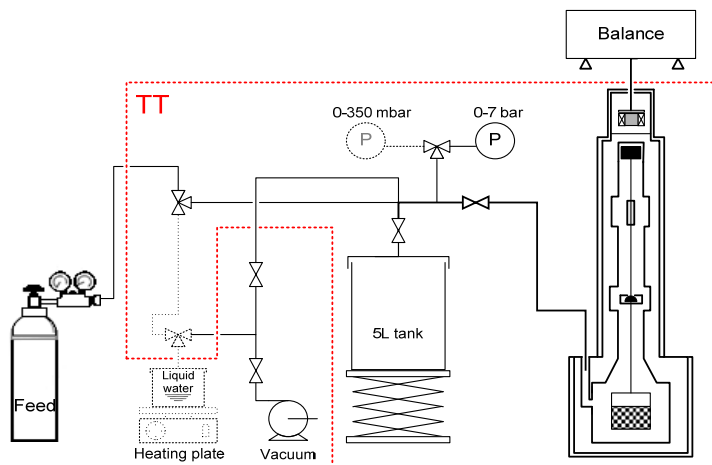
Figure 2.15 – Schematic representation of the gravimetric apparatus adapted for water vapor studies (adapted from [26]).

2.2.4. Results and discussion

2.2.4.1. Thermogravimetric analysis

Proximate analysis by thermogravimetry has been performed for MSC3K-162 and HF CM. The mass fraction of the sample is represented in Figure 2.16, employing the heating protocol described previously.
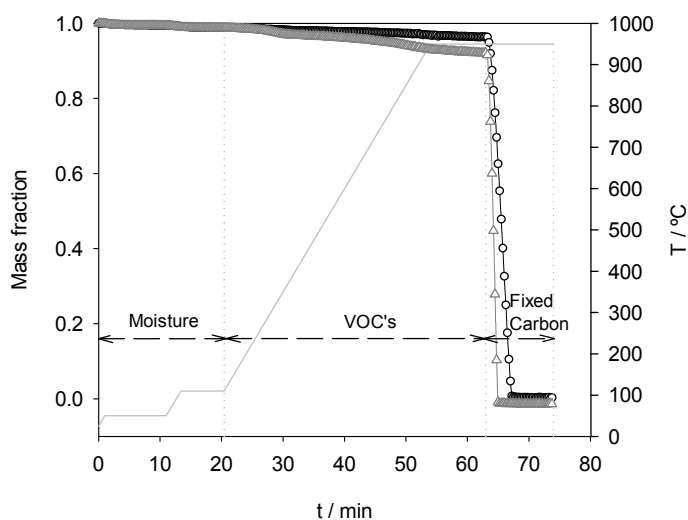
Figure 2.16 – Proximate analysis of MSC3K-162 (black circles) and HF CM (gray triangles) by thermogravimetric method. The species removed at different time intervals are identified.

The weight results are presented in a dry basis and are summarized in Table 2.7.

Table 2.7 – Dry basis (d.b.) results of proximate analysis by thermogravimetry of MSC3K-162 and HF CM.

	MSC3K-162	HF CM
Volatile matter (% d.b.)	2.27	16.3
Fixed Carbon (% d.b.)	97.4	83.7
Ash (% d.b.)	0.35	0

It is evidenced that both MSC3K-162 and HF CM present a high yield of fixed carbon. In fact, the carbon structure of each material is the result of the heat treatment employed; the higher the heat temperature achieved, the greater the stability of carbon structure [31]. Probably the carbonization step for MSC3K-162 occurred up to higher temperatures (700-900 ^{o}C) [74] yielding a more stable structure richer in fixed carbon. On the other hand, the HF CM prepared up to 600 ^{o}C most likely originated a carbon structure with some unstable atoms susceptible of chemisorbing oxygen when exposed to air. The ash content is very low for MSC3K-162 and absent in HF CM.

2.2.4.2. X-ray microanalysis

In Figure 2.17 the X-ray microanalyses of the materials' surfaces are shown.

It can be seen that in both cases the major element is carbon, as expected. Oxygen is also present, which confers the hydrophilic shift to the carbon surfaces. The C/O ratios obtained through X-ray microanalyses of MSC3K-162 are approximately 45 and 68, for respectively, outside and cross side (inside) surfaces, while HF CM exhibited much lower C/O ratios, 30 and 34 for, respectively, shell and bore sides. The lower C/O ratios obtained for HF CM should be responsible for the higher hydrophilic character of this material when compared to MSC3K-162. The hollow fiber membranes also show the presence of residual chlorine. In fact, as written in literature [8], the producer used HCl as catalyst for producing these carbon membranes.
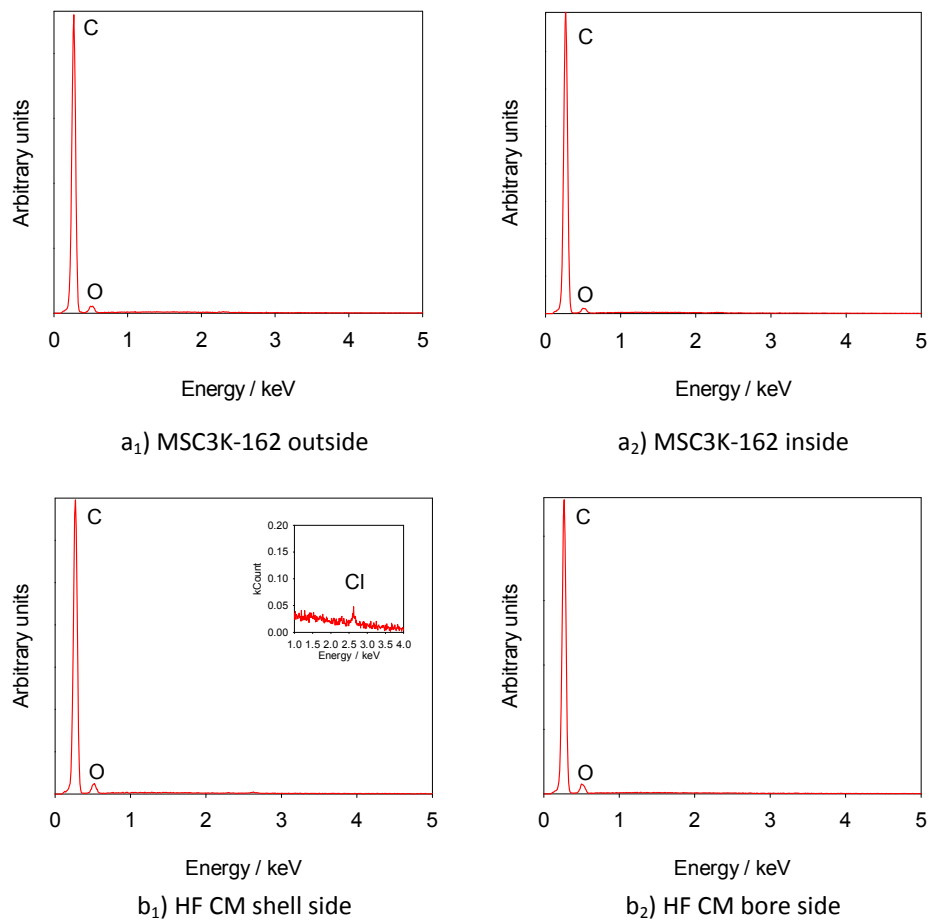
Figure 2.17 – Microanalysis of a_1) inside and a_2) outside of MSCK-162 and b_1) shell side and b_2) bore side of HF CM.

2.2.4.3. Water vapor adsorption Equilibrium

Experimental equilibrium data

Adsorption and desorption equilibrium data of water vapor in MSC3K-162 and HF CM was obtained by the gravimetric method at 29.5 $^{\circ}$C. The experimental values are given in Figure 2.18; the graphics are plotted in terms of relative pressure, considering 41.27 mbar the saturated water vapor pressure at 29.5 $^{\circ}$C.
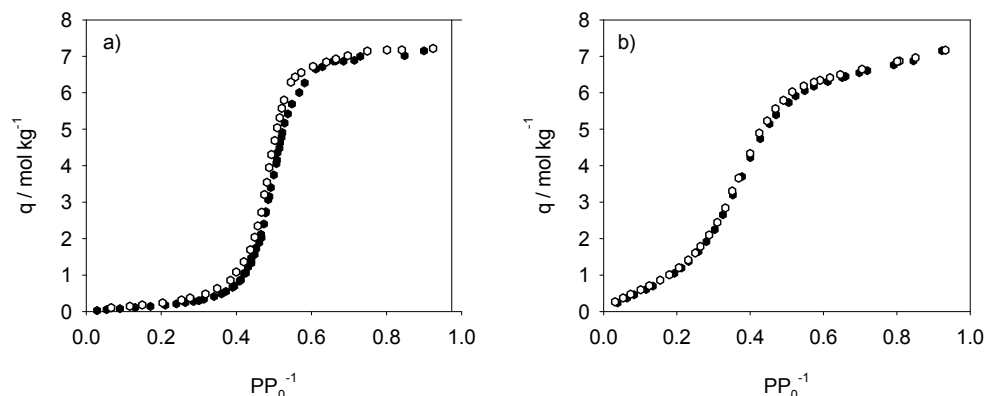
Figure 2.18 – Adsorption and desorption equilibrium of water vapor on a) MSC3K-162 and b) HF CM at 29.5 °C. The filled circles correspond to adsorption values while empty ones are related to desorption values.

Both materials present adsorption S-shaped equilibrium isotherms to water vapor, as suggested in Figure 2.18. Despite some differences, the type V isotherms show a very small hysteresis loop. The first slope shown for both isotherms a) and b) traduces the adsorption of water molecules on primary sites [75, 76]. Here, vertical interactions between the fluid and the surface occur. It is clear that HF CM present much higher concentration of oxygenated groups on the surface of the carbon matrix due to the significant adsorption at very low loading [75, 77, 78], which is in agreement with the X-ray microanalysis. On the other hand, MSC3K-162 presents an almost negligible adsorption in this range. Afterwards, the steepest part reflects the clusters formation, where lateral interactions among water molecules take place. This rise up occurs sooner for HF CM, around 0.3, and ends around 0.5, and later and sharper for MSC3K-162 just after 0.4, ending even before 0.5. Finally the last flatten slope, reveals that the micropore filling is limited to a finite amount. From this analysis it is seen that HF CM presents a stronger hydrophilic behavior than MSC3K-162. This is in conformity with the results shown in the previous sections concerning thermogravimetry analysis and X-ray microanalysis, which indicated a higher C/O ratio in the MSC3K-162 sample.

Semi-empirical and theoretical models

The description of experimental data related to water vapor adsorption on carbonaceous materials has been performed by many authors. Each one of them presumes a set of assumptions for the mechanism behind experimental data. Dubinin and coworkers proposed the semi empirical models widely used to describe water vapor adsorption equilibrium in carbons for its understanding [61, 64, 79-81]. However, these models demonstrate thermodynamic inconsistencies for very low pressures, disrespecting the Henry law limit. Due to this limitation, the Dubinin approach only successfully predicts some carbon-water systems. In this work, the modified Dubinin-Astakhov equation proposed by Stoeckli to describe water vapor adsorption in activated carbons has been used [79]. This modification results in the contribution of two type isotherms: type I, describing the low pressure range of the isotherm where adsorption on surface functional groups occurs and type V, for higher pressures, accounting for adsorption in micropores. In the modified Dubinin-Astakhov equation, the fitting parameters are: $q_0(I)$ and $q_0(V)$ respectively, the adsorbed concentration related to the functional groups and in the micropores (mol kg^{-1}), $E(I)$ and $E(V)$ the characteristic energies (kJ mol^{-1}) and n_1 and n_2, describing the heterogeneity of the system - see Table 2.8.

In 1996, Talu and Meunier [82] came up with a theory based on three assumptions: 1) at low relative pressure the water molecules are primarily adsorbed on the surface at oxygenated sites, 2) the adsorbed water molecules associate with each other via H-bonding forming clusters and, finally, 3) at high relative pressures, the adsorption volume is limited by the micropore volume, yielding a plateau. The proposed model involves three parameters with physical meaning: H, the Henry's law constant (kPa kg mol^{-1}), k, the constant for cluster formation in the micropores (kg mol^{-1}), and q_m, the saturation capacity (mol kg^{-1}) – see Table 2.8. This approach only predicts water vapor adsorption for microporous systems, neglecting any condensation at meso or macropore level.

In 2000, Malakhov and Volkov [83], developed a theory called "Cooperative multimolecular sorption" (CMMS) to predict adsorption equilibrium of alcohols in a

polymer. A couple of years later, Rutherford [84] proposed the use of this same theory to describe water adsorption in carbons. Here a water molecule adsorbs onto a primary site and promotes the adsorption of other two molecules forming a triad. These adsorbed water molecules are called secondary sites allowing the association of further water molecules forming dimers, trimers, etc. The original model is characterized by four parameters which in the case of type V isotherm can be reduced to a three parameter model also known as the Ising equation [85]. The parameters are the adsorption capacity, q_m (mol kg^{-1}), and the equilibrium constants for adsorption on primary sites of the central and side units, respectively, k_0 and k_1 - see Table 2.8.

In 1999, Do and Do [65] developed a mechanism for describing water vapor adsorption in activated carbon. This research resulted in a model that accounts for water adsorption into functional groups located at the mesopores, called primary sites, by means of H-bonding. These water adsorbed molecules are then assumed as secondary sites, where other water molecules will adsorb also establishing H-bonds, thus weaker than the first ones. The growth of this cluster formed by the association of water molecules occurs up to an extent where a 5-molecule cluster is then energetically sufficient to leave the "train" and adsorb onto hydrophobic carbon micropore walls. The model parameters are: S_0 (mol kg^{-1}), the concentration of functional groups, K_f, the chemisorption equilibrium constant, q_s (mol kg^{-1}), the saturation concentration of water in the micropores and K_μ, the micropore equilibrium constant – see Table 2.9. This work performed by Do and Do has inspired many other authors who have modified this model. Neitsch et al. [76], introduced the concept of a variable cluster size and consequently the addition of a parameter, m, to account for this. This new parameter does not represent a fixed number of water molecules, but an average number. This new model is called as "cluster formation induced micropore filling" and will be named here as Do-CIMF. In 2005, in the scope of a study performed on carbon molecular sieve membranes, Lagorsse et al. [71], also reformulated the adsorption mechanism by Do and Do and proposed a mechanism

for desorption. The other main differences from the original model consist on considering that the hydrophilic sites are concentrated at the micropores, instead of at the mesopores, and that the nature of the H-bondings established between primary sites-water and water-water is the same. Another difference is the number of water molecules that form a cluster. Instead of 5-molecules like in the original work by Do and Do, Lagorsse and coworkers proposed a 7-molecule cluster formation. The clusters with enough dispersion energy detach from the hydrophilic sites to adsorb on the hydrophobic walls. The five parameters of this model represent the concentration of hydrophilic groups, S_0 (mol kg^{-1}), the H-bonding equilibrium constant, K, the water adsorption capacity, q_s (mol kg^{-1}) and the adsorption and desorption constants, respectively, K_a and K_d - see Table 2.9.

The models presented above were used to fit experimental adsorption equilibrium data. Table 2.8 presents Dubinin-Astakhov, Talu-Meunier and CMMS equations and Table 2.9 compiles Do-based equations.

Table 2.8 – Dubinin-Astakhov, Talu-Meunier and CMMS fitting equations and respective parameters for predicting adsorption equilibrium of water vapor.

Model	Parameters			
Dubinin-Astakhov (I/V)	Sample	$q_0(I)/q_0(V)$	$E(I)/E(V)$	n_1/n_2
	MSC3K-162	1.79 / 5.26	2.46 / 1.81	2.9 / 8.4
$q = q_{0(I)} \exp\left[-\left(A/E_{(I)}\right)^{n_1}\right]$	HF CM	2.17 / 4.65	2.64 / 4.98	1.6 / 4
$+q_{0(V)} \exp\left[-\left(A/E_{(V)}\right)^{n_2}\right]$				
$A = \Re T \ln\left(P_v/P\right)$		(6th order)		
Talu and Meunier	Sample	H	k	q_m
	MSC3K-162	36.6	17.9	7.29
$P = \dfrac{H\psi}{1+k\psi} \exp\left(\dfrac{\psi}{q_m}\right)$	HF CM	2.02	1.23	7.80
where $\psi = \dfrac{-1+\sqrt{1+4k\xi}}{2k}$		(3rd order)		
and $\zeta = q_m \cdot q /\left(q_m - q\right)$				
CMMS Theory	Sample	k_0	k_1	q_m
	MSC3K-162	0.011	2.01	7.28
$q = q_m \dfrac{k_0 x}{k_0 x + w^2}$ where	HF CM	0.183	2.68	7.46
$w = \dfrac{1}{2}\left(1 - k_1 x + \sqrt{\left(1-k_1 x\right)^2 + 4k_0 x}\right)$		(3rd order)		

Table 2.9 - Do-based fitting equations for predicting water vapor adsorption equilibrium and their parameters.

Models	Parameters					
Do and Do	Sample	S_0	K_f	q_s	K_μ	
$$q = S_0 \frac{K_f \sum_{n=1}^{\infty} n x^n}{1 + K_f \sum_{n=1}^{\infty} x^n} + q_s \frac{K_\mu \sum_{n=6}^{\infty} x^n}{K_\mu \sum_{n=6}^{\infty} x^n + \sum_{n=6}^{\infty} x^{n-5}}$$	MSC3K-162	0.001	0.03	7.28	27.2	
	HF CM	0.025	5.46	6.70	172	
		(4th order)		Cluster size =5 molecules		
Do-CIMF	Sample	S_0	K_f	q_s	K_μ	m
$$q = S_0 \frac{K_f \sum_{n=1}^{m+1} n x^n}{1 + K_f \sum_{n=1}^{m+1} x^n} + q_s \frac{K_\mu\, x^{m+1}}{K_\mu\, x^{m+1} + x}$$	MSC3K-162	0.096	10.0	6.69	9604	13
	HF CM	0.565	31.1	5.37	164	5
		(5th order)				
Lagorsse	Sample	S_0	K	q_s	K_a	K_d
$$q_{ads} = S_0 \frac{\sum_{n=1}^{7} n (Kx)^n}{1 + \sum_{n=1}^{7} (Kx)^n}\left(1 - \frac{K_a (Kx)^7}{1 + K_a (Kx)^7}\right) + q_s \frac{K_a (Kx)^7}{1 + K_a (Kx)^7}$$	MSC3K-162	0.051	4.17	7.54	0.006	186
	HF CM	0.956	2.64	6.84	0.123	159
$$q_{des} = S_0 \frac{\sum_{n=1}^{7} n (Kx)^n}{1 + \sum_{n=1}^{7} (Kx)^n}\left(1 - \frac{K_d x^7}{1 + K_d x^7}\right) + q_s \frac{K_d x^7}{1 + K_d x^7}$$		(5th order)		Cluster size = 7 molecules		

The obtained fitting parameters are also given corresponding to the fitting curves illustrated in Figure 2.19-Figure 2.22.
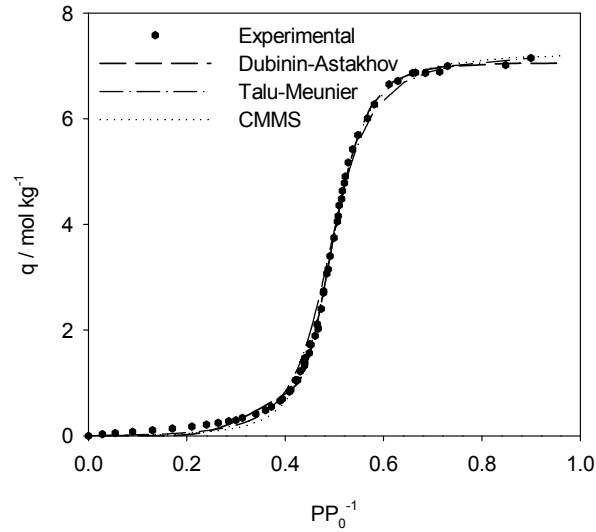
Figure 2.19 – Representation of water vapor experimental adsorption equilibrium values for MSC3K-162 and respective theoretical fitting equations presented in Table 2.8.
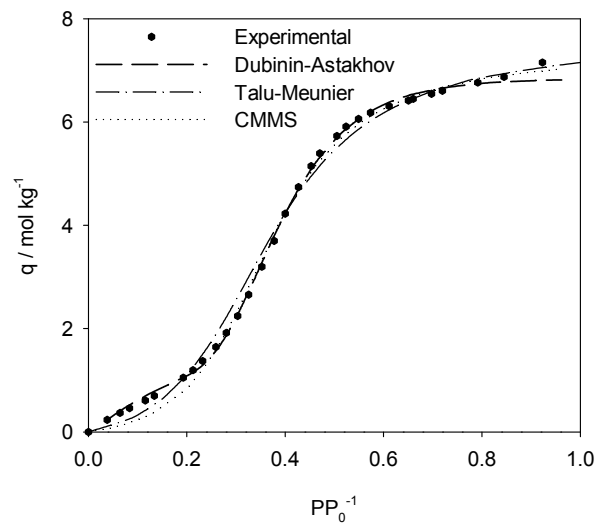
Figure 2.20 - Representation of water vapor experimental adsorption equilibrium values for HF CM and respective theoretical fitting equations presented in Table 2.8.

It is seen from Figure 2.19 and Figure 2.20 that the Dubinin-Astakhov equation with type I and V contributions describes reasonably both water vapor equilibrium isotherms in MSC3K-162 and HF CM. For the MSC3K-162 equilibrium line, the Dubinin-Astakhov equation slightly shifts to the left the inflexion part of the isotherm and underestimates the amount adsorbed; besides that, it seems to perform a good fitting for relative pressures higher than 0.4. For HF CM, the model equation describes well the whole range of relative pressure with the exception of the last two values, really close to the saturation. From the fitting parameters obtained it is observed that type I contribution is more significant for the HF CM than for the MSC3K-162.

The Talu and Meunier model better describes MSC3K-162 than HF CM, but in both cases presents some deviations for relative pressures just before the first inflexion zone.

The CMMS simplified to the Ising equation also provides a good approximation to experimental data, though with a little underestimation at low pressures.
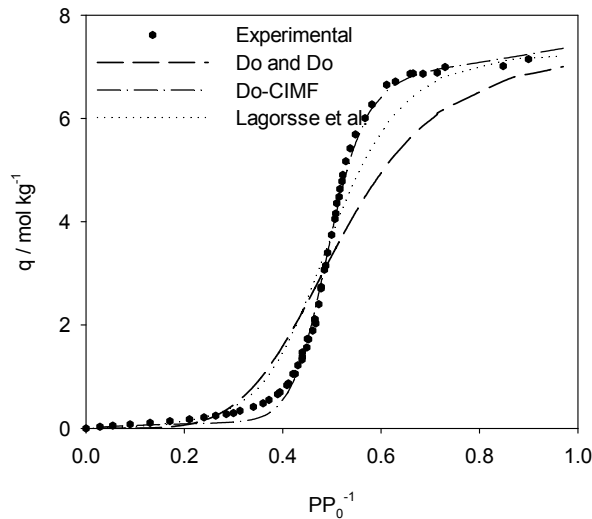
Figure 2.21 - Representation of water vapor experimental adsorption equilibrium values for MSC3K-162 and respective theoretical fitting equations presented in Table 2.9.
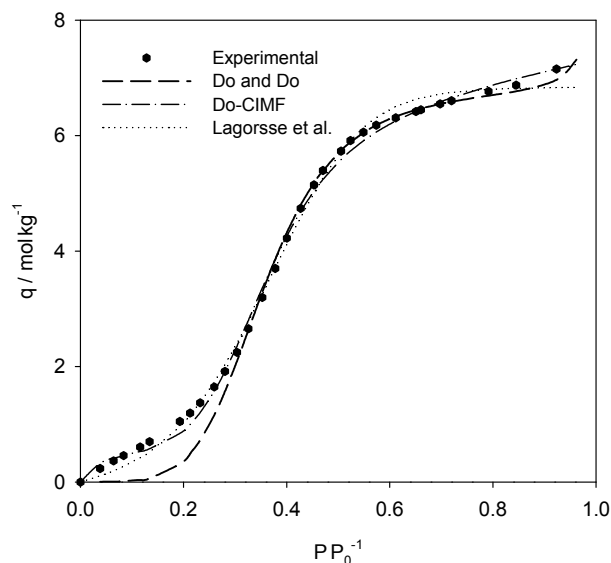
Figure 2.22 - Representation of water vapor experimental adsorption equilibrium values for HF CM and respective theoretical fitting equations presented in Table 2.9.

It can be observed from Figure 2.21 and Figure 2.22 that the original model by Do et al. [65] presents considerable deviations from the experimental equilibrium values for both materials. This model, as mentioned before, is based on the fact that a cluster of 5-molecules is formed. However, this assumption does not reflect the reality of water adsorption in MSC3K-162; the form of the curve suggests that clusters are formed by more than just five water molecules. For HF CM, the major deviation occurs for low relative pressures up to 0.3.

The modification to the Do model proposed by Lagorsse et al. [71] assumes a heptamer and also a mechanism for desorption. However, this model considerably deviates from the experimental data obtained for MSC3K-162. Concerning the HF CM, the model seems to fit better the experimental data but still with some misestimation: for low pressures the model underestimates the experimental data and just before reaching the plateau the model overestimates the amount adsorbed ending underestimating. The concept of a variable sized cluster introduced by Neitsch et al. [76] in the Do-CIMF model seems to be a good attempt for describing the water vapor adsorption in MSC3K-162 and HF CM materials. It does follow the shape of the experimental curves for the entire range of relative pressures. As suggested by the

experimental data, the water-clusters formed in the MSC3K-162 should be bigger than the ones formed in the HF CM. It is believed that the higher concentration of functional groups on the HF CM, suggested by the significant adsorption of water at very low pressures, is traduced in the formation of smaller water-clusters. On the other hand, the MSC3K-162 material exhibit a much lower concentration of hydrophilic groups reflected in a lower water-adsorption up to P/P_0 = 0.4, sharper rise up of the water adsorption and formation of bigger water-clusters inside.

Mechanism for adsorption/desorption in CMS

The most significant water adsorption models concerning carbon molecular sieve materials were reviewed in the previous section. Generally, these models present a considerable number of parameters for what accurate experimental isotherms are needed. In the present work, closely spaced experimental values were obtained to assure that the water sorption equilibrium is well represented. Therefore, it was possible to develop a more precise model; this model was derived following the work by Do et al. [65] and Lagorsse et al. [71]. The main assumptions for the adsorption mechanism of the model are:

- The water molecules are firstly adsorbed on the hydrophilic groups presented on the material's surface through H-bonding. The adsorption equilibrium is traduced by an equilibrium constant, K_1;

- When the first water molecule is attached to the hydrophilic group, other water molecules may successively establish H-bonding with the previous water molecule until a m sized cluster is reached. These equilibria are also traduced by K_1 as they still reflect the establishment of H-bondings; *(different from Do et al. [1] who have considered that the equilibrium constants for the water-hydrophilic group bonding and water-water bonding are different.)*

- The resulting cluster composed by m water molecules has enough dispersion energy to be released from the hydrophilic group and adsorb on

79

the carbon surface; *(different from Lagorsse et al. [2] who consider that a heptamer is formed.)*

As referred in the first and second assumptions the equilibrium relations are traduced by:
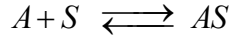
$$A + S \; \rightleftarrows \; AS$$

$$K_1 = \frac{[AS]}{[A][S]} \Rightarrow [AS] = K_1[A][S] \tag{2.20}$$
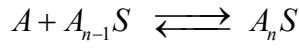
$$A + A_{n-1}S \; \rightleftarrows \; A_nS$$

$$K_1 = \frac{[A_nS]}{[A][A_{n-1}S]} \Rightarrow [A_nS] = K_1[A][A_{n-1}S]$$

$$= K_1^{\,n}[A]^n[S] \text{ for } n = 1,2,3,\dots \tag{2.21}$$

where A and S represent, respectively, a water molecule and hydrophilic site. The overall concentration of hydrophilic sites, S_0, in the micropores is the sum of the occupied and not-occupied sites, as follows:

$$S_0 = [S] + [AS] + [A_2S] + [A_3S] + \cdots + [A_nS] \tag{2.22}$$

The water complexes may be related to the adsorbed-gas phases partition through the eqs. (2.20) and (2.21):

$$S_0 = [S]\left(1 + K_1[A] + K_1^{\,2}[A]^2 + K_1^{\,3}[A]^3 + \cdots + K_1^{\,n}[A]^n\right)$$

$$= [S]\left(1 + \sum_{n=1}^{\infty} K_1^{\,n}[A]^n\right) \tag{2.23}$$

The concentration of water attached to the hydrophilic groups, w_a, can be obtained rearranging eqs. (2.20), (2.21) and (2.23):

$$w_a = [AS] + 2[A_2S] + 3[A_3S] + \cdots + n[A_nS]$$
$$= K_1[A][S] + 2K_1^2[A]^2[S] + 3K_1^3[A]^3[S] + \cdots + nK_1^n[A]^n[S]$$
$$= [S]\sum_{n=1}^{\infty} nK_1^n[A]^n$$
$$= S_0 \frac{\sum_{n=1}^{\infty} nK_1^n[A]^n}{1 + \sum_{n=1}^{\infty} K_1^n[A]^n} \tag{2.24}$$

A water cluster attached to a hydrophilic group is released when it comprises m water molecules. This m sized cluster has enough dispersion energy to detach from the hydrophilic site and to adsorb on the hydrophobic carbon surface. The hydrophilic sites rest then with $n - m$ adsorbed water molecules or even with no water molecule adsorbed, as given below:

$$A_nS \underset{k_d}{\overset{k_a}{\rightleftarrows}} A_m + A_{n-m}S \text{ for } n \geq m$$
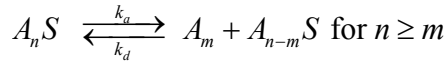
The available hydrophobic sites for water clusters to adsorb is given by $(q_m - w_a - c_a)$, where c_a is the concentration of water adsorbed on the carbon surface of the micropores. The velocities of adsorption and desorption are then given by:

$$r_a = k_a (q_m - w_a - c_a) \sum_{n=m}^{\infty} [A_nS] \tag{2.25}$$

$$r_d = k_d (c_a) \sum_{n=m}^{\infty} [A_{n-m}S] \tag{2.26}$$

The system reach the adsorption equilibrium when $r_a = r_d$:

$$K_a = \frac{k_a}{k_d} = \frac{(c_a) \sum_{n=m}^{\infty} [A_{n-m}S]}{(q_m - w_a - c_a) \sum_{n=m}^{\infty} [A_nS]} \tag{2.27}$$

where K_a is the adsorption equilibrium constant that is related to the clusters release from hydrophilic sites and consequent adsorption on the hydrophobic space. Combining this equation with eq. (2.21), and solving it in order to c_a, it comes:

$$c_a = (q_m - w_a) \frac{K_a \sum_{n=m}^{\infty} K_1^n [A]^n}{\sum_{n=m}^{\infty} K_1^{n-m} [A]^{n-m} + K_a \sum_{n=m}^{\infty} K_1^n [A]^n}$$

(2.28)

The water concentration in the micropores, q_a, can now be determined adding the water amount attached to the hydrophilic sites and the water in the form of a clusters adsorbed in the hydrophobic space:

$$(q_a = w_a + c_a)$$

(2.29)

Substituting now eq. (2.24) and (2.28) in eq. (2.29), it yields:

$$
q_a = S_0 \frac{\sum_{n=1}^{\infty} n K_1^n [A]^n}{1 + \sum_{n=1}^{\infty} K_1^n [A]^n} \left(1 - \frac{K_a \sum_{n=m}^{\infty} K_1^n [A]^n}{\sum_{n=m}^{\infty} K_1^{n-m} [A]^{n-m} + K_a \sum_{n=m}^{\infty} K_1^n [A]^n} \right)
$$
$$
+ q_m \frac{K_a \sum_{n=m}^{\infty} K_1^n [A]^n}{\sum_{n=m}^{\infty} K_1^{n-m} [A]^{n-m} + K_a \sum_{n=m}^{\infty} K_1^n [A]^n}
$$

(2.30)

Eq. (2.30) gives the adsorption equilibrium isotherm of water in the micropore volume of carbon molecular sieve materials.

The mechanism for water vapor desorption proposed considers, in analogy with the work by Lagorsse et al. [71], that the clusters have to dissociate into separate molecules. The difference to these authors is that they had considered a heptamer and the present model considers a cluster of size m:

$$A_m \xrightleftharpoons[k_d']{k_a'} mA$$
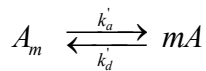
The adsorption and desorption rates, during the desorption process, are given by:

$$r_a' = k_a' \, c_d \tag{2.31}$$

$$r_d' = k_d' \left(q_m - w_d - c_d \right) [A]^m \tag{2.32}$$

where $\left(q_m - w_d - c_d \right)$ is the available adsorption capacity and $c_d = m[A_m]$. At the equilibrium the adsorption and desorption rates become equal:

$$c_d = \frac{[A]^m}{K_d + [A]^m} \left(q_m - w_d \right) \tag{2.33}$$

$$K_d = k_a' k_d'^{-1} \tag{2.34}$$

where K_d is the equilibrium constant for clusters' dissociation into separate molecules.

From eqs. (2.20), (2.21) and (2.24) the water concentration attached to the hydrophilic groups, w_d, during desorption is:

$$w_d = w_a = S_0 \frac{\sum_{n=1}^{\infty} n K_1^{\,n} [A]^n}{1 + \sum_{n=1}^{\infty} K_1^{\,n} [A]^n} \tag{2.35}$$

The total adsorbed concentration of water in the micropores during desorption is then expressed by:

$$q_d = w_d + c_d \tag{2.36}$$

Substituting eq. (2.24) and (2.28) in eq. (2.35), it yields:

$$q_d = S_0 \frac{\sum_{n=1}^{\infty} n K_1^{\,n} [A]^n}{1 + \sum_{n=1}^{\infty} K_1^{\,n} [A]^n} \left(1 - \frac{[A]^m}{K_d + [A]^m} \right) + q_m \left(\frac{[A]^m}{K_d + [A]^m} \right) \tag{2.37}$$

Rewriting now eq. (2.30) and (2.37) in terms of relative pressure, x, and considering that $x = K_1 A$, and $K = K_1^{-1}$, the adsorption and desorption branches of the water isotherm are given by:

Adsorption:

$$q_a = S_0 \frac{\sum_{n=1}^{\infty} n x^n}{1 + \sum_{n=1}^{\infty} x^n} \left(1 - \frac{K_a \sum_{n=m}^{\infty} x^n}{\sum_{n=m}^{\infty} x^{n-m} + K_a \sum_{n=m}^{\infty} x^n} \right) + q_m \frac{K_a \sum_{n=m}^{\infty} x^n}{\sum_{n=m}^{\infty} x^{n-m} + K_a \sum_{n=m}^{\infty} x^n} \qquad (2.38)$$

Desorption:

$$q_d = S_0 \frac{\sum_{n=1}^{\infty} n x^n}{1 + \sum_{n=1}^{\infty} x^n} \left(1 - \frac{(Kx)^m}{K_d + (Kx)^m} \right) + q_m \left(\frac{(Kx)^m}{K_d + (Kx)^m} \right) \qquad (2.39)$$

The proposed model has four parameters to describe the adsorption branch: S_0, q_m, K_a and m, and requires additionally two more parameters: K and K_d, for describing the desorption branch. Parameters S_0, q_m and m are the same for both adsorption and desorption branches. The model follows the Henry law for low pressures: $\lim_{x \to 0} q \approx S_0 x$.

This model was used to fit the water vapor equilibrium data for MSC3K-162 and HF CM, minimizing the sum of the square differences – Figure 2.23 and Figure 2.24. As a first estimative, the adsorption capacity obtained experimentally for a relative pressure near the saturation was used as the total adsorption capacity, q_m.
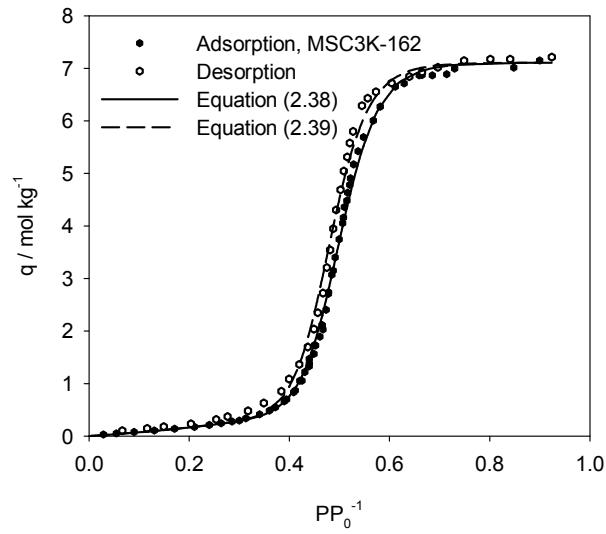
Figure 2.23 - Water vapor experimental adsorption and desorption equilibrium values for MSC3K-162 and respective fitting, eqs. (2.38) and (2.39).
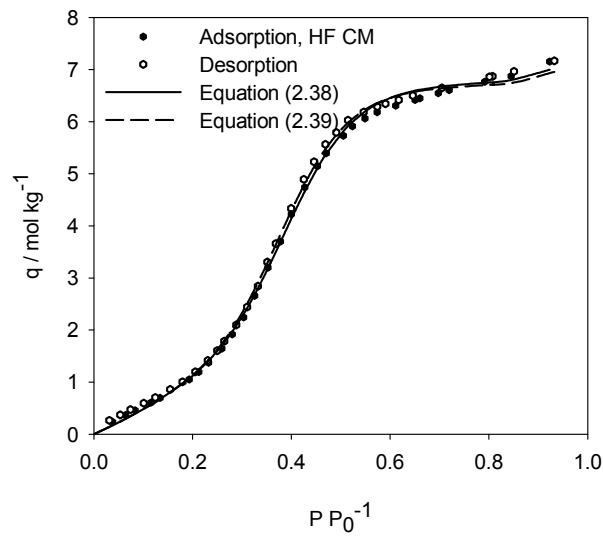
Figure 2.24 - Representation of water vapor experimental adsorption and desorption equilibrium values for HF CM and respective fitting, eqs. (2.38) and (2.39).

The fitting parameters obtained for MSC3K-162 and HF CM are given in Table 2.10.

Table 2.10 – Fitting parameters of the proposed model of the experimental water vapor adsorption and desorption equilibrium data on MSC3K-162 and HF CM.

	Fitting parameters, eqs. (2.38) and (2.39)					
	S_0 (mol kg^{-1})	q_m (mol kg^{-1})	K_a	K_d	K (mol kg^{-1})	m
MSC3K-162	0.66	7.16	7420	129	3.00	13
HF CM	4.31	6.45	133	28	4.07	6

It was previously mentioned that the cluster formation around hydrophilic sites is shifted to higher relative pressures in the case of MSC3K-162. As suggested by Do et al. [86] in their recent work reporting water vapor adsorption in activated carbon, the larger the cluster, the slower the onset of adsorption with a consequent quicker increase in the amount adsorbed. This fact is in agreement with the parameters found for the proposed model, Table 2.10, namely the 13-water molecules cluster and the greater value of K_a obtained for MSC3K-162. On the other hand, the higher adsorption values for very low pressures in HF CM reflect the gentler but sooner rise in the isotherm; a cluster of 6 water molecules was obtained from the fitting model, which is significantly smaller than for MSC3K-162. It seems that the higher the concentration of hydrophilic groups, the smaller the water cluster.

It is also seen that both MSC3K-162 and HF CM isotherms present just a little hysteresis, already attributed to the different mechanisms of adsorption and desorption. This behavior is less pronounced in the case of the membranes, probably due to the formation of smaller clusters that impairs the dissociation into individual water molecules. On the other hand, the larger cluster formed in the adsorbent should be more easily divided into individual water molecules.

The adsorbed water density d_a obtained by fitting the proposed model to the experimental data is d_a = 0.69 g cm^{-3} for both MSC3K-162 and HF CM, cf. Table 2.11. In the literature, and concerning microporous carbonaceous materials, different water adsorbed density values can be found, ranging from 0.57-0.66 g cm^{-3} [71], 0.81-0.86 g cm^{-3} [87], 0.9 g cm^{-3} [77] up to 0.92 g cm^{-3} [67, 88]; the value obtained in this work is then within the density range found in the literature.

Table 2.11 – Water density, d_a, inside micropores assuming that it fills the overall micropore volume, W_{0,CO_2}.

	W_{0,CO_2} (cm^3 kg^{-1})	d_a (g cm^{-3})
MSC3K-162	185.7 [a]	0.69
HF CM	168.7 [a]	0.69

a) Previously reported in Table 2.4.

These densities were determined under the assumption that water fully fills the micropore volume. Carrott [89], and later Lagorsse et al. [71] stated that the different values of micropore volumes obtained from water data are due to the impossibility of a water cluster to enter pores with sizes close to the dimension of just one water molecule. A water molecule can pass through constrictions but it will only adsorb in the form of a cluster at a certain minimum pore width capable of comprising a cluster. A cluster of 13-water molecules and 6-water molecules for respectively, CMS adsorbent and CMS membrane will only fit pores larger than the cluster size. In fact, if the density of water in the adsorbed state is considered to be 0.92 g cm^{-3}, as proposed by Alcaniz-Monge et al. [88], then the micropore volume obtained would be inferior to that obtained from CO_2 adsorption. This is an indication that there might be pores, smaller than the cluster sizes, which are not filled with water vapor.

2.2.4.4. Kinetics of water vapor adsorption

Together with adsorption equilibrium data, the kinetics of water adsorption may provide important information about the materials under study. Kinetics can in fact help understanding the adsorption mechanism.

There is a lack of information in the literature concerning the kinetics of water vapor adsorption in carbon molecular sieve materials. Most cases consider a linear driving force (LDF) model [60, 66, 78, 90-92]:

$$F = 1 - e^{-kt} \tag{2.40}$$

where F is the fractional uptake, t is the time and k is the LDF rate constant.

Uptake curves of water vapor have been determined for MSC3K-162 and HF CM, at 29.5 ºC for the entire range of relative pressures. Figure 2.25 shows an example of uptake curves for MSC3K-162 and HF CM, at respectively 0.58 and 0.35 relative pressure. The LDF model represents accurately the experimental data for the relative pressures shown. Similar results were obtained for all the pressures studied. The dependence of the LDF rate constants with the relative pressure is shown in Figure 2.26.
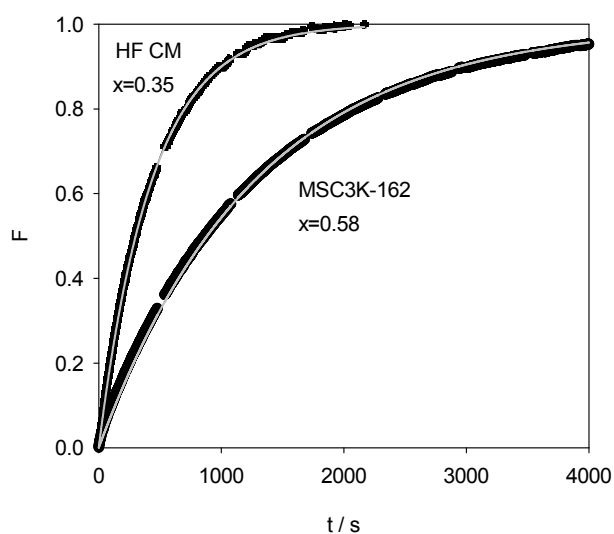
Figure 2.25 - Uptake curves for water vapor on MSC3K-162 and HF CM at 29.5 ºC. The circles represent the experimental values and the line the LDF fitting.
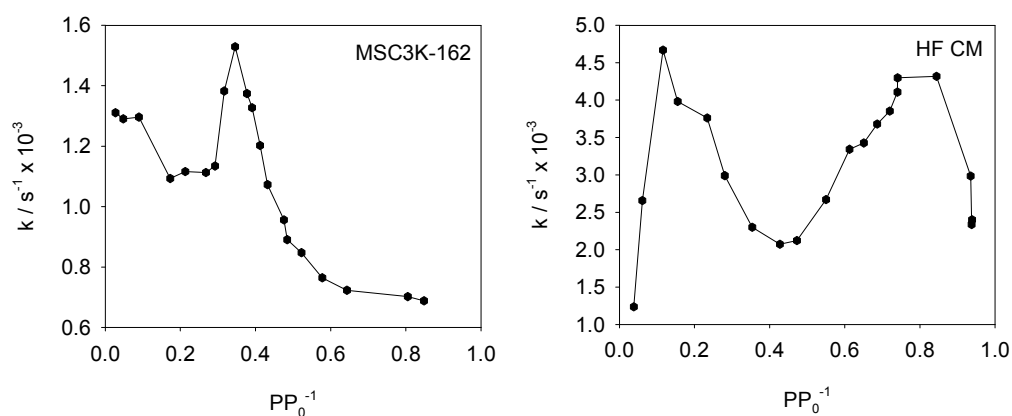
Figure 2.26 - LDF rate constants as a function of the water vapor relative pressure at 29.5 ºC for MSC3K-162 and HF CM.

As suggested in the previous section, the primary sites are responsible for the strongest interactions with the water molecules. Nevertheless, it is known that depending on the nature and number of the functional groups, which are primary water adsorption sites, interactions can be more or less strong, leading to different rates of adsorption [91]. In agreement with this, both materials show high adsorption rates at low relative pressures, cf. Figure 2.26. In addition, these values are higher for HF CM than for MSC3K-162. Back to Figure 2.18, the first legs of the S-shape curves for adsorption correspond to the highest rates of adsorption: P/P_0 < 0.4 for MSC3K-162 and < 0.2 for HF CM. Afterwards, the steepest parts of both isotherms, in the relative pressure range of 0.4-0.6 for MSC3K-162 and 0.2-0.45 for HF CM, are related to the cluster release from the hydrophilic sites, corresponding to the minimum rate of adsorption. Finally, for P/P_0 > 0.6, the clusters released from the hydrophilic sites, in the MSC3K-162, adsorb on hydrophobic walls with no increase in the adsorption rate. From the equilibrium isotherm, for P/P_0 > 0.6, the plateau for adsorption is almost attained. On the other hand, for P/P_0 = 0.45-0.8, HF CM presents an increase in the adsorption rate associated to the stage of cluster adsorption in hydrophobic carbon. This particular behavior is probably associated to the cluster size, which is also related to the concentration of hydrophilic sites. HF CM originates an average of 6-water molecules per cluster, while MSC3K-162 originates an average of 13-water molecules per cluster. In the latter case, the cluster might probably face a greater blocking or difficulty entering the pores, caused by other water clusters [60, 85]. Finally, for P/P_0 > 0.8, HF CM presents a decrease on the adsorption rate. This may be justified by the complete surface coverage by water molecules, as suggested by others [60, 90, 91].

2.2.5. Conclusions

Water vapor adsorption and desorption equilibrium isotherms were determined and compared for a carbon molecular sieve adsorbent, MSC3K-162, and a carbon hollow fiber membrane, HF CM. Both materials exhibited a type V behavior, with a well

defined S-shaped curve. Since these are carbonaceous materials, the water vapor adsorption is attributed to the existence of oxygenated functional groups, where water molecules firstly adsorb [61, 64]. The X-ray microanalyses confirmed the existence of oxygen in addition to carbon. In fact, up to relative pressures of 0.3 and 0.4, respectively for HF CM and MSC3K-162, it is considered that adsorption around hydrophilic groups occurs. The second and steepest part of each isotherm occurs in the range of 0.2-0.45 and 0.4-0.6 relative pressures for respectively HF CM and MSC3K-162. At this stage, the cluster has enough dispersion energy to be released from the functional groups and to adsorb on hydrophobic space or carbon walls. Finally, the last plateau represents the filling up of pores with water clusters. It was also conclude that HF CM has a greater hydrophilic character than MSC6K-162. This was sustained by TG analyses, which showed a larger content of heteroatoms for HF CM, and by the significant adsorption at very low pressures.

Several models were applied to fit adsorption experimental data. The model by Do et al. [65], considering a cluster of 5 water molecules, did not describe well the experimental data for MSC3K-162, suggesting that a different cluster size should be considered. The model developed by Lagorsse et al. [71] to describe both adsorption and desorption branches, considering a cluster of 7 molecules, was also unsuccessful. A new model was developed, as an extension of the previous two models. It describes the adsorption and desorption branches and assumes that clusters of a generic size m are formed. This model fit the experimental results quite well for both materials.

The adsorption kinetics was assessed for both carbon molecular sieves and was well described by a LDF model. The different adsorption rate intervals obtained were related to the distinguishable stages of the adsorption isotherms.

2.2.6. Acknowledgements

MSC3K-162, and to CEMUP which allowed the SEM/EDS analysis (REEQ/1062/CTM/2005 and REDE/1512/RME/2005 funding provided by FCT).

2.3. References

[1]   R.T. Yang, Adsorbents: Fundamentals and Applications, John Wiley & Sons, Inc., New Jersey, 2003.

[2]   D.M. Ruthven, S. Farooq, K.S. Knaebel, Pressure Swing Adsorption, John Wiley & Sons, Inc., New York, 1994.

[3]   H.J. Schröter, H. Jüngten, Gas separation by pressure swing adsorption using carbon molecular sieves, in: A.E. Rodrigues, M.D. LeVan, D. Tondeur (Eds.), Adsorption: Science and Technology, Kluwer Academic Publishers, Vimeiro, 1989, pp. 269-283.

[4]   X.S. Feng, C.Y. Pan, J. Ivory, D. Ghosh, Integrated membrane/adsorption process for gas separation, Chem. Eng. Sci. 53 (1998) 1689-1698.

[5]   I.A.A.C. Esteves, J.P.B. Mota, Simulation of a new hybrid membrane/pressure swing adsorption process for gas separation, Desalination 148 (2002) 275-280.

[6]   R.W. Baker, Future directions of membrane gas separation technology, Ind. Eng. Chem. Res. 41 (2002) 1393-1411.

[7]   J.E. Koresh, A. Soffer, Molecular-Sieve Carbon Permselective Membrane .1. Presentation of a New Device for Gas-Mixture Separation, Sep. Sci. Technol. 18 (1983) 723-734.

[8]   A. Soffer, J. Gilron, S. Saguee, R. Hed-Ofek, H. Cohen, Process for the production of hollow carbon fiber membranes, US005925591, 1999.

[9]   A. Soffer, M. Azariah, A. Amar, H. Cohen, D. Golub, S. Saguee, H. Tobias, Method for improving the selectivity of carbon membranes by carbon chemical vapor deposition, US005695818, 1997.

[10]   A. Soffer, J. Koresh, S. Saggy, Separation device, US004685940, 1987.

[11]   M.B. Hagg, J.A. Lie, A. Lindbrathen, Carbon molecular sieve membranes - A promising alternative for selected industrial applications, Ann. N.Y. Acad. Sci. 984 (2003) 329-345.

[12]   I. Menendez, A.B. Fuertes, Aging of carbon membranes under different environments, Carbon 39 (2001) 733-740.

[13]   S. Lagorsse, F.D. Magalhães, A. Mendes, Aging study of carbon molecular sieve membranes, J. Membr. Sci. 310 (2008) 494-502.

[14]   K. Abe, Carbon molecular sieve, US005238888, 1993.

[15]   T. Aibe, K. Shibata, Activated carbon adsorbent and applications thereof, US005403548, 1995.

[16]   S.R. Auvil, M.S. Joan, S. Rajagopalan, Air separation by pressure swing adsorption with a high capacity carbon molecular sieve, US 5240474, 1993.

[17] A.L. Cabrera, J.N. Armor, Modified carbon molecular sieve adsorbents, US005071450, 1991.

[18] K. Itoga, Y. Tsutsumi, M. Tsuji, A. Tatebayashi, Nitrogen-cointaining molecular sieving carbon, a process for preparing the same and use thereof, US005670124, 1997.

[19] T. Ohsaki, S. Abe, Process for manufacturing a carbon molecular sieve, US004742040, 1988.

[20] C. Pak, J. Kim, H. Lee, Carbon molecular sieve and method for manufacturing the same, US006812187B1, 2004.

[21] R. Ryoo, S. Jun, S.H. Joo, C.H. Ko, Carbon molecular sieve material with structural regularity, method for preparing the same and use thereof, US006585948, 2003.

[22] T. Takeuchi, M. Kameno, Moldable compositions of activated carbon and molded articles produced therefrom, US005043310, 1991.

[23] S. Lagorsse, F.D. Magalhães, A. Mendes, Carbon molecular sieve membranes - Sorption, kinetic and structural characterization, J. Membr. Sci. 241 (2004) 275-287.

[24] D. Cazorla-Amoros, J. Alcaniz-Monge, A. Linares-Solano, Characterization of activated carbon fibers by CO2 adsorption, Langmuir 12 (1996) 2820-2824.

[25] D. Lozano-Castello, D. Cazorla-Amoros, A. Linares-Solano, Usefulness of CO2 adsorption at 273 K for the characterization of porous carbons, Carbon 42 (2004) 1233-1242.

[26] F. Dreisbach, H.W. Losch, P. Harting, Highest pressure adsorption equilibria data: Measurement with magnetic suspension balance and analysis with a new adsorbent/adsorbate-volume, Adsorption 8 (2002) 95-109.

[27] R. Hussain, R. Qadeer, M. Ahmad, M. Saleem, X-ray diffraction study of heat-treated graphitized and ungraphitized carbon, Turkish Journal of Chemistry 24 (2000) 177-183.

[28] Y.Z. Song, G.T. Zhai, G.S. Li, J.L. Shi, Q.G. Guo, L. Liu, Carbon/graphite seal materials prepared from mesocarbon microbeads, Carbon 42 (2004) 1427-1433.

[29] D. Cazorla-Amoros, J. Alcaniz-Monge, M.A. de la Casa-Lillo, A. Linares-Solano, CO2 as an adsorptive to characterize carbon molecular sieves and activated carbons, Langmuir 14 (1998) 4589-4596.

[30] N.D. Hutson, R.T. Yang, Theoretical Basis for the Dubinin-Radushkevitch (D-R) Adsorption Isotherm Equation, Adsorption 3 (1997) 189-195.

[31] H. Marsh, F. Rodríguez-Reinoso, Activated Carbon, Mater. Sci., Elsevier, 2006, pp. 31-34.

[32] F. Stoeckli, A. Slasli, D. Hugi-Cleary, A. Guillot, The characterization of microporosity in carbons with molecular sieve effects, Microporous Mesoporous Mater. 51 (2002) 197-202.

[33] F. Stoeckli, T.A. Centeno, On the characterization of microporous carbons by immersion calorimetry alone, Carbon 35 (1997) 1097-1100.

[34] C. Nguyen, D.D. Do, Adsorption of supercritical gases in porous media: Determination of micropore size distribution, J. Phys. Chem. B 103 (1999) 6900-6908.

[35] C. Nguyen, D.D. Do, K. Haraya, K. Wang, The structural characterization of carbon molecular sieve membrane (CMSM) via gas adsorption, J. Membr. Sci. 220 (2003) 177-182.

[36] S. Lagorsse, A. Leite, F.D. Magalhães, N. Bischofberger, J. Rathenow, A. Mendes, Novel carbon molecular sieve honeycomb membrane module: configuration and membrane characterization, Carbon 43 (2005) 809-819.

[37] S.M. Wang, Y.X. Yu, G.H. Gao, Grand canonical Monte Carlo and non-equilibrium molecular dynamics simulation study on the selective adsorption and fluxes of oxygen/nitrogen gas mixtures through carbon membranes, J. Membr. Sci. 271 (2006) 140-150.

[38] Y.G. Seo, G.H. Kum, N.A. Seaton, Monte Carlo simulation of transport diffusion in nanoporous carbon membranes, J. Membr. Sci. 195 (2002) 65-73.

[39] W.A. Steele, The Interaction of Gases with Solid Surfaces, Pergamon Press, Oxford, 1974.

[40] S.W. Rutherford, C. Nguyen, J.E. Coons, D.D. Do, Characterization of carbon molecular sieves using methane and carbon dioxide as adsorptive probes, Langmuir 19 (2003) 8335-8342.

[41] P.I. Ravikovitch, A. Vishnyakov, R. Russo, A.V. Neimark, Unified approach to pore size characterization of microporous carbonaceous materials from N2, Ar, and CO2 adsorption isotherms, Langmuir 16 (2000) 2311-2320.

[42] J. Koresh, A. Soffer, Study of Molecular-Sieve Carbons. 1. Pore Structure, Gradual Pore Opening and Mechanism of Molecular-Sieving, J Chem Soc Farad T 1 76 (1980) 2457-2471.

[43] D.D. Do, Adsorption Analysis: Equilibria and Kinetics, Imperial College Press, London, 1998.

[44] S. Sircar, Basic research needs for design of adsorptive gas separation processes, Ind. Eng. Chem. Res. 45 (2006) 5435-5448.

[45] D.M. Ruthven, L.K. Lee, H. Yucel, Kinetics of Non-Isothermal Sorption in Molecular-Sieve Crystals, AlChE J. 26 (1980) 16-23.

[46] D.M. Ruthven, Principles of adsorption and adsorption processes, Wiley & Sons, Inc, New York, 1984.

[47]   S.W. Rutherford, D.D. Do, Characterization of carbon molecular sieve 3A, Langmuir 16 (2000) 7245-7254.

[48]   D.D. Do, A model for surface diffusion of ethane and propane in activated carbon, Chem. Eng. Sci. 51 (1996) 4145-4158.

[49]   Y.S. Bae, C.H. Lee, Sorption kinetics of eight gases on a carbon molecular sieve at elevated pressure, Carbon 43 (2005) 95-107.

[50]   P.J.M. Carrott, I.P.P. Cansado, M.M.L.R. Carrott, Carbon molecular sieves from PET for separations involving CH4, CO2, O2 and N2, Appl. Surf. Sci. 252 (2006) 5948-5952.

[51]   C.R. Reid, I.P. O'koye, K.M. Thomas, Adsorption of gases on carbon molecular sieves used for air separation. Spherical adsorptives as probes for kinetic selectivity, Langmuir 14 (1998) 2415-2425.

[52]   C.R. Reid, K.M. Thomas, Adsorption of gases on a carbon molecular sieve used for air separation: Linear adsorptives as probes for kinetic selectivity, Langmuir 15 (1999) 3206-3218.

[53]   M.B. Rao, S. Sircar, Performance and pore characterization of nanoporous carbon membranes for gas separation, J. Membr. Sci. 110 (1996) 109-118.

[54]   H. Suda, K. Haraya, Gas permeation through micropores of carbon molecular sieve membranes derived from Kapton polyimide, J. Phys. Chem. B 101 (1997) 3988-3994.

[55]   H.W. Habgood, The Kinetics of Molecular Sieve Action - Sorption of Nitrogen-Methane Mixtures by Linde Molecular Sieve 4a, Can. J. Chem. 36 (1958) 1384-1397.

[56]   Y.D. Chen, R.T. Yang, Concentration-Dependence of Surface-Diffusion and Zeolitic Diffusion, AIChE J. 37 (1991) 1579-1582.

[57]   S.K. Bhatia, D. Nicholson, Anomalous transport in molecularly confined spaces, J. Chem. Phys. 127 (2007) 124701-124710.

[58]   J.K. Brennan, T.J. Bandosz, K.T. Thomson, K.E. Gubbins, Water in porous carbons, Colloids Surf., A 187 (2001) 539-568.

[59]   I. Avraham, A. Danon, J.E. Koresh, Water coadsorption effect on the physical adsorption of N2 and O2 at room temperature on carbon molecular sieve fibers, Phys. Chem. Chem. Phys. 1 (1999) 479-484.

[60]   A.W. Harding, N.J. Foley, P.R. Norman, D.C. Francis, K.M. Thomas, Diffusion barriers in the kinetics of water vapor adsorption/desorption on activated carbons, Langmuir 14 (1998) 3858-3864.

[61]   M.M. Dubinin, E.D. Zaverina, V.V. Serpinsky, The Sorption of Water Vapour by Active Carbon, J. Chem. Soc. (1955) 1760-1766.

[62]   S. Furmaniak, P.A. Gauden, A.P. Terzyk, G. Rychficki, Water adsorption on carbons - Critical review of the most popular analytical approaches, Adv. Colloid Interface Sci. 137 (2008) 82-143.

[63]   N.J. Foley, K.M. Thomas, P.L. Forshaw, D. Stanton, P.R. Norman, Kinetics of water vapor adsorption on activated carbon, Langmuir 13 (1997) 2083-2089.

[64]   M.M. Dubinin, Water-Vapor Adsorption and the Microporous Structures of Carbonaceous Adsorbents, Carbon 18 (1980) 355-364.

[65]   D.D. Do, H.D. Do, A model for water adsorption in activated carbon, Carbon 38 (2000) 767-773.

[66]   L. Cossarutto, T. Zimny, J. Kaczmarczyk, T. Siemieniewska, J. Bimer, J.V. Weber, Transport and sorption of water vapour in activated carbons, Carbon 39 (2001) 2339-2346.

[67]   J. Alcaniz-Monge, A. Linares-Solano, B. Rand, Mechanism of adsorption of water in carbon micropores as revealed by a study of activated carbon fibers, J. Phys. Chem. B 106 (2002) 3209-3216.

[68]   Q. Nan, M.D. LeVan, Adsorption equilibrium modeling for water on activated carbons, Carbon 43 (2005) 2258-2263.

[69]   C.L. McCallum, T.J. Bandosz, S.C. McGrother, E.A. Muller, K.E. Gubbins, A molecular model for adsorption of water on activated carbon: Comparison of simulation and experiment, Langmuir 15 (1999) 533-544.

[70]   T. Iiyama, Y. Kobayashi, K. Kaneko, S. Ozeki, Situ small-angle X-ray scattering study of cluster formation in carbon micropores, Colloids Surf., A 241 (2004) 207-213.

[71]   S. Lagorsse, M.C. Campo, F.D. Magalhães, A. Mendes, Water adsorption on carbon molecular sieve membranes: Experimental data and isotherm model, Carbon 43 (2005) 2769-2779.

[72]   S.S. Barton, M.J.B. Evans, S. Liang, J.A.F. McDonald, The influence of surface modification of BPL carbons on aging, Carbon 34 (1996) 975-982.

[73]   M. Ottaway, Use of Thermogravimetry for Proximate Analysis of Coals and Cokes, Fuel 61 (1982) 713-716.

[74]   T.S. Farris, C.G. Coe, J.N. Armor, J.M. Schork, High capacity coconut shell char for carbon molecular sieves, US 5164355, 1991.

[75]   C. Vagner, G. Finqueneisel, T. Zimny, J.V. Weber, Water vapour adsorption on activated carbons: comparison and modelling of the isotherms in static and dynamic flow conditions, Fuel Process. Technol. 77 (2002) 409-414.

[76]   M. Neitsch, W. Heschel, M. Suckow, Water vapor adsorption by activated carbon: a modification to the isotherm model of Do and Do, Carbon 39 (2001) 1437-1438.

[77]   S.W. Rutherford, Modeling water adsorption in carbon micropores: Study of water in carbon molecular sieves, Langmuir 22 (2006) 702-708.

[78]   A.J. Fletcher, Y. Yuzak, K.M. Thomas, Adsorption and desorption kinetics for hydrophilic and hydrophobic vapors on activated carbon, Carbon 44 (2006) 989-1004.

[79]   F. Stoeckli, Water adsorption in activated carbons of various degrees of oxidation described by the Dubinin equation, Carbon 40 (2002) 969-971.

[80]   M.M. Dubinin, V.V. Serpinsky, Isotherm Equation for Water-Vapor Adsorption by Microporous Carbonaceous Adsorbents, Carbon 19 (1981) 402-403.

[81]   F. Stoeckli, T. Jakubov, A. Lavanchy, Water-Adsorption in Active Carbons Described by the Dubinin-Astakhov Equation, Journal of the Chemical Society-Faraday Transactions 90 (1994) 783-786.

[82]   O. Talu, F. Meunier, Adsorption of associating molecules in micropores and application to water on carbon, AIChE J. 42 (1996) 809-819.

[83]   A.O. Malakhov, V.V. Volkov, Cooperative multimolecular sorption equation: Application to an alcohol-poly(1-trimethylsilyl-1-propyne) system, Polymer Science Series A 42 (2000) 1120-1126.

[84]   S.W. Rutherford, Application of cooperative multimolecular sorption theory for characterization of water adsorption equilibrium in carbon, Carbon 41 (2003) 622-625.

[85]   S.W. Rutherford, J.E. Coons, Equilibrium and kinetics of water adsorption in carbon molecular sieve: Theory and experiment, Langmuir 20 (2004) 8681-8687.

[86]   D.D. Do, S. Junpirom, H.D. Do, A new adsorption–desorption model for water adsorption in activated carbon, Carbon 47 (2009) 1466-1473.

[87]   T. Iiyama, M. Ruike, K. Kaneko, Structural mechanism of water adsorption in hydrophobic micropores from in situ small angle X-ray scattering, Chem. Phys. Lett. 331 (2000) 359-364.

[88]   J. Alcaniz-Monge, D. Lozano-Castello, Assessment of ultramicroporosity on carbon molecular sieves by water adsorption, Adsorpt. Sci. Technol. 21 (2003) 841-848.

[89]   P.J.M. Carrott, Molecular-Sieve Behavior of Activated Carbons, Carbon 33 (1995) 1307-1312.

[90]   A.J. Fletcher, Y. Uygur, K.M. Thomas, Role of surface functional groups in the adsorption kinetics of water vapor on microporous activated carbons, J. Phys. Chem. C 111 (2007) 8349-8359.

[91]   P. Kim, Y.J. Zheng, S. Agnihotri, Adsorption equilibrium and kinetics of water vapor in carbon nanotubes and its comparison with activated carbon, Ind. Eng. Chem. Res. 47 (2008) 3170-3178.

[92]   J. Bedia, J. Rodriguez-Mirasol, T. Cordero, Water vapour adsorption on lignin-based activated carbons, J. Chem. Technol. Biotechnol. 82 (2007) 548-557.

Chapter III

Chapter 3 - Preparation and Characterization of CMSM

3.1. Influence of pyrolysis parameters on the performance of CMSM[3]

3.1.1. Abstract

Carbon hollow fiber membranes have been prepared by pyrolysis of a P84/S-PEEK blend. Proximate analysis of the precursor was performed using thermogravimetry (TGA) and a carbon yield of approximately 40 % can be obtained. This study aimed at understanding the influence of pyrolysis parameters - end temperature, quenching effect and soaking time - on the membrane properties. Permeation experiments were performed with N_2, He and CO_2. Scanning electron microscopy (SEM) has been done for all carbon hollow fibers. The highest permeances were obtained for the membrane submitted to an end temperature of 750 $^{\circ}$C and the highest ideal selectivities for an end temperature of 700 $^{\circ}$C. In both cases, the membranes were quenched to room temperature.

3.1.2. Introduction

Carbon molecular sieve membranes (CMSM), pioneered by Koresh and Soffer in the 80's, are a very recent research topic in the area of gas separation. These inorganic materials present great advantages over polymeric membranes, since they have comparatively high permeabilities and selectivities, together with high thermal and chemical stability [1-4]. The main applications for this type of membranes are, among

---

others, air separation, landfill gas recovery, olefin/paraffin separation, hydrogen recovery and natural gas processing.

Carbon membranes are produced by pyrolysis of a polymeric precursor under an inert atmosphere [1, 3]. The main precursors mentioned in literature are, among others, polyimide, polyfurfuryl alcohol polyacrylonitrile, phenolic resins and cellulose [3]. Theprecursor material should have a high carbon yield and be thermosetting [2]. To further improve the separation capacity of CMSM, some authors have functionalized the carbon matrix by adding metals with affinity towards one of the permeating species [5]. This strategy was followed by Barsema et al. [6, 7]. These authors used a blend of P84/Ag-S-PEEK to produce flat sheet carbon membranes and determined the influence of Ag on the membranes' separation performance. However, the influence of the pyrolysis end temperature, soaking time or cooling procedure was not assessed. In the present work, a P84/S-PEEK blend is used for the first time as a hollow fiber precursor for preparing carbon membranes and to study some of the pyrolysis parameters on the final performance. The hollow fiber configuration provides higher mechanical stability than flat sheet membranes.

The preparation of CMSM should be directed towards the tailoring of the final carbonaceous micropore network. The influence of the pyrolysis parameters and complementary treatments used for producing the final carbon membranes should be studied in order to better suit a certain application [1, 8]. Examples of these complementary treatments are pore closing by carbon vapor deposition using a carbon-containing source, or pore widening by activation under an oxidative atmosphere [3, 9-11]. The temperature programs followed in the pyrolysis, the cooling steps and the gas atmosphere employed, are all important aspects that have to be studied and optimized according to the selected precursor, having in mind the final application.

CMSM have two major disadvantages that still have to be overcome: mechanical brittleness and aging effects [4, 12]. Aging is caused by oxygen chemisorption on the carbon surface, which reduces the membrane performance due to reduction of pore size [12]. The presence of oxygenated functional groups on the surface of CMSM was reported by other authors [12-14]. The resulting adsorption of species with affinity to

102

these oxygenated functional groups, such as CO_2 may also contribute to this fact [15]. When the feed mixture is humidified, the oxygen content on the carbon matrix may lead to the adsorption of water vapor, which may block the passage of other species [16]. In this work the use of P84/S-PEEK hollow fibers is suggested for overcoming these problems. Evidences of aging effects will also be looked for in carbon membranes out of this precursor.

3.1.3. Experimental

3.1.3.1. Materials and Precursor preparation

The precursor asymmetric hollow fiber membranes were prepared from a blend of 3.5 wt% S-PEEK and 96.5 wt% P84. P84 (BTDA-TDI/MDI) is a commercial available co-polyimide from Lenzing and S-PEEK is a custom made polymer obtained by sulphonation of poly (ether ether ketone) (PEEK, Victrex). A few % of S-PEEK in the blend introduces additional hydrophilicity and may help suppressing macrovoids in spinning fibers. The P84/S-PEEK hollow fibers were obtained by the dry/wet phase separation process using spinning technology. For this purpose the dope used consisted of 71 % of NMP (N-methyl-pyrrolidone, Merck 99 %), and 18 % P84/S-PEEK blend. Additives were 6 wt% polyvinylpyrrolidone (PVP K90, Acros) and 5 wt% glycerol (Merck > 99 %) and the coagulant medium was tap water. In order to induce pore formation on the inside and outside skin, a bore and shell liquid were used with 80/20 and 90/10 wt% NMP/H_2O, respectively. An air gap was used of 20 mm and the fibers were spun at room temperature. More details about the spinning process can be found elsewhere [17, 18].

3.1.3.2. Thermogravimetric analysis of precursor

The precursor used in this study was a co-polyimide P84/S-PEEK blend. The thermogravimetric proximate analysis performed is a method developed by Ottaway [19] to determine the moisture, volatile matter, fixed carbon and ash contents of a sample. The heating procedure consists on rising the temperature at 25 °C min^{-1} under nitrogen, with dwelling times at 50 °C and 110 °C (10 and 7 min, respectively)

and at 950 ºC (9 min under nitrogen plus 11 min under oxygen). After the first dwell at 110 ºC, humidity is removed. Up to the second dwell, under nitrogen, volatile matter is released. Finally, after 11 min under oxygen at 950 ºC, all the fixed carbon is lost, yielding ashes, if existent.

The proximate analysis of the precursor was performed in a Netzsch TG 209 F1 Iris thermogravimetric balance.

3.1.3.3. Fabrication of carbon hollow fiber membranes

The pyrolysis occurred inside a quartz tube installed in a Carbolite® TZF 12/100 High Temperature Tubular Furnace with a Eurotherm 2408 CP temperature controller, under a 50 ml_N min^{-1} nitrogen atmosphere. The hollow fibers were supported on a stainless steel grid and introduced into the furnace with a cane as illustrated in Figure 3.1.
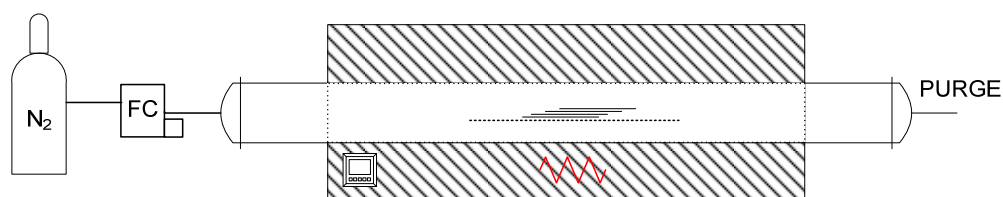
Figure 3.1 - Scheme of the pyrolysis set-up.

The temperature program employed is based on a program developed by Barsema et al. [6, 20] and shown in Figure 3.2. The membranes were heated from room temperature up to 150 ºC at 50 ºC min^{-1}, remaining 15 min at this temperature. This step allowed the removal of any possible adsorbed water or residual solvents. Thereafter, the membranes were heated up to 350 ºC at 5 ºC min^{-1}. The heating rate up to the final temperature was then 1 ºC min^{-1}. This low heating rate prevents cracks from occurring during the formation of the carbon matrix. After achieving the maximum temperature of pyrolysis, here designated as end temperature, the membranes were submitted to quenching or to natural cooling. In some cases, they were kept at the end temperature for a certain time before cooling (soaking step).

The main differences from Barsema's protocol relate to the end temperature, quenching procedure and soaking time.

The quenching consisted on fast cooling inside a jacketed container, refrigerated with cold tap water, under nitrogen. *"No"* quenching means that the sole driving force for cooling was the temperature difference between the inside of the furnace and the surrounding room atmosphere. The transfer of the carbon hollow fibers from the furnace into the quenching container was performed as fast as possible, in order to minimize air exposure. Afterwards the membranes were stored in a box flushed with nitrogen.
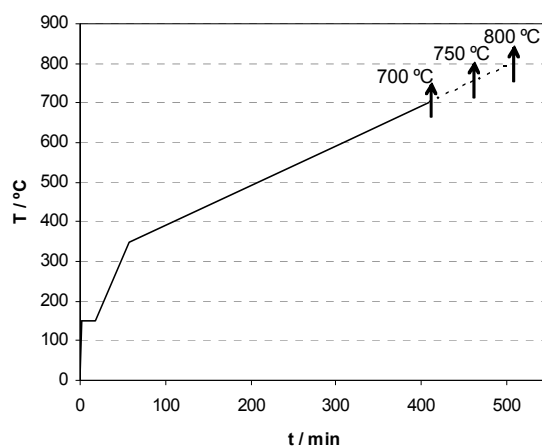
Figure 3.2 - Heating procedure to prepare carbon membranes based in literature [6, 7].

The influence of a final step – soaking time – in which the oven end temperature was kept constant for 2 h before quenching was also analysed.

These two steps, soaking and quenching, may probably lead to microstructural rearrangements, affecting the pore size distribution and, consequently, the membrane selectivity.

Table 3.1 shows the identification of each carbon membrane prepared, concerning its pyrolysis' parameters.

Table 3.1 - Identification of the samples and pyrolysis' parameters.

Sample	T_{END} (ºC)	Soaking time (h)	Quenching
HF-700-A	700	0	Yes
HF-700-B	700	0	No
HF-750-A	750	0	Yes
HF-750-B	750	0	No
HF-800-A	800	0	Yes
HF-800-B	800	0	No
HF-700-ST2h	700	2	Yes

3.1.3.4. Scanning electron microscopy

All samples identified in Table 3. were characterized by means of scanning electron microscopy (SEM) using a JEOL JSM 5600 LV SEM; the fibers were fractured and the cross sections analyzed. All the samples were previously sputtered with gold using a Balzers Union SCD 040 to allow better conductivity for SEM. Through the pictures taken it was possible to measure the thickness, ℓ , of the selective layer located in the fiber bore side, the inner and outer diameter of each fiber, D_{in} and D_{out} , and consequently the wall thickness, ℓ_w. This information, together with the length of the carbon hollow fiber, L , allowed the calculation of the effective area of the selective layer of the membrane, A_m .

3.1.3.5. Permeation

After pyrolysis, the resulting carbon membranes were assembled in a module. Figure 3.3 illustrates the membrane module, where it is evidenced that feed circulates on the shell side, whereas permeate is removed from the bore side. These individual modules were then connected to a stainless steel housing which was introduced in a temperature controlled cabinet.
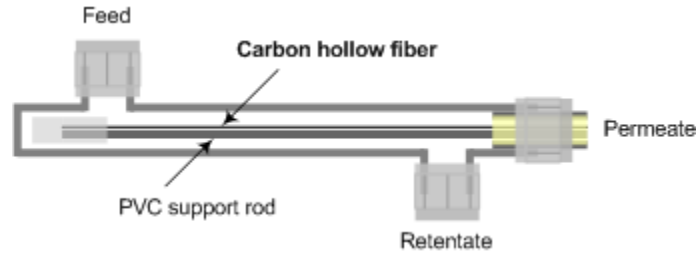
Figure 3.3 - Scheme of the membrane module.

The permeation experiments were conducted at 30 °C, using a pressure increment method. The several carbon membranes were tested towards N_2, He and CO_2. All the modules were submitted to 2 bar feed pressure on the shell side whereas vacuum was applied from the bore side. Here, ideal gas behavior was assumed and, hence, the monocomponent permeance, P/ℓ was calculated according to eq. (3.1),

$$\frac{P}{\ell} = \frac{V_P\, \upsilon_M\, \left(p_l^t - p_l^0\right)}{\Re\, T\, t\, A_m\left(p_h - p_l\right)}$$
(3.1)

where V_P is the volume of the tank where the permeate is collected, p_l and p_h are respectively, the permeate pressure and the feed pressure, A_m is the effective area of the fiber, T is the absolute temperature, υ_M is the molar volume of the gas, $\Re$ is the gas constant, and t is the time. The ideal selectivity $\alpha_{i/j}$ for a certain pair of gases i and j is obtained from eq. (3.2),

$$\alpha_{i/j} = \frac{P_i}{P_j}$$
(3.2)

where P_i and P_j are the permeabilities of species i and j, respectively.

3.1.4. Results and Discussion

3.1.4.1. Thermogravimetry

Proximate analysis is normally performed in order to determine the percentage of humidity, volatile matter, fixed carbon and ashes [19]. The most important variable in this study is the yield of fixed carbon. This percentage accounts for the carbon content of the final carbon membrane. Higher fixed carbon content indicates that the resultant membranes have the potential to become mechanically more stable. Yields of fixed carbon are usually in the range of 25-50 %, depending on the precursor material [21]. Figure 3.4 presents the results of the proximate analysis. The normalized sample mass is represented as a function of time and the heating procedure is referred to the secondary axis. The yield of fixed carbon is determined from the difference between the final mass and the mass at 63 min, being approximately 40 %. In the literature some polymers are reported to have carbon yields of almost 60 % [22]. However, the result of 40 % for P84/S-PEEK blend can still be considered quite good. Probably due to the high P84 content in the blend, this value is similar to those reported in the literature for P84 alone [20, 23].

It is known that S-PEEK and P84 have different thermal stabilities, but it is difficult to distinguish the precise contribution of each component for the shape of the thermogravimetric curve. Nevertheless, the first slope around $200\,^{\circ}C$ should be caused by the degradation of the sulphonic acid group present in S-PEEK. Around $400\,^{\circ}C$, a new slope is observed, due to the degradation of P84 [23]. Since the polymeric chain of S-PEEK decomposes at about $550\,^{\circ}C$, this might be the cause for the final slope [24].
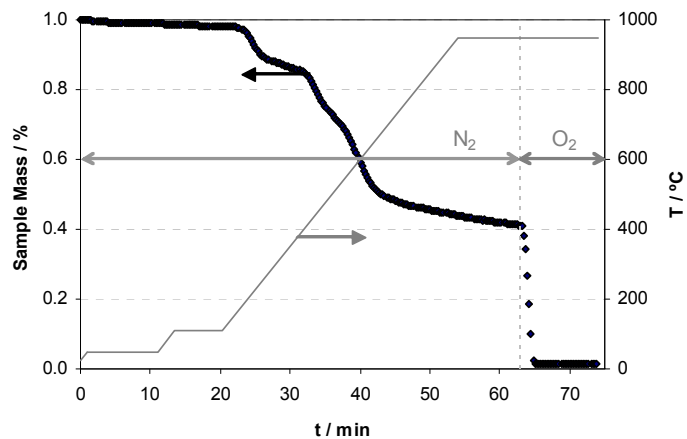
Figure 3.4 - Typical sample mass and temperature histories during proximate analysis procedure.

3.1.4.2. Scanning electron microscopy

SEM pictures were taken to compare the structures of the different samples. The pyrolysis operating variables, such as, end temperature, soaking time and natural cooling procedure, have affected the dimensions of all studied fibers. Besides that, no other considerable changes are observed through SEM. Figure 3.5 provides an example of micrographs taken for sample HF 700B. This membrane was pyrolysed up to 700 ºC and naturally cooled.
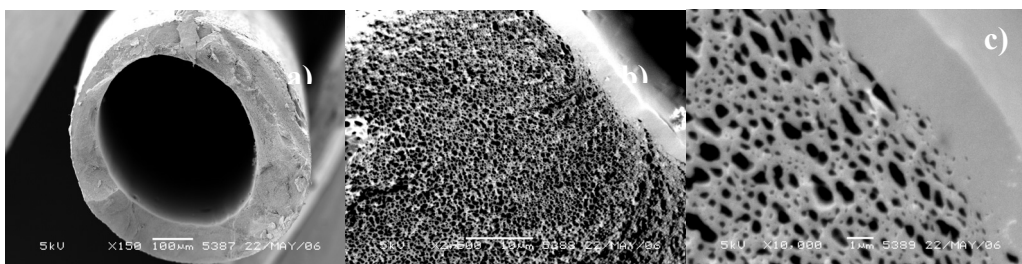
Figure 3.5 - SEM pictures from HF 700 B carbon hollow fiber membrane cross sections: a) global view, x150 magnification, b) inner view, x2500 magnification and c) inner view, x10 000 magnification.

In Table 3.2 the dimensions of all carbon membranes studied are summarized.

Table 3.2 - Characteristics of the carbon membranes.

Sample	D_{in} (μm)	D_{out} (μm)	ℓ_w (μm)	ℓ (μm)	L (cm)	A_m (cm^2)
HF-700-A	401	600	199	3.2	6.9	0.87
HF-700-B	397	588	190	3.1	6.4	0.80
HF-750-A	386	583	197	2.8	6.4	0.78
HF-750-B	387	570	183	2.8	7.5	0.91
HF-800-A	366	562	196	2.7	5.3	0.61
HF-800-B	356	536	180	2.9	6.3	0.70
HF-700-ST2h	397	585	188	2.8	5.4	0.67

It is seen that an increase in the pyrolysis end temperature originates a decrease of the inner and outer diameters of the fibers. This fact is sustained by the results of the proximate analysis, presented in Figure 3.4, which show that between 700 up to 800 °C mass loss still occurs, as volatile matter is still being released. It is during this stage that heteroatoms are set free that the pore network is created. Also in Table 3.2, but regarding the A/B pairs pyrolysed at the same end temperature but with different cooling procedures, it is noticeable that the non-quenched membranes have lower diameters. This may be related to higher mass loss and rearrangement of the carbon matrix occurring during the slow cooling. In agreement with these results, the membrane kept for 2 h at 700 °C before quenching (HF-700-ST2h) shows smaller dimensions than the one quenched with no soaking time (HF-700-A).

3.1.4.3. End temperature effect

The effect of the end temperature on the performance of carbon hollow fiber membranes can be studied by determining single component permeances. Table 3.3 lists permeances and ideal selectivities for samples pyrolysed up to 700, 750 and 800 °C towards N_2, He and CO_2.

Table 3.3 - Effect of end temperature on the permeance of carbon hollow fibers.

Sample	Permeance $(10^{-8} \times m^3_N\ m^{-2}\ kPa^{-1}\ s^{-1})$			Ideal Selectivity		
	N_2	He	CO_2	CO_2/N_2	CO_2/He	He/N_2
HF-700-A	9	107	153	18	1.5	12
HF-750-A	28	176	416	15	2.4	6.4
HF-800-A	14	97	144	10	1.5	7.0

These results are plotted in Figure 3.6.
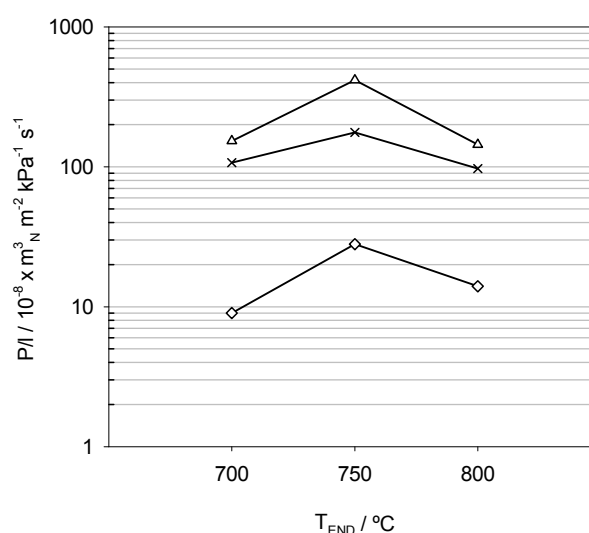
Figure 3.6 - Permeation data of carbon membranes prepared up to 700, 750 and 800 °C: ◇ - N_2, × - He and △ - CO_2.

These results show that the membranes prepared up to 750 °C display the highest permeance towards all the species studied. For all the membranes, the species with lower permeance is N_2, the species with larger size (Lennard-Jones kinetic diameter 0.364 nm). On the other hand, CO_2 has higher permeance than He, despite its larger kinetic diameter (0.33 nm and 0.26 nm, respectively). However, it is known that CO_2 has high adsorption affinity towards carbon matrixes, in opposition to He, which mostly does not adsorb. It is being assumed that adsorption plays a significant role in the mass transport mechanism through these membranes: molecular sieving combined with surface diffusion.

The highest ideal selectivity values are achieved for an end temperature of 700 °C. The increase in permeances observed for all species when the temperature increases up to 750 °C, might indicate that the total pore volume has increased, in the sense that more path ways are created enhancing the transport of the species. On the other hand, the decrease in selectivity for the pairs CO_2/N_2 and He/N_2 suggests that the mean pore width is also increasing, which impairs the sieving effect. At 800 °C end temperature sintering mechanisms explain the decrease in permeances [2, 10, 25].

3.1.4.4. Quenching effect

In this study, as previously mentioned, it was intended to analyze the permeance dependency on the way membranes are cooled from the pyrolysis end temperature down to room temperature.

Table 3.4 summarizes the permeation data and ideal selectivities of the membranes obtained at different end temperatures - 700 up to 800 °C.

Table 3.4 - Quenching effect on the permeance of carbon hollow fibers.

Sample	Quenching	Permeance $(10^{-8} \times m^3_N \, m^{-2} \, kPa^{-1} \, s^{-1})$			Ideal Selectivity		
		N_2	He	CO_2	CO_2/N_2	CO_2/He	He/N_2
HF-700-A	Yes	9	107	153	18	1.5	12
HF-700-B	No	5	84	66	14	0.8	18
HF-750-A	Yes	28	176	416	15	2.4	6.4
HF-750-B	No	16	116	236	14	2.0	7.1
HF-800-A	Yes	14	97	144	10	1.5	7.0
HF-800-B	No	8	44	119	16	2.7	5.8

For each end temperature, the quenched membranes show larger permeances over the ones that were slowly cooled. This qualitatively indicates that the total pore volume created during the heat treatment is maintained when the membrane is quenched. On the other hand, slow cooling allows for structural rearrangements of

the carbon graphene layers, leading to pore narrowing. In the case of the carbon membranes prepared at 700 ºC, the He/N_2 selectivity is higher for the naturally cooled membrane. Furthermore, the fact that the CO_2/He selectivity turned smaller than unity indicates that the pore width has decreased together with the pore volume, revealing the onset of a molecular sieving effect towards CO_2. It is also observed that the highest permeances were generically obtained when the membranes were quenched just after reaching 750 ºC. For 750 ºC, the quenching effect essentially affected the permeance but not the selectivities. Concerning the membranes prepared at 800 ºC, the selectivities have decreased with quenching, except for the pair He/N_2. The pore volume and the pore width are disfavoring the permeation of the more adsorbed species, i.e. CO_2 and N_2.

3.1.4.5. Soaking time effect

The soaking time consisted on keeping the membranes at the end temperature for a certain time interval, just before quenching. The effect of such a soaking time on the performance of carbon membranes is presented in Table 3.5.

Table 3.5 - Effect of soaking time on the permeance of carbon hollow fibers.

Sample	Permeance (10^{-8} x m^3_N m^{-2} kPa^{-1} s^{-1})			Ideal Selectivity		
	N_2	He	CO_2	CO_2/N_2	CO_2/He	He/N_2
HF-700-A	9	107	153	18	1.5	12
HF-700-ST2h	16	134	180	11	1.3	8.2

In this case, from Table 3.5, all the permeances are enhanced by the existence of a final isothermal step at 700 ºC end temperature, but all the selectivities are lower. In fact, it can be seen in Figure 3.4 that mass loss is still occurring at this temperature. By keeping the membranes at 700 ºC for 2 hr, pores are enlarged, but this causes a decrease in selectivity. As expected, this decrease is more accentuated for pairs CO_2/N_2 and He/N_2, since the larger molecule N_2 is more easily penetrating the pore

network. Once again, higher permeances allied to lower selectivities might be an indication that the total pore volume has increased together with the mean pore width.

3.1.4.6. CO₂ exposure

After exposure to CO_2, a check run was performed with N_2 to assess any possible decrease in the membranes permeances. The presence of oxygenated functional groups on the surface of CMSM was reported by other authors [12-14] and the studies done in the scope of this work were to confirm the presence of such groups. CO_2 is electron-deficient and thus acts as a Lewis-acid [15]. Although the membranes are essentially carbon, there may be some oxygenated groups on the surface [26], acting as a Lewis-bases and enhancing interactions with CO_2. Hagg et al. [13] has shown that CO_2 could plug pores leading to a decrease in permeances and suggested regeneration procedures at 200 °C under inert atmosphere. Nevertheless, in the present work the experiments showed no loss in permeance due to CO_2 exposure. The permeance of N_2 after CO_2 exposure matched the one obtained when the membrane was virgin or fresh. This means that, if those oxygenated groups do exist in the carbon matrix, they do not interfere with the membrane's performance which means that carbon membranes done from this precursor have that advantage over the others.

3.1.5. Conclusions

The pyrolysis parameters studied influence the characteristics of the resulting carbon membranes. The highest permeances were obtained for the membranes submitted to an end temperature of 750 °C and to quenching. The highest ideal selectivities were accomplished for the membrane submitted to 700 °C and also to quenching. It was also concluded that the existence of a final soaking time, after reaching the end temperature, just before quenching, improved the permeance of the carbon membranes, but causes a decrease in selectivity. Furthermore, it was observed that the membranes quenched after reaching the end of the process revealed higher

permeances than the ones naturally cooled. No decrease in the performance of the membrane due to CO_2 exposure was observed.

3.1.6. Acknowledgments

3.2. Carbon molecular sieve membranes from cellophane paper[4]

3.2.1. Abstract

Carbon molecular sieve membranes (CMSM) were successfully prepared from cellophane paper by one single pyrolysis step. The influence of pyrolysis parameters on the membranes' structure, morphology and performance were examined through scanning electron microscopy, X-ray microanalysis, X-ray diffraction and single component permeation experiments towards He, H_2, Ar, N_2, CO_2, O_2, CH_4 and water vapor at 29.5 °C. The pyrolysis end temperature was allowed to change from 450 up to 850 °C and the soaking time from 60 to 480 min at 550 °C. The permeabilities reached a maximum for CMSM heated up to 550 °C, without significantly compromising selectivities. The soaking time at this temperature led to pore closing and, consequently, decrease in permeability and an enhancement in selectivity. These membranes were also considerably permeable to water vapor (1000 barrer), and very selective concerning H_2O/CH_4 ($\alpha = 921\text{-}7\,518$) and H_2O/N_2 ($\alpha = 364\text{-}9\,936$) separations. No aging effects were observed due to oxygen or water vapor exposure. The permselectivities of the CMSM prepared up to 550 °C overtook the Robeson bound for polymeric membranes, especially regarding O_2/N_2 ($\alpha = 13\text{-}18$), H_2/N_2, H_2/O_2, H_2/CH_4 and H_2/CO_2 separations.

3.2.2. Introduction

The use of membranes for gas separations has seen significant developments in the past few decades. When compared to other processes, like cryogenic distillation, alkanolamines absorption or condensation, membrane technology shows advantages, such as: no need for phase change, lower implementation complexity and simplicity in scale-up [27]. Nowadays, the main gas separations involving membranes are: recovery of nitrogen from air, separation of hydrogen from nitrogen in ammonia

---

plants or from hydrocarbons in petrochemistry and carbon dioxide and water removal from natural gas [27]. Polymeric membranes are the most used in such industries. However, they can only operate under mild chemical and thermal conditions. On the other hand, inorganic membranes show improved chemical and thermal stability, can operate under larger pressure gradients and exhibit promising permeabilities and selectivities, despite having a less favorable surface to volume ratio and being more expensive and fragile.

The particular interest on carbon molecular sieve membranes (CMSM) for gas separation started back in the 80's with the work of Koresh and Soffer [1, 28]. The research on carbon molecular sieve adsorbents inspired these authors to prepare carbon membranes with molecular sieving properties by controlling and adjusting sequential steps of carbonization, activation and sintering [28], leading to the creation of an adjustable narrow pore size distribution. These carbon membranes present a porous structure where the permeation mechanism is a result of molecular sieving (pore range 0.3-0.5 nm) and/or a surface diffusion (0.5-0.8 nm). The molecular sieving mechanism occurs when smaller permeants are allowed to pass through narrow constrictions rather than larger permeants which cannot pass; the surface diffusion, on the other hand, is based on the selective adsorption/diffusion of permeants on the carbon walls – those which adsorb and diffuse the most will preferentially cross the membrane, in detriment of the more weakly adsorbable and slow permeants. These membranes result from high temperature treatments of a polymeric precursor membrane. The most reported precursors have been polyimides, polyfurfuryl alcohol, phenolic resins, cellulose, etc. [3]. Koresh and Soffer began their work by preparing CMSM for air separation from a cellulosic precursor [29]. Almost 10 years later, Rao and Sircar [30], obtained nanoporous carbon membranes from poly(vinylidene chloride) that could efficiently separate hydrocarbons from hydrogen. In 1994, Jones and Koros [31] prepared hollow fiber carbon membranes based on polyimide precursors with good productivity for air separation. In the following years several other researchers continued using polyimides to further understand the heat treatment parameters and improving the performances of CMSM. Good results concerning other separations H_2/N_2, He/N_2, CO_2/N_2 were also obtained with this type

of precursor. By the same time, Chen and Yang [32] used polyfurfuryl alcohol on a macroporous support to prepare CMSM that applied for the binary separation of CH_4/C_2H_6. The same precursor was also used by Acharya and Foley [33] to prepare carbon membranes for air separation. In 1999, Centeno and Fuertes [34] have coated a macroporous support with a film of phenolic resin; after carbonization the membranes were suitable for O_2/N_2, CO_2/N_2 and CO_2/CH_4 separations. These authors have also tried different polymers such as commercial polyimides, polyetherimide and poly(vinylidene chloride-co-vinyl chloride) [35-37]. Recently, cellulose based precursors for CMSM have been studied by Lie and Hägg [38, 39] and Grainger and Hägg [40] specially for hydrogen purification.

In this work a commercial film of cellophane paper has been used to prepare carbon molecular sieve membranes by employing one single heating step. This is the first time that cellophane paper is studied for CMSM preparation. Cellophane is regenerated cellulose obtained by the viscose process; it is a natural polymer of glucose, 100 % biodegradable and inexpensive. Its chemical components are carbon, hydrogen, and oxygen. The fact that it is industrially produced is advantageous, since it minimizes problems related to the reproducibility and homogeneity of the film properties. The effect of the gas atmosphere employed in the carbonization step on the CMSM structure was assessed by thermogravimetry. The gas permeation performance of the membranes was related to the effect of the end temperature of pyrolysis and of the time interval spent at the final temperature, designated as soaking time. The CMSM were tested for He, H_2, CO_2, O_2, Ar, N_2, CH_4 and water vapor permeation. The separation effectiveness of a prepared membrane for a certain gas mixture is given by its positioning on the empirical upper bound for membrane separation of gases published by Robeson [41] for real binary gas separations in polymeric membranes. However, even for single component experiments of a certain pair of gases, and consequently ideal selectivities, the positioning on the Robeson graph might indicate whether the membranes are promising or not. Further morphologic and structural characterization studies were also performed. The membranes revealed good ideal selectivities with separation performances above the recently revised Robeson's upper bound for polymeric membranes. Due to the high

permeabilities found for water vapor, these membranes may provide a good opportunity for water vapor removal from natural gas or other gaseous streams. They might also be considered in important industrial applications such as separation of nitrogen from air or recovery of hydrogen from synthesis gas.

3.2.3. Experimental

3.2.3.1. Materials

In this study a transparent commercial cellophane paper from Sadipal Stationery Papers, Girona, Spain, was used as a precursor film. Cellophane is regenerated cellulose obtained by the viscose process. The carbon membranes produced in this work were all obtained by a single carbonization of cellophane.

All gases used in this work were from Air Liquid (99.999 % pure), except methane that was from Linde (99.995 % pure).

3.2.3.2. Thermogravimetric analysis

Thermogravimetric analyses were carried in a Netzsch TG 209 F1 Iris, thermogravimetric balance, with 10^{-5} g precision. The amount of sample provided for each batch was about 5 mg. In order to determine the yield of fixed carbon, proximate analysis of cellophane was performed. The heating protocol employed was modified [42], but follows essentially the work by Ottaway et al. [19] and can be summarized as follows:

- Temperature rise from room temperature up to 110 °C at 25 °C min^{-1} under nitrogen flow at 30 ml min^{-1}, with two dwells at 50 °C for 10 min and at 110 °C for 7 min. All humidity present should be released.

- Temperature rise from 110 °C up to 950 °C under nitrogen, with a 9 min dwell at 950 °C under the same conditions. In this step the weight loss is attributed to the release of volatile matter;

- Finally, the sample is kept for 11 min at 950 °C under oxygen, while fixed carbon is burned, leaving only ashes, if present.

Characteristic curves for cellophane were also determined under three different atmospheres, N_2, Ar and CO_2, from 20 up to 950 °C, using a heating rate of 10 °C min^{-1} and a flow rate of 30 ml min^{-1}.

3.2.3.3. Preparation of CMSM

Carbon molecular sieve membranes derived from cellophane were prepared in the set-up described in Figure 3.7. The pyrolysis of the precursor occurred inside a quartz tube (80 mm in diameter and 1.5 m in length) placed inside a horizontal tubular Termolab TH furnace, equipped with three different heating elements. These heating elements are actuated by three distinct control actions, using a Shimaden MR13 temperature controller, to better guarantee the temperature homogeneity along the quartz tube. A gas feed system is connected to the quartz tube inlet. Software was developed using NI LabVIEW, to control and monitor the gas feed flowrates and the temperature history inside the tube.
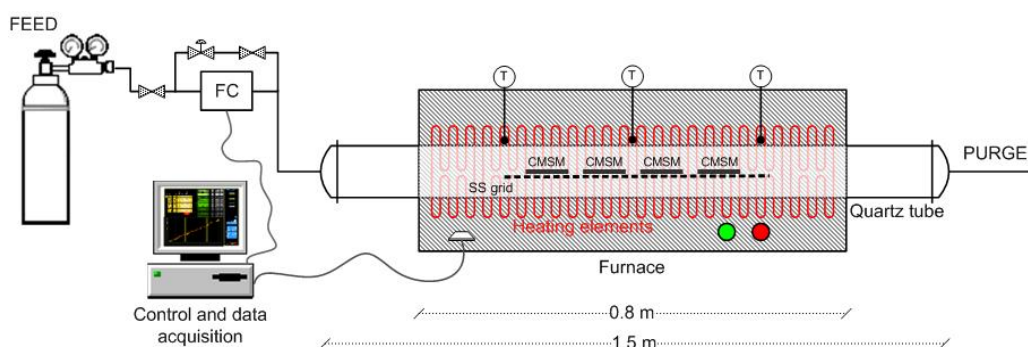
Figure 3.7 – Scheme of the pyrolysis set-up.

The cellophane precursor disks were cut with 70 mm in diameter and introduced into the quartz tube, supported on a horizontal stainless steel grid. The temperature program used is shown in Figure 3.8. It basically consists on slow heating rates [43] of 0.5 °C min^{-1} with several 30 min dwells in order to avoid a quick release of residual solvents and volatile matter that could damage the carbon matrix, causing micro cracks or defects. The end temperature varied between 400 and 850 °C, as shown in Figure 3.8a). The lower limit temperature was chosen according to the thermogravimetric results, which indicate that the main weight loss occurs from

300 ºC up to 400 ºC, as will be discussed in section 3.2.3.2. For studying the soaking parameter, the end temperature was 550 ºC and several soaking times where analyzed: 60, 120, 240 and 480 min, as suggested in Figure 3.8 b). The end temperature for this study was fixed at 550 ºC, since this temperature has originated the carbon membranes with the highest permeances, as described in section 3.2.4.5.
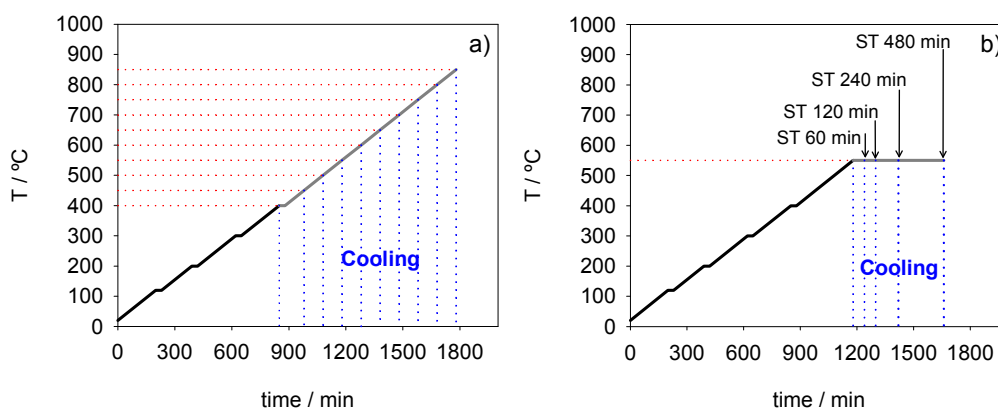
Figure 3.8 – Temperature history employed to prepare carbon membranes derived from cellophane: a) different pyrolysis end temperatures; b) different soaking times at 550 ºC.

The resultant carbon membranes are identified in Table 3.6.

Table 3.6 – Identification of the membranes produced according to pyrolysis conditions.

Membrane ID	T_{end} (ºC)	Soaking (min)	Gas atmosphere
Celo400	400	0	N_2
Celo450	450	0	N_2
Celo500	500	0	N_2
Celo550	550	0	N_2
Celo600	600	0	N_2
Celo650	650	0	N_2
Celo700	700	0	N_2
Celo750	750	0	N_2
Celo800	800	0	N_2
Celo850	850	0	N_2
Celo550-ST60	550	60	N_2
Celo550-ST120	550	120	N_2
Celo550-ST240	550	240	N_2
Celo550-ST480	550	480	N_2
Celo550-G-Ar	550	0	Ar
Celo550-G-CO2	550	0	CO_2

3.2.3.4. Scanning electron microscopy and X-ray microanalysis

Scanning electron microscopy has been performed on cellophane and its derived carbon membranes; X-ray microanalysis was also done. A FEI Quanta 400FEG / EDAX Genesis X4M with 1.2 nm resolution was used. Due to the low electron conductivity of cellophane, the low-vacuum technique was applied.

3.2.3.5. X-ray diffraction

The analyses were performed in a Philips X'Pert MPD diffractometer with a CuKα radiation of 0.154056 nm wavelength (40 kV; 50 mA). The samples were milled and submitted to X-ray diffraction by the powder method.

3.2.3.6. CO$_2$ Adsorption at 0 ^{o}C

The adsorption equilibrium isotherm of CO_2 at 0 ^{o}C was determined to assess ultramicroporosity on Celo550. The equilibrium values were obtained using the gravimetric method and a magnetic suspension balance from Rubotherm® (metal version) was used. The balance was connected to two pressure sensors (Drück 0-7 bar and 0-350 mbar, 0.1 % FS) and a vacuum pump (Edwards, model RV5). The set-up is illustrated in Figure 3.9. The temperature was controlled with a thermostatic bath (Huber, model CC1).

Legend:
1 – 5L tank;
2 – Vacuum pump
3 – Vessel with liquid water in equilibrium with vapour;
4 – Heating plate;
5 – Feed gases;
P – Pressure sensor;
HP – High precision pressure sensor.
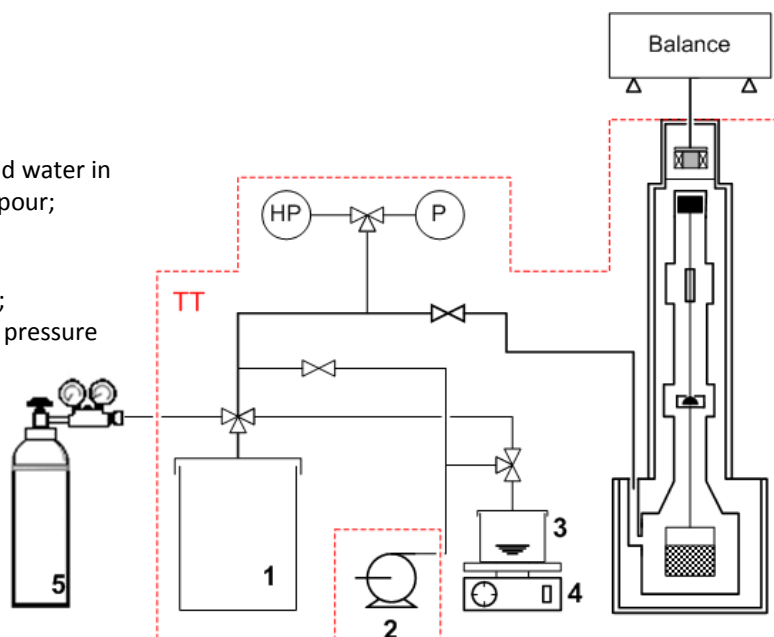
Figure 3.9 – Schematic representation of the gravimetric method apparatus (adapted from [44]).

3.2.3.7. Permeation

The pyrolysed membranes were glued to aluminum O-rings to prevent them from breaking when assembled into the permeation cell; vacuum was applied from the bottom part of the membranes, for flattening them as much as possible. The epoxy glue (Araldite®) was then used to seal the interface membrane/o-ring.

All the permeation experiments were performed in a setup sketched in Figure 3.10.
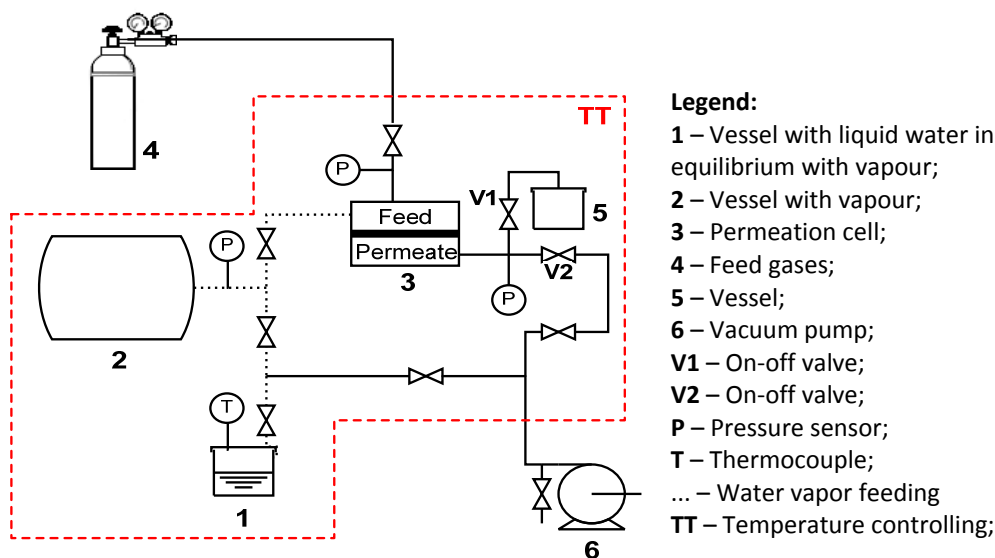
Figure 3.10 – Pressure increment set-up for measuring permeabilities. The dashed line illustrates the part of the set-up used to feed water vapor to the permeation cell.

The method behind this technique consists on measuring the time for a certain increment in pressure to occur at the permeate side. The system includes two calibrated volumes at the permeate side: 1) a small volume (valves V1 and V2 closed) to measure the permeabilities towards slower diffusing species and 2) a large volume (valves V1 open and V2 closed) to characterize the membrane towards faster species. The water vapor permeation experiments were also performed in this system. The set-up was placed inside a thermostatic cabinet. The valves are located inside the cabinet and handled from the outside, therefore avoiding condensation. Water vapor is generated in vessel 1 up to the saturation pressure dictated by the temperature set-point and then transferred to a larger tank, vessel 2, that feeds the permeation cell.

The single component experiments were performed at 29.5 °C using N_2, H_2, He, Ar, CO_2, CH_4 and O_2 with 2 bar feed pressure and vacuum at the permeate side. In the case of experiments with water vapor the feed pressure employed was the vapor pressure at 29.5 °C and the permeate side was also evacuated. After exposure to each gas or vapor, helium was used to regenerate the membrane at 65 °C (limit temperature to avoid the epoxy resin degradation) and its permeability rechecked; this way, any aging due to the exposure to a certain gas could be assessed.

The permeability of the membrane, L_i^*, to pure component i is given by:

$$L_i^* = \frac{F_i \cdot \delta}{\Delta p_i}$$ (3.3)

where F_i is the flux of species i, Δp_i the partial pressure difference of component i across the membrane, which in a single component experiment is equal to the total pressure difference, and δ is the membrane thickness. Therefore, after achieving the steady state, the single component permeability, L^*, was computed from the experimental data as follows:

$$L^* = \frac{\delta \, V_P \, \upsilon_M \, \Delta p_l}{\Re \, T \, t \, A_m \left(p_h - p_l\right)}$$ (3.4)

where V_P is the calibrated volume where the permeate is collected, p_h and p_l are respectively, the feed pressure (high pressure) and the permeate pressure (low pressure), A_m is the effective area of the flat membrane, T is the absolute temperature, υ_M is the molar volume of the gas at normal conditions, $\Re$ is the gas constant, and t is the time to a certain increment in pressure, Δp_l to occur at the permeate side.

The ideal selectivity for a pair of gases, $\alpha\left(i/j\right)$ is given by the ratio between the permeability of species i and j:

$$\alpha\left(i/j\right) = \frac{L_i^*}{L_j^*}$$ (3.5)

3.2.4. Results and Discussion

3.2.4.1. Thermogravimetric analysis

The proximate analysis by thermogravimetry revealed that cellophane is ash free presenting 84 % (dry basis, d.b.) of volatile matter and 16 % (d.b.) of fixed carbon. The characteristic curves of cellophane were obtained under three different atmospheres, N_2, Ar and CO_2 and are presented in Figure 3.11.
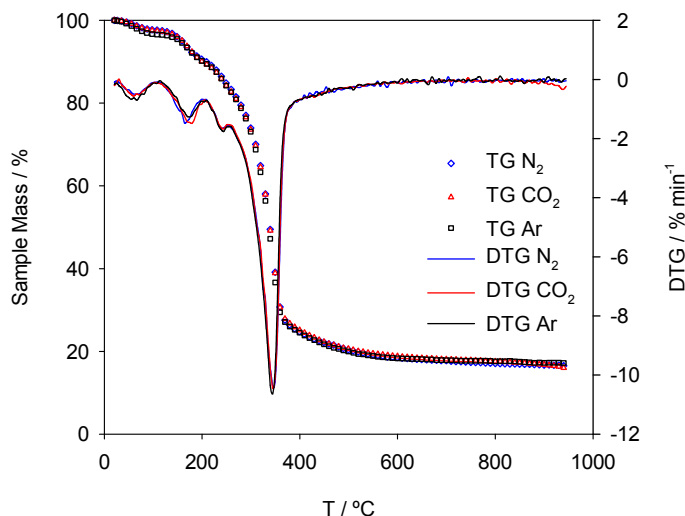
Figure 3.11 – Thermogravimetric analysis of cellophane.

It is seen that all the curves present the same behavior which means that the decomposition of cellophane occurs in the same way by using N_2, Ar or CO_2 atmospheres. Up to 100 ºC, the first derivative of mass loss curve shows a negative peak related with the release of humidity presented in the sample. The peak around 170 ºC probably indicates the release of residual solvents used during the production process. Finally, the peak around 345 ºC indicates the degradation of the polymer [45]. This peak corresponds to the larger mass loss, leaving only the carbon membrane skeleton. Some mass loss is still occurring until 950 ºC, but at a much slower rate. Since N_2 is the most inexpensive inert gas, it was chosen for the subsequent membrane preparations.

3.2.4.2. Preparation of CMSM

The resultant carbon membranes are identified in Table 3.7. The precursor disks, initially circles with a diameter of D = 70 mm, shrank during the pyrolysis process, giving place to elliptic carbon membranes. This fact may be caused by a preferential orientation of the macromolecules in cellophane. Table 3.7 presents two values of final diameters and shrinkage percentages, associated to the two characteristic

dimensions in the final elliptical membranes. The shrinkage percentages were determined as follows:

$$SH = \frac{\left(D - D_{after}\right)}{D} \times 100 \qquad (3.6)$$

Table 3.7 – Identification of carbon membranes derived from cellophane.

Membrane ID	Before pyrolysis D (mm)	After pyrolysis		
		D_{after} (mm)	Shrinkage (%)	Observations
Celo400	70	n.d. [a]	n.d. [a]	Dark brown; some flexibility
Celo450	70	43.4 – 51.4	38.0 – 26.5	Turning black; some flexibility
Celo500	70	42.4 – 50.3	39.4 – 28.2	Black; brittle
Celo550	70	41.6 – 49.6	40.5 – 29.2	Black; brittle
Celo600	70	41.2 – 48.9	41.1 – 30.2	Black; brittle
Celo650	70	40.6 – 48.0	42.0 – 31.4	Black; very brittle
Celo700	70	39.5 – 46.9	43.6 – 33.0	Black; very brittle
Celo750	70	38.3 – 45.1	45.3 – 35.6	Black; very brittle
Celo800	70	37.4 – 44.2	46.6 – 36.8	Black; extremely brittle
Celo850	70	n.d. [a]	n.d. [a]	Black; extremely brittle
Celo550-ST60	70	41.5 – 49.0	40.7 – 30.0	Black; brittle
Celo550-ST120	70	n.d. [a]	n.d. [a]	Black; brittle
Celo550-ST240	70	41.3 – 48.4	41.0 – 30.9	Black; brittle
Celo550-ST480	70	41.0 – 48.0	41.4 – 31.4	Black; brittle
Celo550-GAr	70	n.d. [a]	n.d. [a]	Black; brittle
Celo550-GCO2	70	n.d. [a]	n.d. [a]	Black; brittle

a) n.d. – not determined

The shrinkage increases with the pyrolysis end temperature and with the soaking time. It is also believed that the existence of a soaking time leads to a rearrangement of the carbon atoms [39] resulting in a more compact structure.

3.2.4.3. Scanning electron microscopy and X-ray microanalysis

Micrographs of cellophane and derived carbon membranes have been taken by low vacuum SEM. Figure 3.12 presents the surface and cross sectional views of samples Celo550 and Celo550-ST480, as examples.
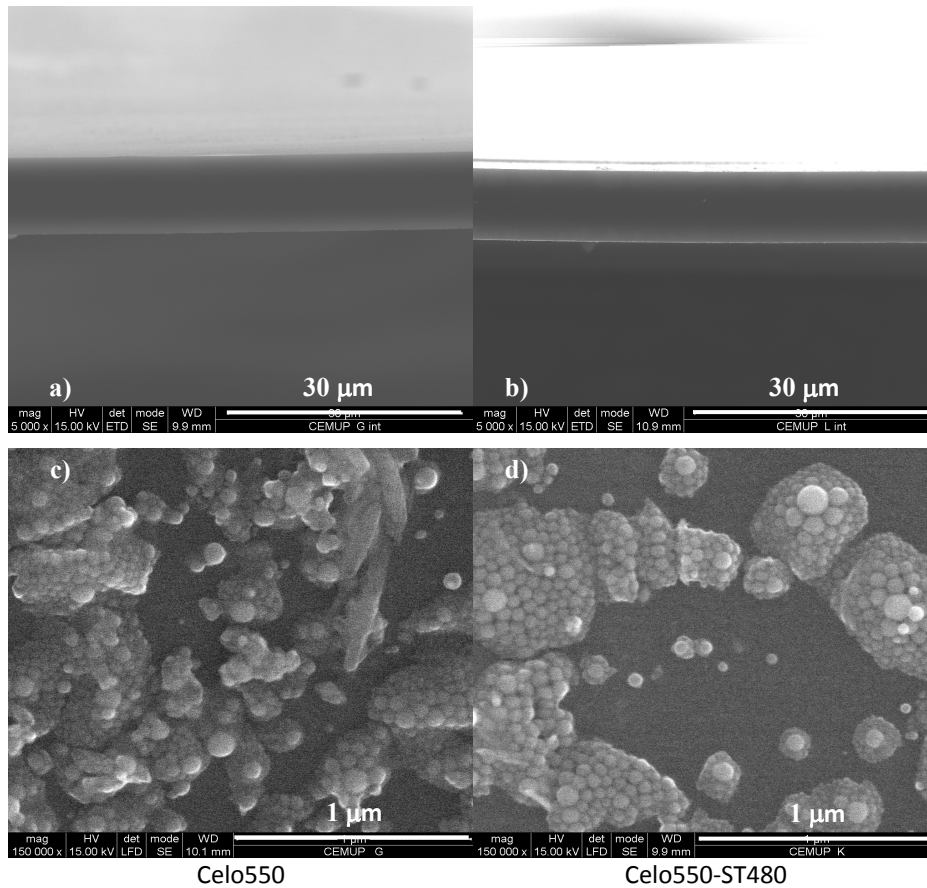
Figure 3.12 – Cross sectional SEM pictures a) and b) x 5000 magnification; surface pictures c) and d) x 150,000 magnification for Celo550 and Celo550-ST480.

Table 3.8 summarizes the thickness of cellophane and of each carbon membrane obtained from SEM. In this table, the effective areas used in the calculation of permeation data are also given.

Table 3.8 – Thickness, δ, of cellophane and carbon membranes flat sheets obtained by SEM and effective area for mass transfer, A_m.

Membrane	δ (μm)	Shrinkage (%)	A_m (cm^2)
Cellophane paper	15-17		36.3
Celo400	9.70	39.4	2.11
Celo450	9.66	39.6	3.08
Celo500	9.62	39.9	3.76
Celo550	9.50	40.6	3.86
Celo600	9.22	42.4	3.81
Celo550-ST60	9.29	41.9	3.39
Celo550-ST120	9.15	42.8	*n.d.* [a]
Celo550-ST240	9.06	43.4	3.97
Celo550-ST480	9.00	43.8	3.29

a) n.d. – not determined

In agreement with the shrinkage macroscopically observed and discussed in the previous section, the measured thicknesses obtained from the cross section views indicate that the increase of the pyrolysis end temperature and soaking time led to a decrease in the membrane thickness. The surface micrographs of all samples were similar. The clusters of microspheres observed in Figure 3.12 are related to a hydrothermal carbonization that happens at around 220 °C. The microspheres are also called "condensed benzene rings" forming more stable oxygen groups in the core (i.e. ether, quinone, pyrrone) and more hydrophilic oxygen groups in the shell (hydroxyl, carbonyl, carboxylic, esther) [46].

Figure 3.13 plots the X-ray microanalysis of various samples; in Figure 3.13 a) the effect of pyrolysis end temperature is analyzed and in b) the soaking time effect is shown.
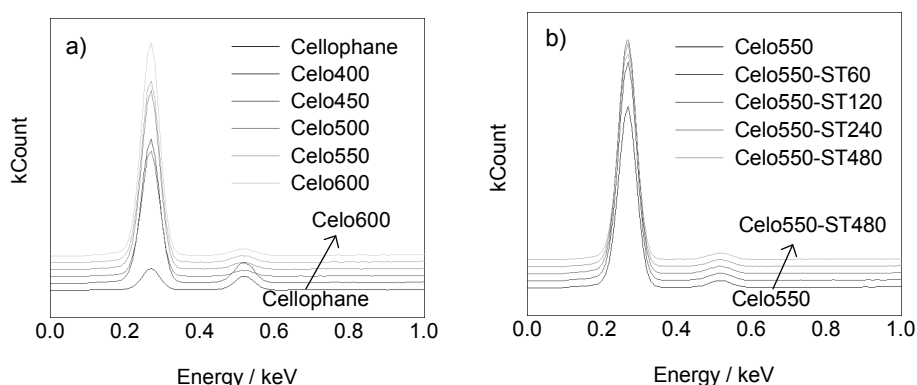
Figure 3.13 – X-ray microanalysis of cellophane and its derived carbon membranes.

Globally, it is seen that the main elements identified for all samples are carbon (C) and oxygen (O). Cellophane paper exhibits a lower C/O ratio than the derived carbonized membranes, as expected. This ratio enlarges with the pyrolysis end temperature. With respect to the soaking time effect, it seems that the C/O ratio suffers some fluctuations, but might be considered mostly constant.

3.2.4.4. X-ray diffraction

Figure 3.14 compiles the spectra of samples prepared at different pyrolysis end temperatures, different pyrolysis environments and different soaking times at end temperatures.
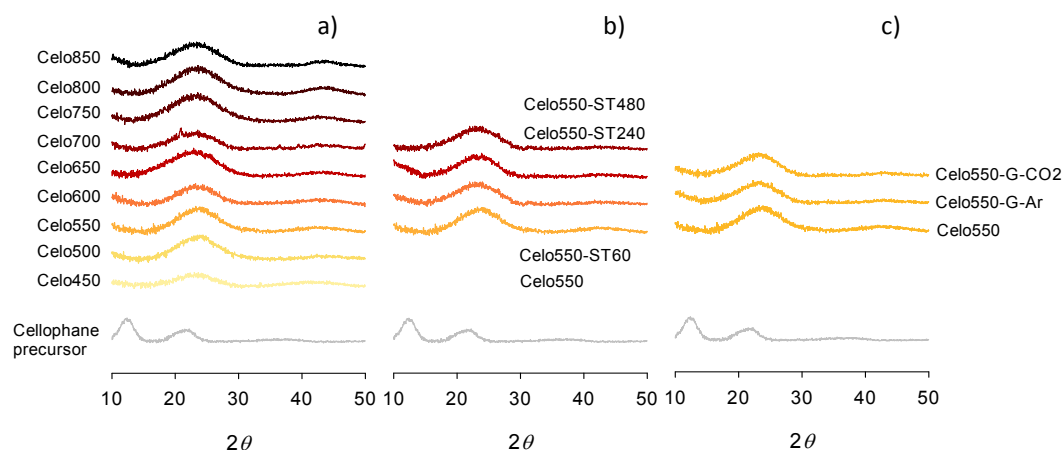
Figure 3.14 – X-ray diffraction spectrum of cellophane precursor and derived carbon membranes.

In Figure 3.14 there are two visible peaks for cellophane precursor, at around 11 and 20 ° (2θ). Indeed, the diffraction pattern typical of cellulose II structure, as should be expected for regenerated cellulose [47], usually presents peaks at around 11.8, 19.9 and 21.6 °; the peaks are related to planes $1\bar{1}0$, 110 and 200, respectively [48]. In Figure 3.14 though, the peaks around 19.9 ° and 21.6 ° should be overlapped in a single peak at around 20 °. On the other hand, when looking at the spectrum of the derived carbon membranes, it seems that cellophane's structure is destroyed by the heat treatment leading to an amorphous structure with diffraction peaks centered at around 23 and 44 °; these peaks are referred to planes 002 and 101, respectively. These values of 2θ are similar to those found in graphite. However, the broadening of the peaks is indicative of the degree of amorphousness typical of porous carbon materials [49]. The distance between adjacent carbon layers relative to the peak at 23 ° is approximately 0.38 nm differing very little from sample to sample. The effect of the pyrolysis end temperature has no significant changes at the positioning of the peaks, evidencing only a slight increase in the intensity of the peaks. No significant changes are observed by comparing the spectra obtained with different soaking times at 550 °C or under different gas atmospheres.

3.2.4.5. Ultramicroporosity of Celo550

An insight over the membrane microstructure was undertaken to provide additional information on the properties of cellophane-based carbon membranes. Sample Celo550 was chosen to be characterized because this membrane revealed to be the best performing one, as will be shown in section 3.2.4.6. From the adsorption equilibrium isotherm of carbon dioxide at 0 °C, the micropore volume, the mean pore width, and the pore size distribution were obtained. The procedure adopted in this characterization was similar to that reported in Chapter II [50].

The adsorption equilibrium isotherm of CO_2 at 0 °C has been determined for Celo550 and is represented in Figure 3.15 a). The micropore volume, W_0, and the

characteristic energy for adsorption, E_0, were determined by fitting the Dubinin-Radushkevitch (DR) equation to experimental data [51] (Figure 3.15 b)).
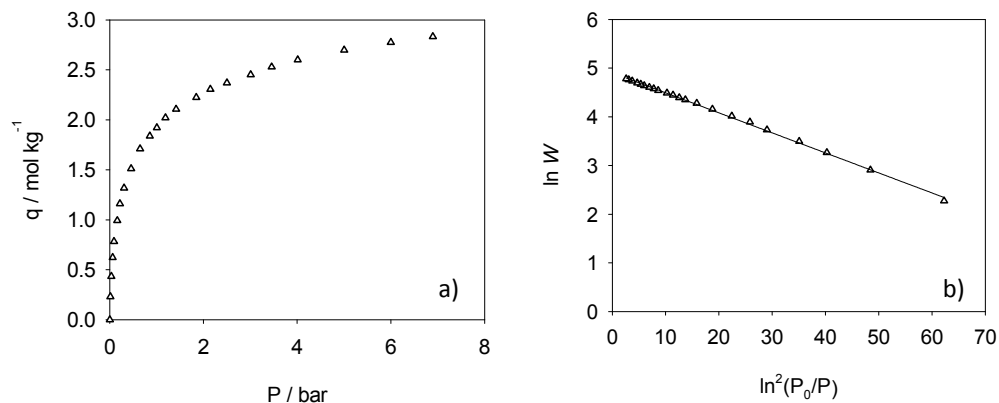
Figure 3.15 – a) Adsorption equilibrium isotherm for CO_2 at 0 ºC for Celo550; b) characteristic curve and DR fitting.

The structural parameters are presented in Table 3.9.

Table 3.9 – Structural parameters for Celo550.

	Celo550
W_0 (cm^3 kg^{-1})	134.8
E_0 (kJ mol^{-1})	32.0
L (nm)	0.525
S_{mic} (m^2 g^{-1})	513.9

The micropore volume of 134.8 cm^3 kg^{-1} is slightly lower when compared to other reported values, e.g. 160 cm^3 g^{-1} [52]. However, the mean pore width obtained is in the range of typical values found for carbon molecular sieves [4, 52].

These results suggest that Celo550 should present a molecular sieve character dictated by the reduced mean pore width, but should exhibit low permeabilities, due

to the low micropore volume, *i.e.* small number of pores, in relation to typical carbon molecular sieve membranes.

The adsorption equilibrium isotherm of CO_2 at 0 °C was also used to determine the pore size distribution based on the method developed by Do et al. [53-55]. The result obtained for Celo550 is given in Figure 3.16. The mathematical analysis used to derive the pore size distribution is detailed in Chapter II.
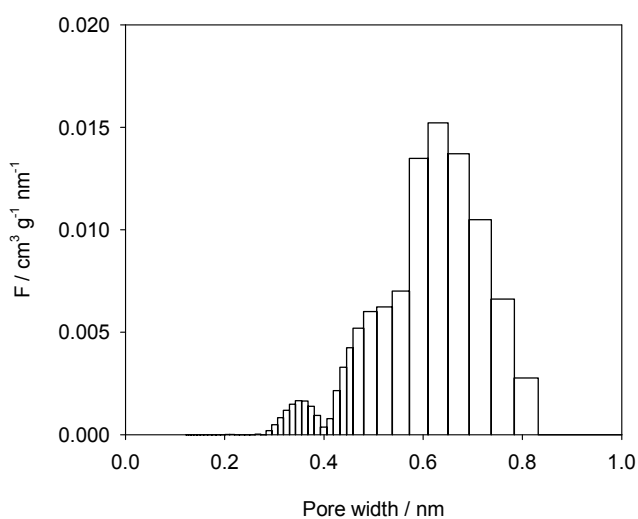
Figure 3.16 – Micropore size distribution for Celo550 obtained from CO_2 adsorption equilibrium data at 0 °C.

From Figure 3.16 it is seen that Celo550 presents small micropores with molecular sieving character, associated to the range 0.3-0.8 nm. There is a well defined small fraction of pores ranging in diameters from 0.3 to 0.4 nm, probably related with the so-called constrictions, responsible for the selectivity of the membrane [2, 50] - these involve open pores and dead-end pores which do not contribute to permeation.

3.2.4.6. Permeation

The membranes were tested for permeation using several probe species: He, H_2, CO_2, O_2, Ar, N_2, CH_4 and water vapor. Table 3.10 presents the results obtained for the cellophane precursor and for the membranes pyrolysed at different end temperatures and prepared at 550 °C with different soaking times.

Table 3.10 - Permeabilities of cellophane derived carbon membranes at 29.5 °C: effect of the pyrolysis end temperature and soaking time at pyrolysis end temperature.

	Permeability (Barrer)*							
	He	H_2	N_2	Ar	CO_2	O_2	CH_4	H_2O
Cellophane precursor	0.01	0.006	0.0007	n.d. [a]	0.001	0.0002	n.d. [a]	n.d. [a]
Celo400	19.3	22.2	0.10	0.23	3.93	0.93	n.d. [a]	139.99
Celo450	34.3	49.6	0.37	0.77	13.9	3.03	n.d. [a]	313.31
Celo500	60.3	79.9	0.20	0.57	9.77	3.50	n.d. [a]	413.63
Celo550	97.6	148.3	0.33	0.67	16.9	4.33	n.d. [a]	962.58
Celo600	55.3	39.3	0.03	0.03	0.67	0.23	n.d. [a]	283.64
Celo550-ST60	101.1	168.1	0.43	0.77	17.0	4.87	0.17	156.6
Celo550-ST240	94.3	108.6	0.10	0.33	5.00	1.67	0.03	107.0
Celo550-ST480	79.25	60.3	0.04	0.07	1.93	0.70	0.01	75.2

a) n.d. – not determined

* 1 Barrer=7.5×10^{-18} m^3_N m m^{-2} s^{-1} Pa^{-1}

Figure 3.17 provides an overview of the permeabilities as a function of the kinetic diameter.
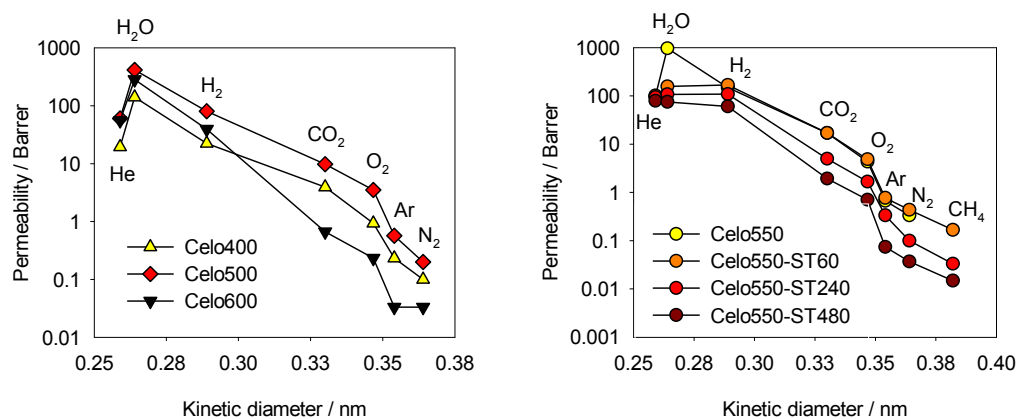
Figure 3.17 – Permeabilities of cellophane derived carbon membranes at 29.5 °C: a) effect of the pyrolysis end temperature and b) of the soaking time at end temperature of 550 °C.

Water permeates faster than He in most cases, despite being a larger species. This should be associated to the hydrophilic character of these membranes. H_2, also a

larger than He, also permeates faster on most of the membranes prepared. This fact has been reported by others [56], indicating that the extent of adsorption, which is assumed to be larger for H_2 than for He, should be playing a role in permeation. For the remaining species, the permeation rates follow the sequence of the kinetic diameters as shown in Figure 3.17, denoting the molecular sieving character of these materials. After exposure to each gas or vapor, the membranes were regenerated with helium at 65 °C and no loss was observed in the performance of any of the membranes studied. Some ideal selectivities were computed and are presented in Table 3.11.

Table 3.11 – Ideal selectivities for carbon membranes derived from cellophane at 29.5 °C.

	Ideal Selectivity						
	H_2/CO_2	H_2/O_2	O_2/N_2	O_2/Ar	CO_2/CH_4	H_2O/H_2	H_2O/CH_4
Celo400	5.6	23.9	9.3	4.0	-	6.3	-
Celo450	3.6	16.4	8.2	3.9	-	6.3	-
Celo500	8.2	22.8	17.5	6.1	-	5.2	-
Celo550	8.8	34.2	13.1	6.5	-	6.5	-
Celo600	58.7	170.9	7.7	7.7	-	7.2	-
Celo550-ST60	9.9	34.5	11.3	6.3	100.0	0.9	921.2
Celo550-ST240	21.7	65.0	16.7	5.1	166.7	1.0	3566.7
Celo550-ST480	31.2	86.1	17.5	10.0	193.0	1.2	7520.0

The carbon membranes produced show permeation rates about 10^3-10^4 times larger than the cellophane precursor, and evidence a molecular sieving behavior. Permeabilities towards all species increase with the pyrolysis end temperature, up to 550 °C, and then start decreasing. In fact, the thermogravimetric analysis given in section 3.2.3.2 suggests that at 550 °C the weight loss becomes negligible. Up to this temperature most of heteroatoms should have been released in the form of volatile matter. The increase in permeability is therefore relatable to the formation of the carbon pore network. However, at 600 °C the membranes seem to lose permeability, suggesting that carbon atoms are rearranging into a tighter structure, by a sintering mechanism [2]. From Table 3.10 and Figure 3.17 b it can be seen that the permeability

of the membrane pyrolysed up to 550 °C starts to slightly increase with the soaking time for decreasing afterwards. The permeability towards water vapour decreases tremendously up to a 60 min of soaking time becoming then mostly stable. The water transport is mainly related to the presence of surface functional groups [57, 58] that should disappear to some extent, allowing the average pore size to increase. Afterwards, the sintering effect overcomes and the net pore size decreases as a function of the soaking time.

The performance of a membrane towards a separation is characterized by the permeability for the target species as well as the corresponding selectivities.

Recently, Robeson has presented a selectivity/permeability upper bound for representative binary gas separations performed with polymeric membranes [41, 59]. Figure 3.18 represents the Robeson upper limits for five gas separations, as well as the results obtained for single gas permeation experiments with the cellophane based carbon membranes produced in this work. For comparison with different cellulose-based carbon membranes, results from the work of Lie et al. [39] and Lagorsse et al. [52] were also included.

Most of the cellophane derived carbon membranes are positioned above the new upper bound for polymeric membranes. In general, the best compromise between permeability and selectivity is achieved for the membranes pyrolysed up to 550 °C, with and without soaking time. Comparatively to the membranes studied by Lagorsse et al. and Lie et al., the membranes presented here exhibit better separation performances for the pairs H_2/O_2, H_2/CO_2 and H_2/CH_4 – see Figure 3.18 b, d and e. This could be related to the fact that hydrogen has difficulty to remove other adsorbed gases from the membrane matrix, underestimating the permeability measurement. The present membranes were cleaned with helium at 65 °C for 1 day, before being tested with hydrogen. Another important industrial application could be the separation of nitrogen from air. These membranes seem to be very promising due to their great O_2/N_2 selectivities (13 and 18). Regarding the CO_2/CH_4 separation, they are worse than those prepared by Lie et al.

A major advantage of the carbon membranes prepared in this work is related to the fact that no traces of aging due to exposure to oxygen or water vapor, or any other

permeant, were observed. Nevertheless, these membranes were extremely permeable to water vapor, making them very promising to be used, for example, on the recovery of methane from natural gas from the retentate side, or even removing humidity from air.
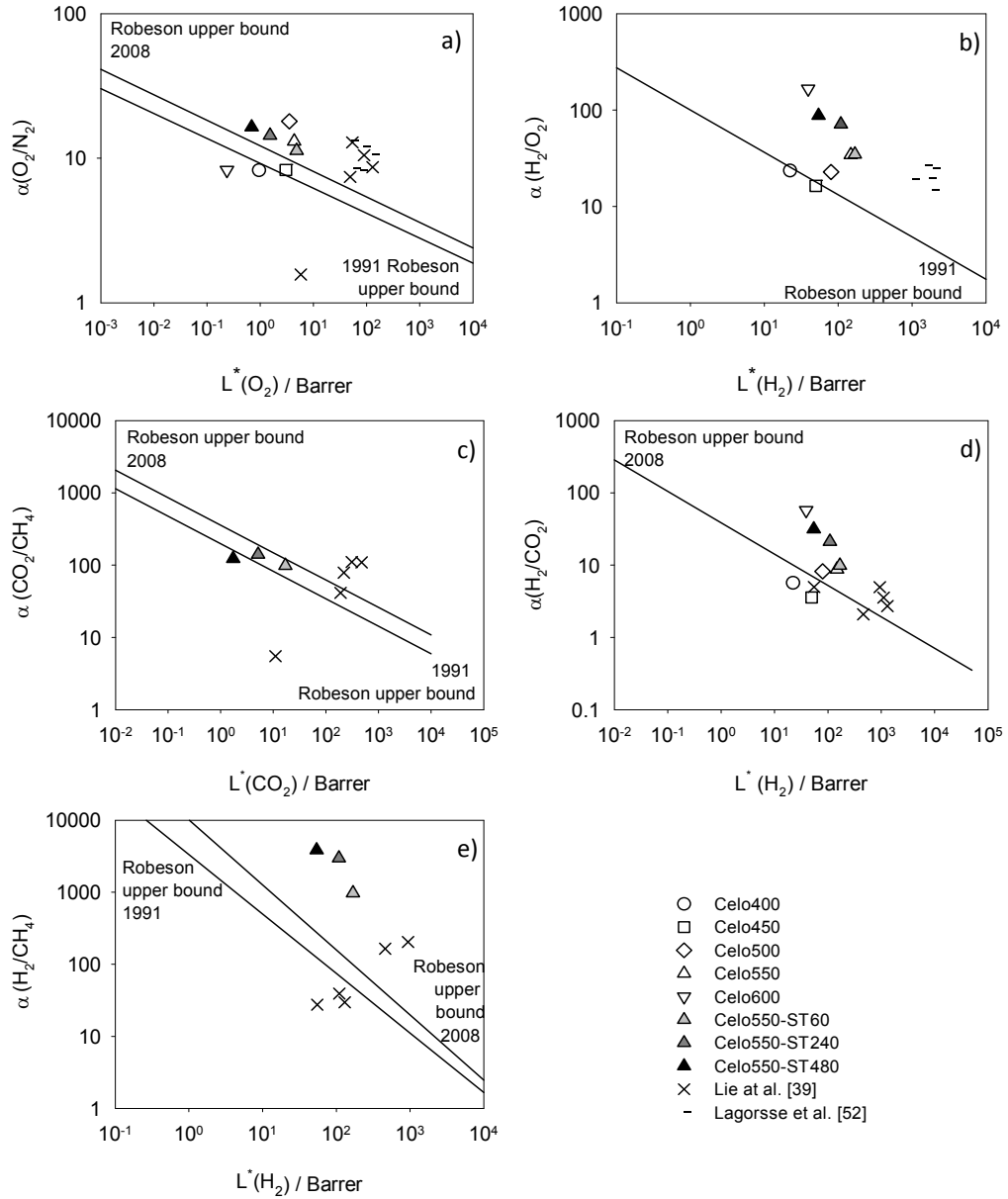
Figure 3.18 – Robeson upper limits [41, 59] and comparison with permeation results obtained with the cellophane derived carbon membranes.

3.2.5. Conclusions

Carbon molecular sieve membranes have been successfully prepared by one single pyrolysis step under nitrogen using cellophane paper as precursor. The effect of the pyrolysis end temperature was assessed from 450 up to 850 °C through several characterization techniques and a maximum permeability was found for sample Celo550. The soaking time seems to influence the final pore network by means of a sintering mechanism; this causes pore widths to decrease, leading to lower permeabilities but increased selectivities.

The permeability versus kinetic diameter towards He, H_2, Ar, N_2, CO_2, O_2, CH_4 and water vapor exhibited a molecular sieve mechanism for all the membranes prepared; this was in agreement with the micropore size distribution obtained for Celo550 (~0.3-0.8 nm).

The new Robeson upper bound for polymeric membranes was overtaken by most of the membranes produced, regarding O_2/N_2, H_2/N_2, H_2/O_2, H_2/CO_2 and H_2/CH_4 separations, specially for the membrane prepared under an end temperature of 550 °C; it should be noted though that the present results are based on single component permeation experiments. In addition, these membranes were extremely permeable to water vapor. X-ray microanalysis has shown that the membranes are essentially carbon-based, but also present elemental oxygen, which justifies the affinity of the carbon matrix towards water vapor. However, the carbon membranes prepared in this work were not susceptible to aging effects due to exposure of oxygen or water vapor, or any other permeant. Therefore, they might be considered in relevant industrial applications such as separation of nitrogen from air or recovery of hydrogen from synthesis gas.

3.2.6. Acknowledgements

3.3. References

[1] J.E. Koresh, A. Soffer, Molecular-Sieve Carbon Permselective Membrane .1. Presentation of a New Device for Gas-Mixture Separation, Sep. Sci. Technol. 18 (1983) 723-734.

[2] J. Koresh, A. Soffer, Study of Molecular-Sieve Carbons .1. Pore Structure, Gradual Pore Opening and Mechanism of Molecular-Sieving, J Chem Soc Farad T 1 76 (1980) 2457-2471.

[3] S.M. Saufi, A.F. Ismail, Fabrication of carbon membranes for gas separation - a review, Carbon 42 (2004) 241-259.

[4] A.F. Ismail, L.I.B. David, A review on the latest development of carbon membranes for gas separation, J. Membr. Sci. 193 (2001) 1-18.

[5] P.S. Tin, Y.C. Xiao, T.S. Chung, Polyimide-carbonized membranes for gas separation: Structural, composition, and morphological control of precursors, Separation and Purification Reviews 35 (2006) 285-318.

[6] J.N. Barsema, J. Balster, V. Jordan, N.F.A. van der Vegt, M. Wessling, Functionalized Carbon Molecular Sieve membranes containing Ag-nanoclusters, J. Membr. Sci. 219 (2003) 47-57.

[7] J.N. Barsema, N.F.A. van der Vegt, G.H. Koops, M. Wessling, Ag-functionalized carbon molecular-sieve membranes based on polyelectrolyte/polyimide blend precursors, Adv. Funct. Mater. 15 (2005) 69-75.

[8] C.H. Liang, G.Y. Sha, S.C. Guo, Carbon membrane for gas separation derived from coal tar pitch, Carbon 37 (1999) 1391-1397.

[9] A.F. Ismail, L.I.B. David, Future direction of R&D in carbon membranes for gas separation, Membrane Technology (2003) 4-8.

[10] A. Soffer, M. Azariah, A. Amar, H. Cohen, D. Golub, S. Saguee, H. Tobias, Method for improving the selectivity of carbon membranes by carbon chemical vapor deposition, US005695818, 1997.

[11] A. Soffer., J. Gilron., S. Saguee., R. Hed-Ofek., H.C. Topic, Process for the production of hollow carbon fiber membranes, US 5925591 Patent, 1999.

[12] I. Menendez, A.B. Fuertes, Aging of carbon membranes under different environments, Carbon 39 (2001) 733-740.

[13] M.B. Hagg, J.A. Lie, A. Lindbrathen, Carbon molecular sieve membranes - A promising alternative for selected industrial applications, Ann. N.Y. Acad. Sci. 984 (2003) 329-345.

[14] S. Lagorsse, F.D. Magalhães, A. Mendes, Aging study of carbon molecular sieve membranes, J. Membr. Sci. 310 (2008) 494-502.

[15]   P. Raveendran, Y. Ikushima, S.L. Wallen, Polar attributes of supercritical carbon dioxide, Accounts of Chemical Research 38 (2005) 478-485.

[16]   S. Lagorsse, M.C. Campo, F.D. Magalhães, A. Mendes, Water adsorption on carbon molecular sieve membranes: Experimental data and isotherm model, Carbon 43 (2005) 2769-2779.

[17]   T. Visser, G.H. Koops, M. Wessling, On the subtle balance between competitive sorption and plasticization effects in asymmetric hollow fiber gas separation membranes, J. Membr. Sci. 252 (2005) 265-277.

[18]   T. Visser, N. Masetto, M. Wessling, Materials dependence of mixed gas plasticization behavior in asymmetric membranes, J. Membr. Sci. 306 (2007) 16-28.

[19]   M. Ottaway, Use of Thermogravimetry for Proximate Analysis of Coals and Cokes, Fuel 61 (1982) 713-716.

[20]   J. Barsema, Carbon Membranes - Precursor, preparation and functionalization, Enschede, PhD Thesis, 2004

[21]   H.C. Foley, Carbogenic Molecular-Sieves - Synthesis, Properties and Applications, Microporous Mater. 4 (1995) 407-433.

[22]   Y.C. Xiao, Y. Dai, T.S. Chung, M.D. Guiver, Effects of brominating matrimid polyimide on the physical and gas transport properties of derived carbon membranes, Macromolecules 38 (2005) 10042-10049.

[23]   P.S. Tin, T.S. Chung, Y. Liu, R. Wang, Separation of CO2/CH4 through carbon molecular sieve membranes derived from P84 polyimide, Carbon 42 (2004) 3123-3131.

[24]   F. Celso, R.S. Mauler, A.S. Gomes, Estudo das Propriedades Térmicas de Filmes Poliméricos Compostos de Speek, Derivados do Benzoimidazol e Ácido Fosfotúngstico, Polímeros: Ciência e Tecnologia 18 (2008) 178-186.

[25]   J.E. Koresh, A. Soffer, The Carbon Molecular-Sieve Membranes - General-Properties and the Permeability of Ch4/H-2 Mixture, Sep. Sci. Technol. 22 (1987) 973-982.

[26]   J.K. Brennan, T.J. Bandosz, K.T. Thomson, K.E. Gubbins, Water in porous carbons, Colloids Surf., A 187 (2001) 539-568.

[27]   M. Freemantle, Membranes For Gas Separation - Advanced organic and inorganic materials being developed for separations offer cost benefits for environmental and energy-related processes. Chemical & Engineering News, 2005, pp. 49-57.

[28]   J.E. Koresh, A. Soffer, Mechanism of Permeation through Molecular-Sieve Carbon Membrane .1. The Effect of Adsorption and the Dependence on Pressure, J Chem Soc Farad T 1 82 (1986) 2057-2063.

[29]   A. Soffer, J. Koresh, S. Saggy, Separation device, US004685940, 1987.

[30]   M.B. Rao, S. Sircar, Nanoporous Carbon Membranes for Separation of Gas-Mixtures by Selective Surface Flow, J. Membr. Sci. 85 (1993) 253-264.

[31]   C.W. Jones, W.J. Koros, Carbon Molecular-Sieve Gas Separation Membranes. 1. Preparation and Characterization Based on Polyimide Precursors, Carbon 32 (1994) 1419-1425.

[32]   Y.D. Chen, R.T. Yang, Preparation of Carbon Molecular-Sieve Membrane and Diffusion of Binary-Mixtures in the Membrane, Ind. Eng. Chem. Res. 33 (1994) 3146-3153.

[33]   M. Acharya, H.C. Foley, Spray-coating of nanoporous carbon membranes for air separation, J. Membr. Sci. 161 (1999) 1-5.

[34]   T.A. Centeno, A.B. Fuertes, Supported carbon molecular sieve membranes based on a phenolic resin, J. Membr. Sci. 160 (1999) 201-211.

[35]   T.A. Centeno, A.B. Fuertes, Carbon molecular sieve gas separation membranes based on poly(vinylidene chloride-co-vinyl chloride), Carbon 38 (2000) 1067-1073.

[36]   A.B. Fuertes, T.A. Centeno, Carbon molecular sieve membranes from polyetherimide, Microporous Mesoporous Mater. 26 (1998) 23-26.

[37]   A.B. Fuertes, D.M. Nevskaia, T.A. Centeno, Carbon composite membranes from Matrimid (R) and Kapton (R) polyimides for gas separation, Microporous Mesoporous Mater. 33 (1999) 115-125.

[38]   J.A. Lie, M.B. Hagg, Carbon membranes from cellulose and metal loaded cellulose, Carbon 43 (2005) 2600-2607.

[39]   J.A. Lie, M.B. Hagg, Carbon membranes from cellulose: Synthesis, performance and regeneration, J. Membr. Sci. 284 (2006) 79-86.

[40]   D. Grainger, M.B. Hagg, Evaluation of cellulose-derived carbon molecular sieve membranes for hydrogen separation from light hydrocarbons, J. Membr. Sci. 306 (2007) 307-317.

[41]   L.M. Robeson, The upper bound revisited, J. Membr. Sci. 320 (2008) 390-400.

[42]   M.C. Campo, T. Visser, K. Nijmeijer, M. Wessling, F.D. Magalhães, A. Mendes, Influence of Pyrolysis Parameters on the Performance of CMSM, International Journal of Chemical Engineering 2009 (2009) 1-7.

[43]   A. Soffer, J. Gilron, S. Saguee, R. Hed-Ofek, H. Cohen, Process for the production of hollow carbon fiber membranes, US005925591, 1999.

[44]   F. Dreisbach, H.W. Losch, P. Harting, Highest pressure adsorption equilibria data: Measurement with magnetic suspension balance and analysis with a new adsorbent/adsorbate-volume, Adsorption 8 (2002) 95-109.

[45]   C.S.R. Freire, A.J.D. Silvestre, C.P. Neto, M.N. Belgacem, A. Gandini, Controlled heterogeneous modification of cellulose fibers with fatty acids: Effect of

reaction conditions on the extent of esterification and fiber properties, J Appl Polym Sci 100 (2006) 1093-1102.

[46]   M. Sevilla, A.B. Fuertes, The production of carbon materials by hydrothermal carbonization of cellulose, Carbon 47 (2009) 2281-2289.

[47]   E. Togawa, T. Kondo, Unique structural characteristics of nernatic ordered cellulose-stability in water and its facile transformation, J Polym Sci Pol Phys 45 (2007) 2850-2859.

[48]   L.N. Zhang, D. Ruan, J.P. Zhou, Structure and properties of regenerated cellulose films prepared from cotton linters in NaOH/Urea aqueous solution, Ind. Eng. Chem. Res. 40 (2001) 5923-5928.

[49]   R. Hussain, R. Qadeer, M. Ahmad, M. Saleem, X-ray diffraction study of heat-treated graphitized and ungraphitized carbon, Turkish Journal of Chemistry 24 (2000) 177-183.

[50]   M.C. Campo, F.D. Magalhães, A. Mendes, Comparative study between a CMS Membrane and a CMS Adsorbent: Part I – Morphology, adsorption equilibrium and kinetics, J. Membr. Sci. 346 (2010) 15-25.

[51]   N.D. Hutson, R.T. Yang, Theoretical Basis for the Dubinin-Radushkevitch (D-R) Adsorption Isotherm Equation, Adsorption 3 (1997) 189-195.

[52]   S. Lagorsse, F.D. Magalhães, A. Mendes, Carbon molecular sieve membranes - Sorption, kinetic and structural characterization, J. Membr. Sci. 241 (2004) 275-287.

[53]   C. Nguyen, D.D. Do, Adsorption of supercritical gases in porous media: Determination of micropore size distribution, J. Phys. Chem. B 103 (1999) 6900-6908.

[54]   C. Nguyen, D.D. Do, K. Haraya, K. Wang, The structural characterization of carbon molecular sieve membrane (CMSM) via gas adsorption, J. Membr. Sci. 220 (2003) 177-182.

[55]   S.W. Rutherford, C. Nguyen, J.E. Coons, D.D. Do, Characterization of carbon molecular sieves using methane and carbon dioxide as adsorptive probes, Langmuir 19 (2003) 8335-8342.

[56]   H. Suda, K. Haraya, Gas permeation through micropores of carbon molecular sieve membranes derived from Kapton polyimide, J. Phys. Chem. B 101 (1997) 3988-3994.

[57]   M.C. Campo, S. Lagorsse, F.D. Magalhães, A. Mendes, Comparative study between a CMS Membrane and a CMS Adsorbent: Part II –Water vapor adsorption and surface chemistry J. Membr. Sci. 346 (2010) 26–36.

[58]   S.W. Rutherford, Modeling water adsorption in carbon micropores: Study of water in carbon molecular sieves, Langmuir 22 (2006) 702-708.

[59]   L.M. Robeson, Correlation of Separation Factor Versus Permeability for Polymeric Membranes, J. Membr. Sci. 62 (1991) 165-185.

Chapter IV

Chapter 4 - Modeling and simulation of a CMSM module

4.1. Separation of nitrogen from air by carbon molecular sieve membranes[5]

4.1.1. Abstract

In this work, the experimental properties of a carbon molecular sieve membrane made out of cellophane were used to model and simulate a membrane module for the production of nitrogen from air. The mass transport across the membrane has been related to its porous structure. The mathematical model developed accounts for counter- and co-current operation modes, pressure-dependent permeabilities and pressure drop along the membranes. A product stream of high pure nitrogen (> 99.9 %) was obtained from the retentate side, with recoveries up to 65 %. It was considered different feed to permeate pressure ratios and different feed pressures. It was concluded that higher ratios and higher feed pressures favor the separation. Furthermore, the pressure drop along the membranes has a negative impact on the performance of the unit.

4.1.2. Introduction

Air is composed essentially by nitrogen, oxygen and argon, with traces of other components, such as carbon dioxide and water vapor. It is used as raw material in the production of nitrogen and oxygen up to various purities. This chapter focuses on the recovery of nitrogen from air. The use of nitrogen is frequent in different kinds of

industry, namely for purging of pipelines and vessels, blanketing of equipment [1] and for inertization in the food and pharmaceutical industry. For several years, nitrogen was produced from air by cryogenic distillation, and more recently by pressure swing adsorption (PSA). Often, the latter technology involves the use of carbon molecular sieve adsorbents packed in two beds [2].

Lately, significant efforts have been directed towards membrane technology. This presents some advantages, since it requires low maintenance. Additionally the separation modules are compact and light-weight and can be positioned either vertically or horizontally [3]. It is expected that this technology will lead to an increasing impact over the gas separation market, including the nitrogen separation from air [4, 5]. The development of more productive membranes and a deeper understanding of the separation mechanisms are meaningful efforts aiming at a better and more efficient membrane separation process.

In the last ten years only a few simulation gas permeator studies have addressed air separation [6-11]. Coker et al. [6] have used a model to predict multicomponent separations with a polysulfone hollow fiber membrane module. Simulations of co-current, counter-current, and cross-flow contacting patterns with permeate purging (or sweep) were analyzed for the particular separation of nitrogen from a four component air mixture. They specified that the numerical approach used on their work was able to include a pressure-dependent permeability coefficient, but did not explore this point. Rautenbach et al. [9] investigated how the fiber properties (fiber skin thickness, diameter and selectivity) affect the performance of defect-free hollow fiber membrane modules for air separation. For this purpose, these authors presented a flexible simulation method capable of modeling the performance of a gas separation module with variations in fiber properties. Lababidi [9] simulated a cascade of polysulfone membrane modules in series and validated the mathematical models with experimental data for co-current and counter-current. The permeances used on the models were obtained as a function of partial pressure of nitrogen and oxygen by correlating experimental data. Chowdhurry et al. [10] proposed a new numerical solution approach for a model accounting for a multicomponent gas

148

separation. The simulations were performed and validated for air separation experiments with asymmetric cellulose acetate hollow fibers. The use of artificial neural network to model a hollow fiber membrane module for the separation of oxygen from air has been employed by Madaeni et al. [11]. Several feed pressures were studied but the permeability of oxygen and nitrogen was kept constant in the simulations.

The present work deals with the simulation of nitrogen production from air using a membrane module equipped with carbon molecular sieve membranes (CMSM). These membranes share the same structural characteristics with carbon molecular sieve adsorbents used in PSA systems: both carbonaceous materials present a narrow pore size network, allowing for the separation of molecules or atoms with very similar sizes, as is the case of nitrogen and oxygen [12]. Therefore, CMSM are a promising alternative to polymeric membranes for low-cost production of high purity nitrogen, due to their increased selectivity O_2/N_2 and high permeabilities [13].

The CMSM considered for the simulation has been synthesized and characterized, as described in Chapter III [14], being prepared by pyrolysis of cellophane. The pyrolysed CMSM revealed to be promising with good permeabilities and high selectivities when compared to polymeric membranes. Thes membrane – designated as Celo550 - was found to yield the best compromise between selectivity and permeability, among the ones produced at different conditions. The lab-prepared samples of Celo550 were flat sheets. However, scale-up should involve hollow fiber configuration, which is better suited for industrial applications [13] - greater surface to volume ratio and improved mechanical stability. This work, therefore, considers a hollow fiber CMSM having the same characteristics as Celo550, operating in co- and counter-current. The mathematical model developed accounts for pressure-dependent permeability and for pressure drop along the membrane.

4.1.3. Model

4.1.3.1. Membrane fundamentals

The flux of component i, J_i, through a membrane is given by

$$J_i = \frac{L_i^*}{\delta} \Delta p_i \tag{4.1}$$

where L_i^* is the permeability of component i, Δp_i is the partial pressure driving force established between retentate and permeate sides of the membrane, and δ is the membrane thickness. On the other hand, inside the membrane the transport is governed by the Fick's law:

$$J_i = -D_i\, \rho_s\, \frac{\partial q_i}{\partial r} \tag{4.2}$$

where D_i is the diffusivity of component i, q_i is its concentration in the adsorbed phase, ρ_s is the skeleton density of the membrane and r is the radial coordinate along the membrane thickness. Combining the previous two equations, a relation among the permeability, diffusivity and the adsorption equilibrium isotherm can be established,

$$L_i^* = -\frac{\rho_s}{\Delta p_i} \int_{q_i(c_i|_{x=0})}^{q_i(c_i|_{x=\delta})} D_i\, \mathrm{d}q_i \tag{4.3}$$

Therefore, to predict the pressure dependence of the permeabilities towards N_2, O_2, CO_2 and H_2O, adsorption data is required.

4.1.3.2. Assumptions and model equations

A gas separation unit is simulated assuming a hollow fiber like module – see schematic representation in Figure 4.19. The module is assumed as a bundle of hollow fibers with the same characteristics as the CMSM Celo550 obtained previously [14]. It is considered that the feed stream flows on the shell side while permeate is collected from the bore side.
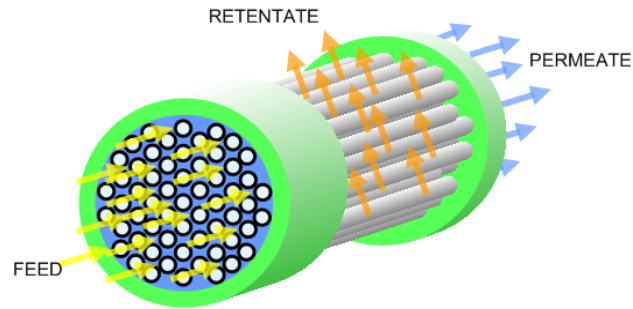
Figure 4.19 – Permeation module.

The main assumptions of the model are:

- The pressure drop on the feed (shell) and permeate (bore) sides is given by the Hagen-Poiseuille equation;

- The mass transport through the membrane thickness is described by the sorption-diffusion model;

- Plug flow and ideal gas behavior are assumed;

- Steady-state operation.

Based on these assumptions the model equations can now be written. The partial balance for a species i at the retentate side is given by,

$$-\frac{\partial\left(uc_i\right)}{\partial z} - N_i = 0 \tag{4.4}$$

where u is the velocity, c_i is the molar concentration of species i, z is the space coordinate along the axial direction and $N_i = \dfrac{N_\mathrm{f}\, 2\pi R}{\varepsilon A_s} J_i$. N_f is the number of fibers in the module, R is the radius of a hollow fiber, A_s is the cross section area of the module and $\varepsilon = 1-\left(N_\mathrm{f} R^2 / R_\mathrm{shell}^2\right)$ is the porosity of the module, which describes the module packing, being R_shell the radius of the modules' shell.

The total mass balance is similarly described as,

$$-\frac{\partial(uc)}{\partial z} - \sum_{i=1}^{nc} N_i = 0 \tag{4.5}$$

where c is the total concentration.

Considering that the permeability L_i^* is constant along the membrane thickness, δ, the mass transfer across the membrane is given by:

$$N_i = \frac{N_f 2\pi R}{\varepsilon A_s} L_i \left(c_i^R - c_i^P \right) \Re T \tag{4.6}$$

$L_i = L_i^* / \delta$ is the permeance of species i, c_i^R and c_i^P are the concentration of species i at the retentate and permeate, respectively, $\Re$ is the ideal gas constant and T is the temperature.

However, according to eq. (4.3), the permeability is given as the product of diffusivity and the adsorption equilibrium isotherm. Therefore, eq. (4.6) becomes:

$$N_i = \frac{N_f 2\pi R}{\varepsilon A_s} \frac{\rho_s}{\delta} \int_{q_i(c_i|_{z=\delta})}^{q_i(c_i|_{z=0})} D_i \, dq_i \tag{4.7}$$

The pressure drop on both retentate and permeate sides is given by the Hagen-Poiseuille equation [15]:

$$-\frac{dp}{dz} = \frac{8\mu}{R^2} u \tag{4.8}$$

where and μ is the viscosity of the gas.

4.1.3.3. Boundary conditions

The boundary conditions for the mass balance equations are defined considering a hollow-fiber module operating in counter- and co-current modes – see Figure 4.20.

Retentate side, counter- and co-current modes:

$$z = 0: \quad uc_i = u^F c_i^F$$
$$u = u^F$$

where u^{F} is the velocity of the feed gas.

Permeate side, co-current mode:

$$z = 0: \quad \frac{\partial c_i}{\partial z} = 0$$
$$u = 0$$

The permeate side, counter-current mode:

$$z = \ell: \quad \frac{\partial c_i}{\partial z} = 0$$
$$u = 0$$

where ℓ is the membrane length.

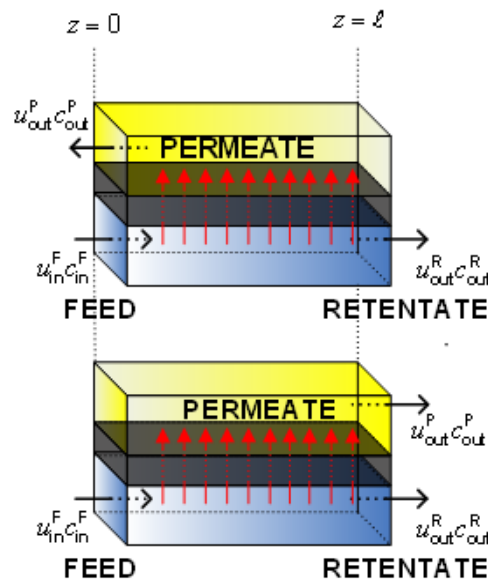Figure 4.20 – Counter- and co-current operating modes.

4.1.3.4. Dimensionless mass balance equations

Eqs. (4.4), (4.5), (4.6), (4.7) and (4.8) were rewritten in their dimensionless form and are given below. The advantage of using dimensionless variables is the decrease on the total number of variables required for the simulation, being therefore unnecessary the specification of design parameters.

Partial mass balance:

$$-\frac{\partial(u^*c_i^*)}{\partial x} - N_i^* = 0 \ , \ i = 1, \text{nc} \tag{4.9}$$

Total mass balance:

$$-\frac{\partial(u^*c^*)}{\partial x} - \sum_{i=1}^{\text{nc}} N_i^* = 0 \tag{4.10}$$

where $c^* = c/c_{\text{ref}}$ is the dimensionless concentration, $c_{\text{ref}} = p_{\text{ref}}/(\Re T_{\text{ref}})$ is the reference concentration at the reference pressure, p_{ref}, and temperature, T_{ref}. The dimensionless velocity is $u^* = u/u_{\text{ref}}$, where $u_{\text{ref}} = u^{\text{F}}$ and u^{F} is the velocity of the feed entering the module.

Mass transfer across the membrane considering pressure-independent permeability:

$$N_i^* = \Gamma \alpha_i \left(c_i^{*R} - c_i^{*P} \right) T^* \tag{4.11}$$

where $N_i^* = N_i \tau_{\text{b}}/c_{\text{ref}}$ is a dimensional variable representing the flux across the membrane, $\tau_{\text{b}} = \ell/u_{\text{ref}}$ is the residence time of the gas in the bulk phase, $x = z/\ell$ is the dimensionless space coordinate, $\alpha_i = L_i/L_{\text{ref}}$ with L_{ref} being the permeance of a reference component and c_i^{*R} and c_i^{*P} are, respectively, the gas phase concentration of species i at the retentate and permeate. Finally, $\Gamma = \dfrac{\tau_{\text{b}} N_{\text{f}}}{\varepsilon} \dfrac{2\pi R}{A_{\text{s}}} L_{\text{ref}} T_{\text{ref}} \Re$, can be designated as a contact time.

Dimensionless mass transfer across considering pressure-dependent permeability:

$$N_i^* = \Gamma' \gamma D_i \left(q_i^{*R} - q_i^{*P} \right) \tag{4.12}$$

where $\Gamma' = \dfrac{\tau_{\text{b}} N_{\text{f}}}{\varepsilon} \dfrac{2\pi R}{A_{\text{s}}} T_{\text{ref}} \Re$, $\gamma = \dfrac{\rho_{\text{s}}}{\delta} \dfrac{q_{\text{ref}}}{c_{\text{ref}}} \dfrac{1}{\Re T_{\text{ref}}}$ and D_i is considered constant, and $q_i^* = q_i/q_{\text{ref}}$ is the dimensionless concentration in the adsorbed phase where q_{ref} is the reference concentration in the adsorbed phase.

Dimensionless Hagen-Poiseuille equation for pressure drop:

$$-\frac{dc^*}{dx} = \beta \frac{u^*}{T^*} \qquad\qquad (4.13)$$

where $\beta = \dfrac{8\mu}{R^2} \dfrac{u_{\text{ref}}}{T_{\text{ref}}} \dfrac{L}{c_{\text{ref}}} \dfrac{1}{\Re}$.

4.1.3.5. Dimensionless boundary conditions

From the retentate side:

$$x = 0: \quad u^* c_i^* = u^{*\text{F}} c_i^{*\text{F}}$$
$$u^* = u^{*\text{F}}$$

From the permeate side in co-current mode:

$$x = 0: \quad \frac{\partial c_i^*}{\partial x} = 0$$
$$u^* = 0$$

From the permeate side in counter-current mode:

$$x = 1: \quad \frac{\partial c_i^*}{\partial x} = 0$$
$$u^* = 0$$

4.1.4. Numerical method

The membrane model was solved using the false transient method [16]. This method consists in adding a time derivative term to the left-hand side of the equations, avoiding numerical instability problems.

The space derivatives were computed using the finite volume method coupled with the WACEB high resolution scheme [17]. The resulting initial value problem was then integrated explicitly in time using the package LSODA [18]. The routine LSODA solves initial boundary problems for stiff or non-stiff systems of first-order ordinary differential equations (ODEs). The algorithm for solving the system of partial

differential equations is sketched in Figure 4.21. The procedure should be followed for both retentate and permeate sides, simultaneously.
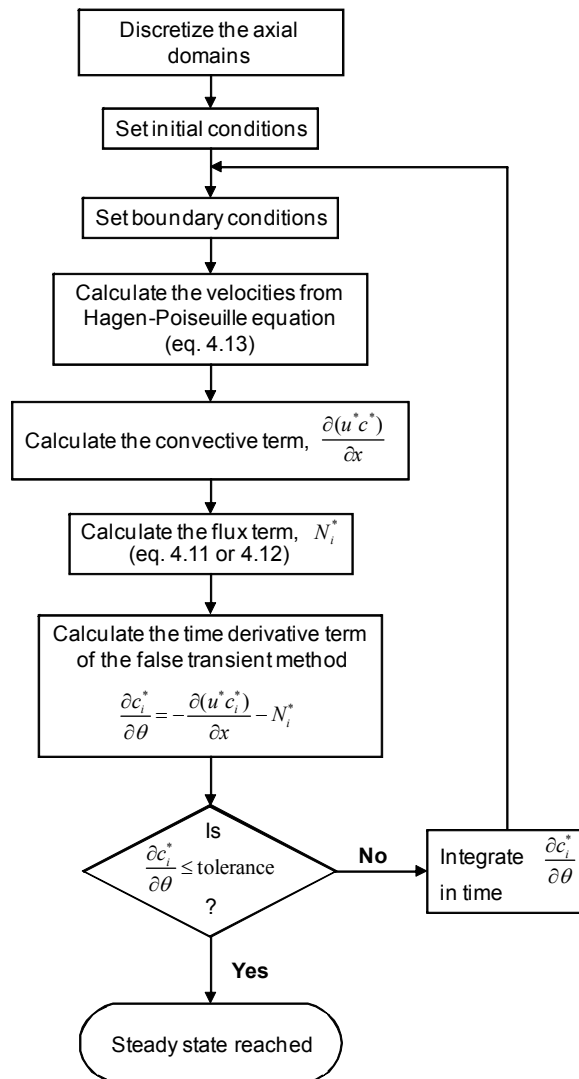

Figure 4.21 – Algorithm for solving partial differential equations.

4.1.5. Experimental

4.1.5.1. Permeation method

The permeabilities of the CMSM membrane Celo550 towards N_2, CO_2, N_2 and H_2O at 2 bar feed pressure and 3 mbar at the permeate side at 29.5 °C have been presented in Chapter III [14].

4.1.5.2. Adsorption experiments using the gravimetric method

The adsorption equilibrium isotherms and uptake curves of N_2, CO_2 and O_2 on Celo550 were determined at 29.5 °C from 0-7 bar by the gravimetric method using a suspension magnetic balance from Rubotherm®. The sample was fragmented into flakes in order to fill the weighing basket. The increments in pressure performed for the uptake curves were small enough to ensure constant diffusivities within the transient range, minimizing thermal effects. The experimental set-up was described in Chapter II [19]. The adsorption and desorption equilibrium isotherms and uptake curves of water vapor were also obtained by the gravimetric method at 29.5 °C up to 0.95 of relative pressure. The skeleton density of the membranes, $\rho_s = 1.48 \times 10^3 \, \text{kg m}^{-3}$, was obtained by helium picnometry.

4.1.6. Results and discussion

4.1.6.1. Adsorption equilibrium of N_2, O_2, CO_2 and water vapor

The Langmuir equation was used to fit the experimental adsorption equilibrium values of N_2 and O_2 and the SIPS equation to fit the adsorption values of CO_2. The Langmuir and SIPS equations are, respectively [20]:

$$q = q_s \frac{bp}{1+bp} \tag{4.14}$$

$$q = q_s \frac{(bp)^{1/n}}{1+(bp)^{1/n}} \tag{4.15}$$

Where q is the concentration in the adsorbed phase, q_s is the saturation capacity, b is the affinity coefficient and n is a parameter. The equations were fitted to experimental data by minimizing the sum of the square of the residues divided by the number of points, np, where q' is the concentration predicted by the equation.

Figure 4.22 presents the experimental adsorption equilibrium values and respective fitting equations. Table 4.1 lists the fitting parameters obtained.
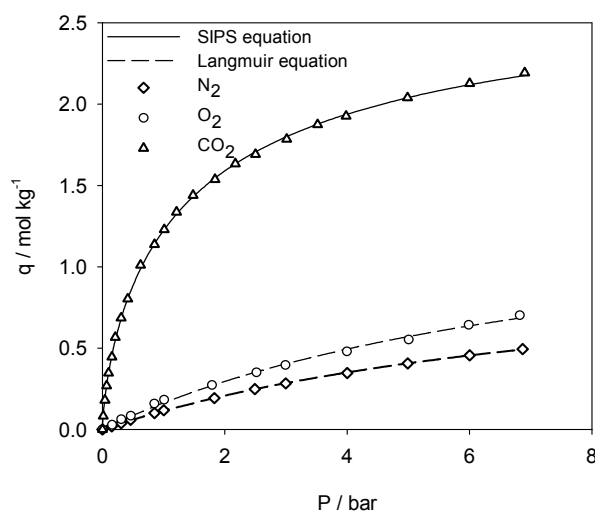
Figure 4.22 – Adsorption equilibrium data for Celo550 at 29.5 $^{\circ}$C.

Table 4.1 - Parameters of the Langmuir and SIPS equation for Celo550 obtained from the adsorption equilibrium values determined by the gravimetric method at 29.5 $^{\circ}$C.

	Langmuir and SIPS parameters			
	q_s (mol·kg^{-1})	b (bar^{-1})	n	$\sum\left(q-q^*\right)^2 \big/ np$
N$_2$	1.126	0.113	-	$3.05 \times 10\text{-}5$
CO$_2$	2.904	0.648	1.369	$2.56 \times 10\text{-}3$
O$_2$	1.513	0.121	-	$1.67 \times 10\text{-}3$

The adsorption equilibrium curves show that CO_2 is the most adsorbable species followed by O_2 and N_2. The equilibrium selectivity of oxygen over nitrogen is significantly higher than usual for this kind of materials. The volume of pores with diameters larger than oxygen, but smaller than nitrogen is equivalent to

0.064 mol kg^{-1}, as obtained from the micropore size distribution derived for Celo550 with CO_2 at 0 °C, presented in Chapter III [14]. The existence of pores with dimensions between oxygen's and nitrogen's diameter will allow oxygen to be adsorbed, but not nitrogen. In fact, the difference between the amounts adsorbed of oxygen and nitrogen at 1 bar is about 0.065 mol kg^{-1}; it is considered that up to 1 bar these ultramicropores are filled up.

The adsorption and desorption equilibrium isotherms of water vapor were obtained for Celo550 by the gravimetric method at 29.5 °C up to 0.95 of relative pressure in the same set-up mentioned before. The experimental values are given in Figure 4.23 as a function of relative pressure, considering 41.27 mbar the water vapor pressure at 29.5 °C. A linear adsorption isotherm is able to describe the experimental adsorption branch reasonably well.
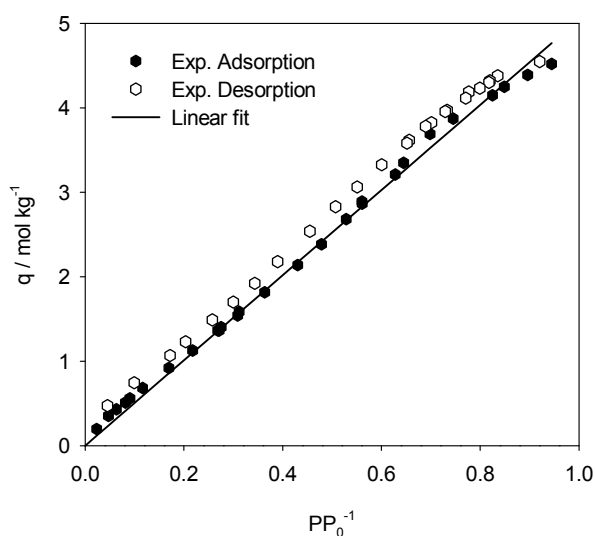
Figure 4.23 – Adsorption and desorption equilibrium isotherms of water vapor on Celo550 at 29.5 °C.

The shape of the adsorption isotherm is in agreement with the large permeabilities found for water vapor; the significant amount adsorbed at very low relative pressures confirms the hydrophilic character of these membranes already discussed in Chapter III [14]. Furthermore, it should be noted that the adsorption of water vapor is reversible as confirmed by replication of adsorption equilibrium values and

diffusivities obtained for nitrogen. As similarly observed on Celo550 [14], the exposure to water vapor did not affect the performance of the membranes, as rechecked by permeating helium afterwards. The linear fit exhibits a slope of 5.04 mol kg^{-1}, which physically corresponds to the Henry constant. There is a little hysteresis, usually attributed to a different desorption mechanism, rather than to capillary condensation.

4.1.6.2. Diffusivities based on uptake curves

The apparent diffusion time constant D/r^2 for each pressure, where D is the diffusivity, was directly computed from the experimental uptake curves, by applying the isothermal diffusion model for slab geometry [20] as represented in eq.(4.16):

$$F = 1 - \frac{2}{\pi^2} \sum_{n=1}^{\infty} \frac{1}{(n-1/2)^2} \exp\left[-(n-1/2)^2 \, \pi^2 \, \frac{D}{r^2} t\right] \qquad (4.16)$$

where F is the fractional uptake at instant t. The obtained apparent time constants were afterwards correlated as a function of loading by using the following pressure-dependent models:

$$D_\mu = D_{\mu 0} \frac{\partial \ln p}{\partial \ln q} \qquad (4.17)$$

This is the Darken relation [20] where $D_{\mu 0}$ is the diffusivity at zero loading and is a parameter of the model. When the Langmuir or SIPS equation are used to describe the adsorption equilibrium, the relation takes the following forms, respectively:

$$D_\mu = D'_{\mu 0} (1 + bp) \qquad (4.18)$$

$$D_\mu = D'_{\mu 0} \left(1 + (bp)^{1/n}\right) \qquad (4.19)$$

However, for some systems the Darken model fails to describe the relation of diffusivities with loading. Do et al. proposed a structural-diffusion relation [21] which accounts for a stronger pressure dependence:

$$D_\mu = \frac{A}{\partial q / \partial p} \qquad (4.20)$$

where A is a constant. When the adsorbed concentration, q, is given by a Langmuir equation it turns to:

$$D_\mu = D'_{\mu 0}\left(1+bp\right)^2$$

(4.21)

Chen and Yang have suggested and developed a new model which includes an extra parameter, Λ, that accounts for the pore blockage effects as well as loading [22]. This model predicts increasing, decreasing or constant pressure-dependences and is presented below:

$$D_\mu = D'_{\mu 0}\frac{1-\theta+\dfrac{\Lambda}{2}\theta\left(2-\theta\right)+H\left(1-\Lambda\right)\left(1-\Lambda\right)\dfrac{\Lambda}{2}\theta^2}{\left(1-\theta+\dfrac{\Lambda}{2}\theta\right)^2}$$

(4.22)

where θ is the surface coverage and Λ is a pore blockage parameter, that accounts for lateral interactions. If no blockage exists, $\Lambda = 0$, and the expression reverts to the Darken relation.

Figure 4.24 represents the pressure-dependence of the apparent time constants for the diffusing species N_2, CO_2 and O_2 on Celo550 and respective fits.
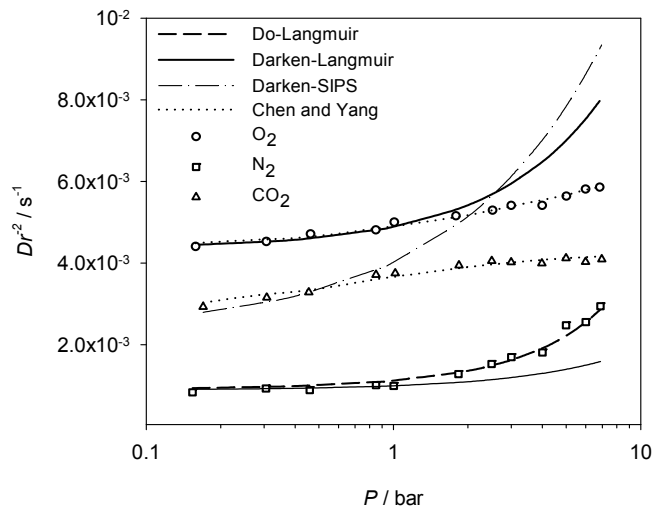

Figure 4.24 – Relationship between the apparent time constant and pressure at 29.5 °C for Celo550.

Table 4.2 lists the parameters obtained.

Table 4.2 – Pressure-dependent models and its parameters for Celo550.

	Do-Langmuir		Chen and Yang	
	b (bar^{-1})	$D_{\mu 0}/r^2$ (s^{-1})	Λ	$D_{\mu 0}/r^2$ (s^{-1})
N_2	1.129×10^{-1}	9.09×10^{-4}	-	-
CO_2	-	-	1.3	2.64×10^{-3}
O_2	-	-	1.7	4.41×10^{-3}

The first model used to fit the obtained pressure dependences was the Darken-Langmuir for N_2 and O_2 and Darken-SIPS for CO_2. However, from Figure 4.24 it is seen that this relation could only predict the tendency for pressures up to 1 bar, failing the remaining increasing pressures; in the case of N_2, the model underestimates the apparent time constants and a stronger pressure-dependent model was successfully used – Do-Langmuir; as for O_2 and CO_2, the Darken relation overestimates the apparent time constants for pressures higher than 1 bar. For O_2 and CO_2, the diffusion time constant increases with the pressure but at slower rate than predicted by the Darken or Do models. Chen and Yang's model (Eq. (4.22)) provided a much better fit. This may be physically associated to pore blockage effects, only evident for these smaller species

The experimental uptake curves of water vapor on Celo550 were well fit according to the Linear Driving Force (LDF) model for each increment in relative pressure. The model is described as follows:

$$F = 1 - e^{kt} \tag{4.23}$$

where F is the fractional uptake, k the LDF rate constant and t the time. The values of k were computed from the uptake curves for all relative pressures and are represented in Figure 4.25.
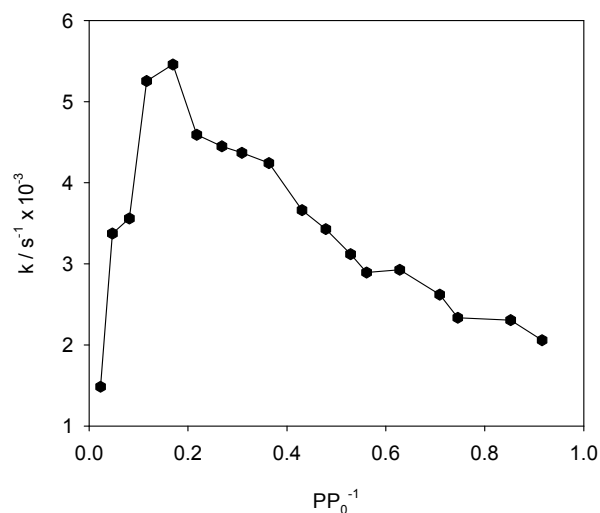
Figure 4.25 – LDF rate constants for water vapor on Celo550 at 29.5 °C.

The LDF rate constants present a maximum for $p/p_0 \approx 0.17$, which corresponds to the adsorption at the primary centers, i.e., at the hydrophilic centers. Afterwards, the rate constants decrease as the saturation pressure is approached.

4.1.6.3. Permeabilities based on steady-state permeation

The permeabilities of the membrane, L^{*P}, were obtained from steady-state permeation experiments at 2 bar feed pressure for N_2, CO_2, O_2 and H_2O. Using eq. (4.3), the experimental values of permeability and the adsorption equilibrium isotherms, it is possible to compute the diffusivities of the studied gases, D_μ^P.

On the other hand, the gravimetric method allowed to obtain the diffusivities based on uptake experiments, D_μ^A. Table 4.3 summarizes the diffusivities and permeabilities of the membrane from permeation and gravimetric methods.

Table 4.3 – Diffusivities of N_2, O_2, CO_2 and water vapor at 29.5 °C on Celo550 and respective permeabilities obtained and calculated from different methods.

	Permeation method		Gravimetric method
$p = 2\,\mathrm{bar}$	L^{*P} / $\mathrm{m^3 \cdot m \cdot m^{-2} \cdot bar^{-1} \cdot s^{-1}}$	D_μ^P ($\mathrm{m^2 \cdot s^{-1}}$)	D_μ^A ($\mathrm{m^2 \cdot s^{-1}}$)
N_2	2.54×10^{-13}	8.91×10^{-14}	8.89×10^{-14}
O_2	3.30×10^{-12}	8.29×10^{-13}	4.19×10^{-13}
CO_2	1.29×10^{-11}	1.46×10^{-12}	0.31×10^{-12}
$p/p_0 = 0.92$			
H_2O	7.22×10^{-10}	5.78×10^{-14}	5.55×10^{-14}

CMSMs present pores available for mass transport across the membrane, which may be named as "effective pores", but also dead-end pores, which do not contribute to mass transport. Both effective and dead-end pores are assessed by the uptake curve method, while the permeation method only has access to the effective pores.

The diffusivities found from the two methods were similar for nitrogen, but different for oxygen and carbon dioxide. This might be an indication that the dead-end pores exist but are not accessible to nitrogen. On the other hand, oxygen and carbon dioxide, both smaller than nitrogen, actually have access to dead-end pores, justifying the decreased diffusivities obtained by the gravimetric method. It is believed that the real mass transfer across the membrane is better described by permeation experiments [23]. The mass transfer model will use the diffusivity obtained by the permeation method combined with the adsorption equilibrium isotherm data, for each species.

4.1.6.4. Simulation

The simulation tool allows to better understanding, designing, and optimizing the separation unit. It is possible to assess the influence of the main factors in the performance of the module such as the dimensional characteristics of the membrane module and operation conditions. In this work the objective is to purify nitrogen from air, using a module made of carbon molecular sieve membranes. These present pressure-dependent permeabilities, as explained before, and for this reason it may be

important to provide a model that describes the real behavior of the membrane. To analyze the relevance of this fact, a comparison between the use of pressure-independent permeability and pressure-dependent approach is provided. Afterwards, different operating conditions such as the feed to permeate pressure ratio, R, are also studied, as well as the effect of pressure range for the same ratio. The influence of the pressure drop along both retentate and permeate sides on the performance of the membrane module was studied; this is important since it can be used for optimizing the aspect ratio of the fibers.

It is assumed that the air feed stream used in the simulations is a four component mixture [24] as presented in Table 4.4.

Table 4.4 – Air molar fraction composition [24].

	Air molar composition			
Components	N$_2$	O$_2$	CO$_2$	H$_2$O
Y	0.79018 d.b.	0.209476 d.b.	0.000344 d.b.	0.04127 / p^{F}

d.b. – dry basis.

The molar fraction in the feed of the species i, y_i^{F}, is obtained from:

$$y_i^F = \frac{Y_i}{\displaystyle\sum_{j=1}^{NC} Y_j} \tag{4.24}$$

In the simulations, the recovery is defined as the amount of nitrogen leaving the module at the retentate side divided by the amount of nitrogen entering the module at the feed side. The recovery of nitrogen from the retentate stream is normally favored when counter-current operation mode is employed. This was also verified in this CMSM module where, for instance, for 65 % recovery, a nitrogen purity of 99.9 % is achieved in counter-current mode, while in co-current, a purity of 95.7 % is obtained. Therefore, in the following simulation studies only counter-current operation is considered.

Pressure-independent vs pressure-dependent permeability

The use of pressure-independent (eq. (4.6)) or pressure-dependent (eq. (4.7)) permeabilites is compared next, to analyze how it influences the separation. The pressure drop is assumed negligible and the feed pressure is considered to be 10 bar. The constant permeability case uses the experimental permeability value, which was obtained at 2 bar. The results are shown in Figure 4.26.
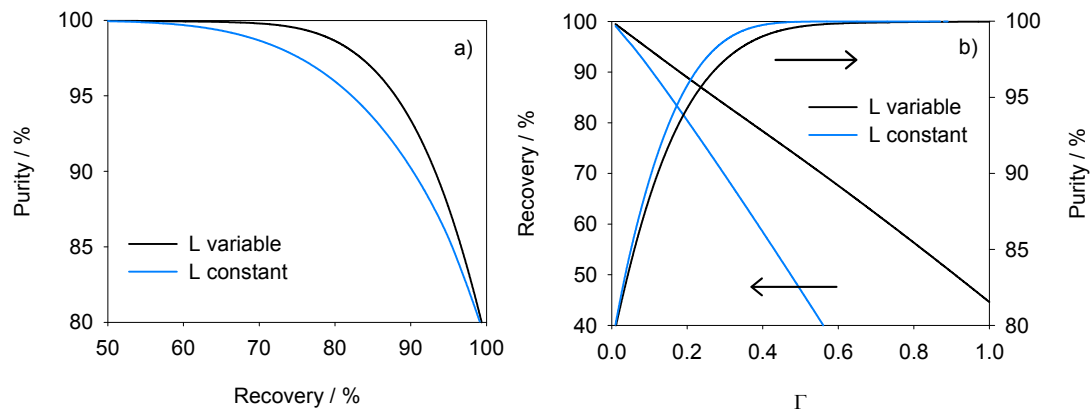

Figure 4.26 – Simulation results considering pressure-independent and pressure-dependent permeability at 29.5 °C, 10 bar feed pressure and 1 bar permeate pressure.

In these conditions, the use of a pressure-independent permeability results in lower recoveries for the same purity than the pressure-dependent permeability approach, as seen in Figure 4.26a. However, the pressure-independent permeability approach results in a smaller contact time (Γ) – see Figure 4.26b, hence it would result in an erroneous prediction of the module performance. Therefore the pressure-dependent permeability approach is considered in the remaining simulations.

Influence of the feed to permeate pressure ratio

For a permeate pressure of 1 bar, the effect of increasing the pressure ratio, R, between the feed and permeate pressure is shown in Figure 4.27.
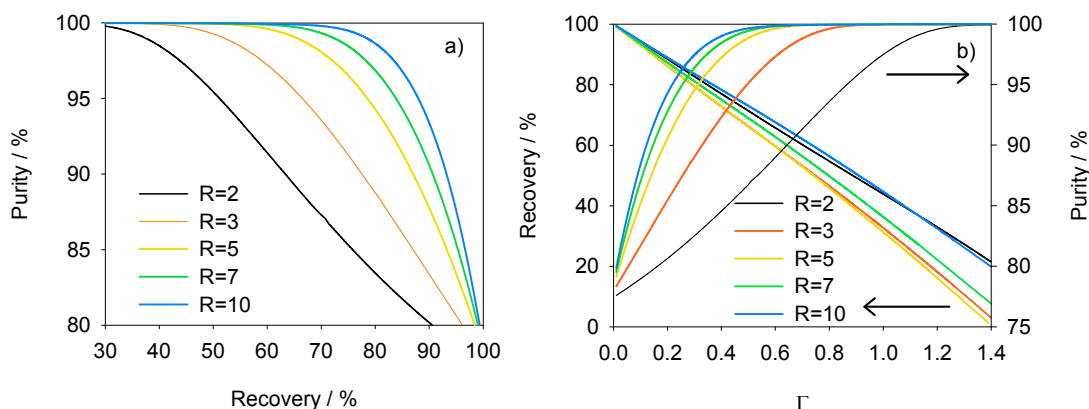
Figure 4.27 – Effect of the feed to permeate pressure ratio (R) on the purity and recovery of nitrogen from air at 29.5 ºC, 1 bar permeate side and $\beta = 10^{-5}$.

From Figure 4.27a, high purity nitrogen (99.99+ %) is achieved by using 2 up to 10 pressure ratio. However, for a 2 bar feed pressure ($R = 2$), a purity of 99.9 % is attained for a recovery of 26.1 %, while for a 10 bar feed pressure ($R = 10$) the same purity is obtained for a recovery of 65.4 %; generally, a higher R favors the separation of nitrogen. Indeed, it is seen that for $R \leq 3$ this tendency is not observed what can be explained by the shape of the isotherms – Figure 4.22. In fact, the decrease of the nitrogen permeability coefficient with pressure increase is greatly affected by the adsorption equilibrium of this component – eq. (4.3). Up to 3 bar the permeability decreases more pronouncedly than for pressures higher than this value. For pressures greater than 3 bar, the permeability decreases not so pronouncedly and at constant rate.

Influence of the pressure range for the same R

Since the model considers a pressure-dependent permeability, the effect of the feed pressure was studied. Figure 4.28 summarizes de simulation curves obtained for $R = 10$ and 2, 3, 5 and 10 bar feed pressures.
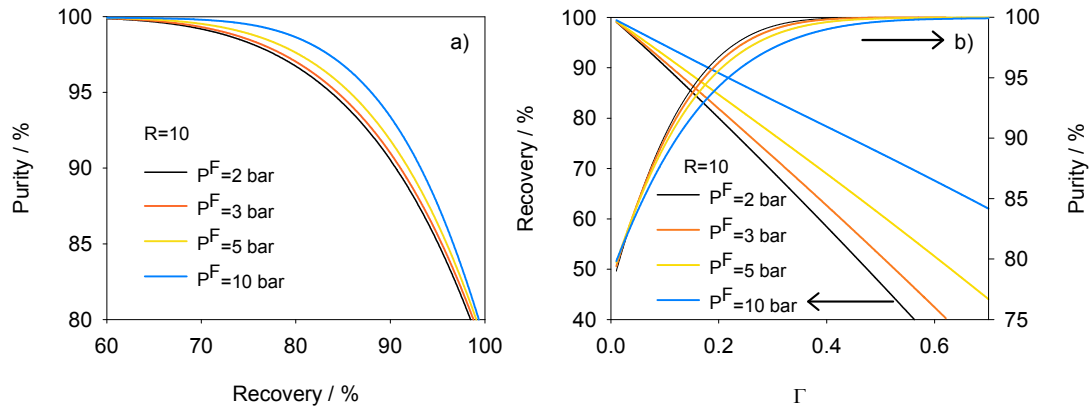
Figure 4.28 – Effect of the feed pressure, p^F, on the purity and recovery of nitrogen from air at 29.5 °C for constant $R = 10$ and $\beta = 10^{-5}$.

It is observed that an increase in feed pressure benefits the relation nitrogen purity *vs.* recovery. Furthermore, higher recoveries are achieved for the same contact time, due to a decrease in permeability with pressure (less product permeates through the membrane). Since the selectivity also decreases with pressure increase, the purity becomes compromised.

Influence of pressure drop

The effect of pressure drop along the membrane module was evaluated and given in Figure 4.29. The smaller the fibers' diameter, the longer the length of the module (fibers) and the tighter the packing, the higher becomes the pressure drop.
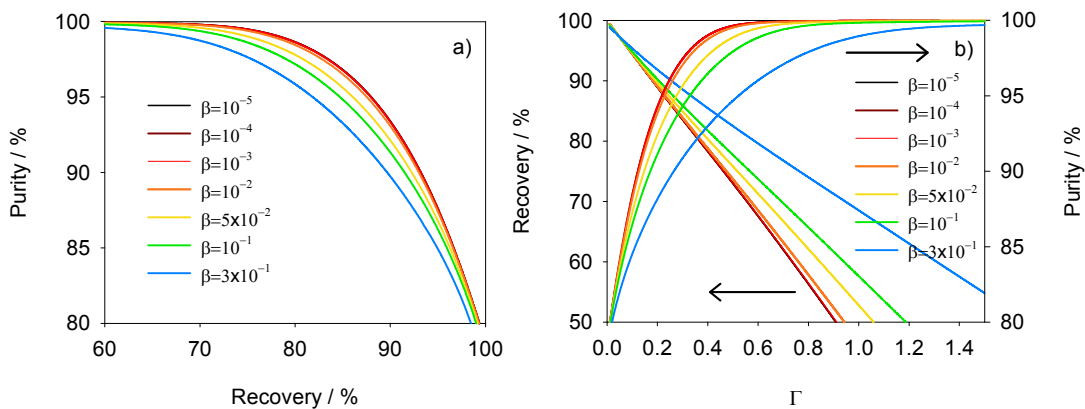

Figure 4.29 – Effect of the pressure drop on the purity and recovery of nitrogen from air at 29.5 °C for $R = 10$, 1 bar permeate side.

As expected, the pressure drop affects negatively the separation. Nevertheless, for values of β from 1x10^{-5} up to 1x10^{-2} no relevant losses are observed. However, for β higher than 1x10^{-2} the separation becomes significantly impaired. The recovery of nitrogen 99.9 % purity falls from 65.4 % for negligible pressure drop ($\beta = 10^{-5}$), to 16.1 % for a pressure drop corresponding to $\beta = 3 \times 10^{-1}$. Besides, the value of Γ in the former case is almost five times higher, corresponding to a module also five times larger or a feed flowrate five times smaller.

4.1.7. Conclusions

The present work deals with the simulation of nitrogen production from air using a membrane module set with carbon molecular sieve membranes (CMSM). The diffusivities of N_2, O_2, CO_2 and water vapor on a CMSM made out of cellophane (Celo550) obtained via gravimetric and permeation experiments were compared. The values of diffusivity found from the two methods were equal for nitrogen, but different for oxygen and carbon dioxide. This could be an indication that the dead-end pores existing in the membrane are not accessible to nitrogen, due to its larger kinetic diameter, but are acceded by oxygen and carbon dioxide.

Assuming pressure-independent permeability in the simulations led to lower recoveries than considering pressure-dependent permeability, for the same purity. The use of a pressure-independent permeability approach would therefore lead to an erroneous dimensioning of the membrane module.

It was also concluded that higher feed to permeate pressure ratios, generally, favor the separation of nitrogen, allowing higher recoveries or smaller contact times for a given purity. In addition, an increase of feed pressure also improves the recovery of the process, but compromises the purity, for the same feed to permeate pressure ratio. It was also observed that increasing the pressure drop significantly impairs the separation. For this reason, pressure drop should be taken into account when designing the module or preparing the fibers.

A key conclusion of this work is that carbon molecular sieve membranes, prepared from pyrolysis of cellophane up to 550 ºC, allow high purity nitrogen production from

air with large recoveries (up to 65 % for a purity of 99.9 % and negligible pressure drop) and using an air feed with 100 % RH.

4.1.8. Acknowledgments

4.1.9. Nomenclature

A Constant (eq.(4.20)), $m^2 \cdot s^{-1} \cdot bar \cdot mol^{-1} \cdot kg$

A_s Effective cross section area of the module, m^2

b Affinity coefficient of Langmuir and SIPS equations, bar^{-1}

c Total concentration in the gas phase, $mol \cdot m^{-3}$

c_i Concentration of component i in the gas phase, $mol \cdot m^{-3}$

D_i Diffusivity of component i through the membrane, $m^2 \cdot s^{-1}$

D/r^2 Apparent time constant, s^{-1}

F Fractional uptake

H Heaviside function

J_i Flux of component i through the membrane, $mol \cdot m^{-2} \cdot s^{-1}$

k LDF rate constant, s^{-1}

L_i Permeance of the membrane to component i, $mol \cdot m^{-2} \cdot Pa^{-1} \cdot s^{-1}$

L_i^* Permeability of the membrane to component i, $mol \cdot m \cdot m^{-2} \cdot Pa^{-1} \cdot s^{-1}$

N_i Molar flow rate of component i, $mol \cdot s^{-1} \cdot m^{-3}$

N_f Number of fibers in the module

nc   Number of components

np   Number of points

n Parameter of SIPS equation

p Total pressure, bar

p_i Partial pressure of component i, bar

q_i Concentration of component i in the adsorbed phase, $mol \cdot kg^{-1}$

q_s Saturation capacity, $mol \cdot kg^{-1}$

z Space coordinate along the membrane thickness, m

R_f Radius of the membrane fiber, m

R_{shell} Radius of the module's shell, m

R Ratio between feed and permeate pressure

$\Re$ Universal gas constant, bar·m³·mol⁻¹·K⁻¹

$\Re$ Universal gas constant, $bar \cdot m^3 \cdot mol^{-1} \cdot K^{-1}$

t Time, s

T Temperature, K

u Velocity, $m \cdot s^{-1}$

x Dimensionless axial coordinate

Y_i Dry basis molar fraction of component i in the air mixture

y_i Molar fraction of component i in the air feed mixture

z Axial coordinate, m

Greek Variables

α_i Selectivity of component i towards reference component

β Dimensionless parameter

ε Module void fraction

Γ Dimensionless contact time

Γ' "Contact time", $bar \cdot m^2 \cdot s \cdot mol^{-1}$

γ Constant, $mol \cdot m^{-4} \cdot bar$

Λ Blockage parameter of Chen and Yang model

μ Viscosity of the gas

θ Surface coverage

ρ_s Skeleton density of the membrane, $mol \, kg^{-1}$

τ_b Residence time, s

Subscripts

ref   Reference conditions

Superscripts

*   Dimensionless

F   Feed

R   Retentate

P   Permeate

4.1.10. References

[1]   M.B. Hagg, Membranes in chemical processing - A review of applications and novel developments, Sep. Purif. Methods 27 (1998) 51-168.

[2]   D.M. Ruthven, S. Farooq, K.S. Knaebel, Pressure swing adsorption, VCH Publishers, Inc., New York, 1994.

[3]   A.D. Ebner, J.A. Ritter, State-of-the-art Adsorption and Membrane Separation Processes for Carbon Dioxide Production from Carbon Dioxide Emitting Industries, Sep. Sci. Technol. 44 (2009) 1273-1421.

[4]   R.W. Baker, Future directions of membrane gas separation technology, Ind. Eng. Chem. Res. 41 (2002) 1393-1411.

[5]   S.P. Nunes, K.V. Peinemann, Gas Separation with Membranes, in: S.P. Nunes, K.V. Peinemann (Eds.), Membrane Technology in the Chemical Industry, Wiley, Weinheim, 2006, pp. 53-75.

[6]   D.T. Coker, B.D. Freeman, G.K. Fleming, Modeling multicomponent gas separation using hollow-fiber membrane contactors, AlChE J. 44 (1998) 1289-1302.

[7]   A. Mourgues, J. Sanchez, Theoretical analysis of concentration polarization in membrane modules for gas separation with feed inside the hollow-fibers, J. Membr. Sci. 252 (2005) 133-144.

[8]   H.M.S. Lababidi, Air separation by polysulfone hollow fibre membrane permeators in series - Experimental and simulation results, Chem Eng Res Des 78 (2000) 1066-1076.

[9]   R. Rautenbach, A. Struck, M.F.M. Roks, A variation in fiber properties affects the performance of defect-free hollow fiber membrane modules for air separation, J. Membr. Sci. 150 (1998) 31-41.

[10]   M.H.M. Chowdhury, X.S. Feng, P. Douglas, E. Croiset, A new numerical approach for a detailed multicomponent gas separation membrane model and AspenPlus simulation, Chemical Engineering & Technology 28 (2005) 773-782.

[11]   S.S. Madaeni, G. Zahedi, M. Aminnejad, Artificial neural network modeling of O2 separation from air in a hollow fiber membrane module, Asia-Pac J Chem Eng 3 (2008) 357-363.

[12]   H.J. Schröter, H. Jüngten, Gas separation by pressure swing adsorption using carbon molecular sieves, in: A.E. Rodrigues, M.D. LeVan, D. Tondeur (Eds.), Adsorption: Science and Technology, Kluwer Academic Publishers, Vimeiro, 1989, pp. 269-283.

[13]   A.F. Ismail, L.I.B. David, A review on the latest development of carbon membranes for gas separation, J. Membr. Sci. 193 (2001) 1-18.

[14] M.C. Campo, F.D. Magalhães, A. Mendes, Carbon molecular sieve membranes from cellophane paper, J. Membr. Sci. (2010), doi:10.1016/j.memsci.2009.1012.1026

[15] R.B. Bird, W.E. Stewart, E.N. Lightfoot, Transport Phenomena, 2nd ed., John Wiley & Sons, New York, 2002.

[16] J.M. Sousa, P. Cruz, F.D. Magalhães, A. Mendes, Modeling catalytic membrane reactors using an adaptive wavelet-based collocation method, J. Membr. Sci. 208 (2002) 57-68.

[17] P. Cruz, J.C. Santos, F.D. Magalhães, A. Mendes, Simulation of separation processes using finite volume method, Comput Chem Eng 30 (2005) 83-98.

[18] L. Petzold, Automatic Selection of Methods for Solving Stiff and Nonstiff Systems of Ordinary Differential-Equations, Siam J Sci Stat Comp 4 (1983) 136-148.

[19] M.C. Campo, F.D. Magalhães, A. Mendes, Comparative study between a CMS Membrane and a CMS Adsorbent: Part I – Morphology, adsorption equilibrium and kinetics, J. Membr. Sci. 346 (2010) 15-25.

[20] D.D. Do, Adsorption Analysis: Equilibria and Kinetics, Imperial College Press, London, 1998.

[21] D.D. Do, A model for surface diffusion of ethane and propane in activated carbon, Chem. Eng. Sci. 51 (1996) 4145-4158.

[22] Y.D. Chen, R.T. Yang, Concentration-Dependence of Surface-Diffusion and Zeolitic Diffusion, AlChE J. 37 (1991) 1579-1582.

[23] A.J. Bird, D.L. Trimm, Carbon Molecular-Sieves Used in Gas Separation Membranes, Carbon 21 (1983) 177-180.

[24] D.R. Lide (Ed.), CRC Handbook of Chemistry and Physics, 89th ed., CRC Press/Taylor and Francis, Boca Raton, 2009.

Chapter V

Chapter 5 - General Conclusions and Future Work

A carbon molecular sieve membrane (hollow fiber) from Carbon Membranes, Israel, and a carbon molecular sieve adsorbent, from Takeda, Japan, for PSA systems (spherical particle), have been compared. The objective of this analysis was to better understand the mass transport mechanism in CMS membranes and relate it to the material's structure. The ultramicroporosity was characterized in terms of micropore volume by the DR approach being for the membrane and adsorbent, respectively, 185.7 and 168.7 $cm^3 kg^{-1}$; the mean pore widths determined using the relation of Stoeckli et al. were, respectively, 0.498 nm and 0.514 nm. Accordingly, the determined micropore size distribution of the hollow fiber membrane was slightly shifted towards larger values of pore width, in relation to that of the adsorbent particle. The adsorption equilibrium isotherms and uptake curves of N_2, Ar, CO_2 and O_2 were determined at 29.5 °C, from 0-7 bar. Both materials exhibited similar shapes for the adsorption equilibrium curves; the experimental equilibrium values of N_2, Ar, and O_2 were fitted by the Langmuir equation while for CO_2 the SIPS equation was used. Concerning the kinetics, different models were employed to fit the uptake curves in order to obtain the apparent time constants. A diffusion model for a spherical homogenous particle was applied to fit experimental uptakes of N_2 and Ar. However, the fast diffusion of CO_2 and O_2 originated non-isothermal effects, implying the use of an appropriate model. As for the hollow fiber membrane, an isothermal diffusion model assuming slab geometry was tried. The pressure dependence of the apparent time constants for the CMS adsorbent followed a Darken-Langmuir relation for the diffusion of species N_2, Ar and O_2, while CO_2, on the other hand, exhibited a more pronounced pressure-dependence, following a Do-SIPS relation. The carbon membrane showed a Darken-Langmuir behavior for the larger species, N_2 and Ar,

while for CO_2 and O_2, showed a first increasing and then decreasing pressure-dependence. This last behavior was well described by a model developed by Chen and Yang, accounting for blockage effects that might occur inside the ultramicropores. In the membrane, the pore widths may allow lateral interactions (along the pore radial direction) of species CO_2 and O_2 rather than only axial interactions when two layers of adsorbed species are formed. When pressure increases the adsorbed concentration also increases and repulsive interactions between neighboring adsorbates lead to an enhancement of wall collisions, causing a decrease in diffusivity. In the adsorbent particle, with slightly smaller pore constrictions, only axial interactions should be relevant and diffusion followed an increasing pressure dependency. This is probably the fundamental difference between these two carbonaceous materials.

Contrarily to what was expected, no aging effects were observed due to oxygen exposure. Despite of that, the behavior towards exposure to water vapor was also studied and related to the surface chemistry of each material. Since these are carbonaceous materials, the water vapor adsorption is attributed to the existence of oxygenated functional groups, where water molecules firstly adsorb. The X-ray microanalyses confirmed the existence of oxygen in addition to carbon. Water vapor adsorption and desorption equilibrium isotherms were determined for both materials at 29.5 ℃ and a type V behavior was found, with well defined S-shaped curves. The first slope of the curves was attributed to adsorption around hydrophilic groups (oxygenated groups), followed by a steepest part, at an intermediate relative pressure range, related to the clusters' release from these sites, and finally, the adsorption of water clusters onto hydrophobic carbon walls. From the comparison between the two curves for the carbon membrane and carbon adsorbent particle, it was also concluded that the membrane has a greater hydrophilic character than the adsorbent particle. This was sustained by TG analyses, which showed a larger content of heteroatoms for HF CM, and by the significant adsorption at very low pressures. A new model was developed, accounting for both adsorption and desorption branches; it assumes that clusters of a generic size are formed. This model fitted the experimental results quite well for both materials. The adsorption kinetics was assessed for both carbon

178

molecular sieve materials and was well described by a LDF model. The different adsorption rate intervals obtained were related to the distinguishable stages of the adsorption isotherms.

Carbon hollow fiber membranes based on a co-polyimide P84/S-PEEK blend have been prepared. The influence of pyrolysis parameters, such as pyrolysis end temperature, soaking time, and quenching, on the properties of the membranes were studied and it was concluded that they affect the performance of the membranes. The highest permeances were obtained for the membranes heated up to 750 °C and quenched. The highest ideal selectivities were accomplished for the membranes submitted up to 700 °C previous to quenching. Furthermore, it was observed that the membranes quenched after reaching the end of the process revealed higher permeances than the ones naturally cooled. It was also concluded that the existence of a final soaking time at the end temperature, just before quenching, did not improve the performance of the carbon membranes, yielding to lower permeabilities. No decrease in the performance of the membrane due to CO_2 exposure was observed.

A different precursor to prepare CMSM was tried. A commercial film of cellophane paper has been used, for the first time, to prepare CMSMs by employing one single heating step. The effect of the pyrolysis end temperature was assessed from 450 up to 850 °C through scanning electron microscopy, X-ray microanalysis, X-ray diffraction and monocomponent permeation experiments at 29.5 °C. The permeability versus kinetic diameter towards He, H_2, Ar, N_2, CO_2, O_2, CH_4 and water vapor exhibited a molecular sieve mechanism for all the membranes prepared; this was in agreement with the micropore size distribution obtained for Celo550 (~0.3-0.8 nm).

Furthermore, the membranes revealed good ideal selectivities with separation performances mostly above the recently revised Robeson's upper bound for polymeric membranes. In addition, these membranes were extremely permeable to water vapor; X-ray microanalysis has shown that the membranes are essentially carbon-based, with traces of elemental oxygen, justifying the affinity of the carbon matrix towards water vapor. However, it was checked that carbon membranes

prepared in this work were not prone to aging effects due to exposure of oxygen or water vapor, or any other permeant, among the ones studied. Therefore, they can be considered in relevant industrial applications such as separation of nitrogen from air or recovery of hydrogen from synthesis gas.

The simulation of nitrogen production from air using a membrane module set with carbon molecular sieve membranes has been studied. For that reason, a mass transfer model for hollow fiber membrane module has been used.

To describe the mass transport through the membrane the diffusivities of N_2, O_2, CO_2 and water vapor on Celo550 were experimentally obtained via gravimetric method and compared to those estimated through permeation experiments. The values of diffusivity found from the two methods were equal for nitrogen, but different for oxygen and carbon dioxide. This suggests the existence of dead-end pores not accessible to nitrogen, due to its larger kinetic diameter, but accessible to oxygen and carbon dioxide. The values of diffusivity used for modeling were the ones obtained from the permeation experiments.

The use of a pressure-independent permeability approach in the simulations led to lower recoveries than the model considering a pressure dependent permeability, for the same purity, at the conditions studied. The use of a pressure-independent permeability model would therefore lead to an erroneous dimensioning of the membrane module.

It was also concluded that, generally, higher feed to permeate pressure ratios (3 up to 10) favor the separation of nitrogen, allowing higher recoveries or smaller contact times for a given purity. In addition, an increase of feed pressure also improves the recovery of the process, when dealing with the same feed to permeate pressure ratio. Increasing the pressure drop significantly impairs the separation. For this reason, pressure drop should be taken into account when designing the module or preparing the fibers.

The last conclusion is that carbon molecular sieve membranes prepared from pyrolysis of cellophane up to 550 °C allow high purity nitrogen production from air

with large recoveries (up to 65 % for a purity of 99.9 %, for negligible pressure drop) and using an air feed with 100 % RH.

Making a retrospective on the work developed in the scope of this thesis, the main difficulties encountered were related with the fragility of the synthesized carbon membranes. Since, they were all self supported, they were extremely brittle and difficult to handle. There were problems during their assembly in the membrane cell for permeation measurements, and there were also problems when submitting the membrane to a pressure difference. Attempting to overcome this mechanical handicap, two different approaches for carbon-based supports are being developed. As a start, disks of composite cellulose pulp (Gescartão SGPS, SA) were prepared for being pyrolyzed and serve as support for the cellophane-based carbon membranes; it is expected that both the support and the selective precursor will shrink similarly during the pyrolysis step, since they are both made of cellulose. More details can be found in Appendix C.

This study was initiated but not finished, and therefore it should be a direction to take in a future research. These supports may be submitted to thermogravimetric analysis, e.g., proximate analysis, to assess the yield of inorganic ashes and fixed carbon. Depending on the fixed carbon resultant of pyrolysis, the addition of a selective layer should be discussed and studied. Different approaches of carbon membranes may be studied, beyond cellophane, as a precursor for the selective film. Furthermore, additional CVD/activation steps might be an option or even the coating of a polymeric solution over the composite cellulose support. Further thermal analysis may be performed with TG to optimize the temperature conditions in scale-up – pyrolysis in the furnace.

The second approach targets the impregnation of α- and/or γ-alumina in the polymeric solution. In fact this work is also already being developed. Different types of polymers, such as, polyfurfuryl alcohol and phenolic resin are being tried. The

membrane film should be cast from the alumina/polymer solution, pyrolysed and characterized.

Finally, it is also suggested to proceed with the work initialized in the first part of Chapter II. This work was performed at MTG, Twente, and this could be a great opportunity to continue with the collaboration between the two research labs. In fact, P84/S-PEEK blends have the possibility to incorporate different types of metals, so that the resultant membrane gains affinity to certain permeating species. Since the methodology for determining the influence of the pyrolysis parameters on the performance of the membranes has been established, the incorporation of metals in the precursor blend can be studied systematically.

Appendix A

Appendix A - Internship at MTG

A.1. Preparation of flat sheet carbon molecular sieve membranes

This work was performed at MTG, University of Twente, The Netherlands, during a three months' internship. The objective of this visit was to learn how to prepare carbon membranes for gas separation, so that a synthesis set-up could be lately designed and assembled at LEPAE.

A.1.1. Preparation of the precursor

Flat membranes were prepared starting from a 13 % wt solution of a co-polyimide P84 in NMP. This solution was used to cast 20 μm thick dense films. Flat membranes with a diameter of about 46 mm have been cut out of these films.

A.1.1.1. Pyrolysis

Carbon membranes were produced by pyrolysis of these films under a N_2 atmosphere in a furnace, following a temperature history program mentioned in Chapter III, section 3.1. These flat films were pyrolysed until different end temperatures, 600, 700 or 800 °C.

A.1.1.2. Permeation

Permeation experiments were performed for N_2, He, CO_2 and O_2 at 35 °C, with a feed pressure of 2 bar and vacuum in the permeate side.

Figure A.1 represents the permeability towards N_2, O_2, He and CO_2 of the flat sheet membranes synthesised up to 600 °C and the permeability of a carbon membrane from a P84 co-polyimide precursor obtained by Jonathan Barsema [1], referred in the figure as MP 600.
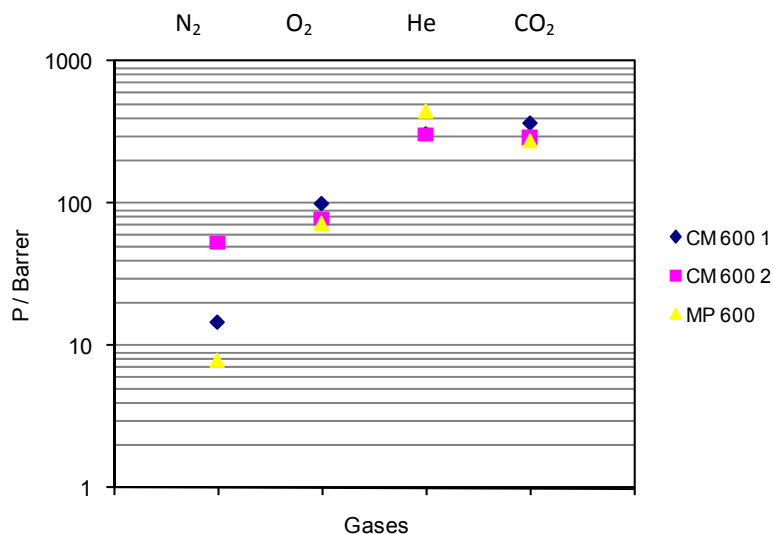
Figure A.1. Permeability towards N_2, O_2, He and CO_2 at 35 °C of carbon flat sheet membranes (1 Barrer=7.5×10^{-18} m^3_N m m^{-2} s^{-1} Pa^{-1}).

Table A.1 presents the selectivities for all the pair of gases considered.

Table A.1 - Ideal selectivities for flat carbon membranes at 35 °C.

Membrane	α O_2/N_2	α CO_2/N_2	α He/O_2	α CO_2/O_2	α He/CO_2
CM 600 1	6.9	25.4	3.3	3.7	0.9
CM 600 2	1.5	5.5	3.9	3.7	1.1
MP 600 [1]	9.3	35.4	6.2	3.8	1.6

According to Figure A.1 and Table A.1 it is noticed that CM 600 1 and 2 have different performances although the precursor and pyrolysis' parameters have been the same for both membranes. This qualitative comparison between these two membranes indicates that it was difficult to obtain reproducible characteristics with the synthesized membranes. The membranes prepared up to 700 and 800 °C broke when assembled into the membranes cell, and could not be tested. This work allowed to realise the importance and difficulties for preparing a homogenous flat film, and consequently, homogenous and reproducible carbon membranes.

A.1.2. Conclusions

Carbon membranes (flat sheets and hollow fibers) were synthesized by pyrolysis in a N_2 atmosphere. However, it was not possible to obtain reproducible performances for these membranes and so the results are not conclusive. Moreover, flat sheet membranes were very difficult to prepare due to their extreme brittleness.

A.1.3. References

[1]   J. Barsema, Carbon Membranes - Precursor, preparation and functionalization, Enschede, PhD Thesis, 2004

Appendix B

Appendix B - Experimental Set-ups

B.1. Synthesis set-up for CMSM

B.1.1. Design of the synthesis set-up at LEPAE

For producing carbon membranes a furnace with a temperature controller was assembled. To control the gas atmosphere passing through the quartz tube located inside the furnace, a panel equipped with flowrate controllers has been sketched (Figure B.1) and designed in real scale in AutoCAD (Figure B.2).
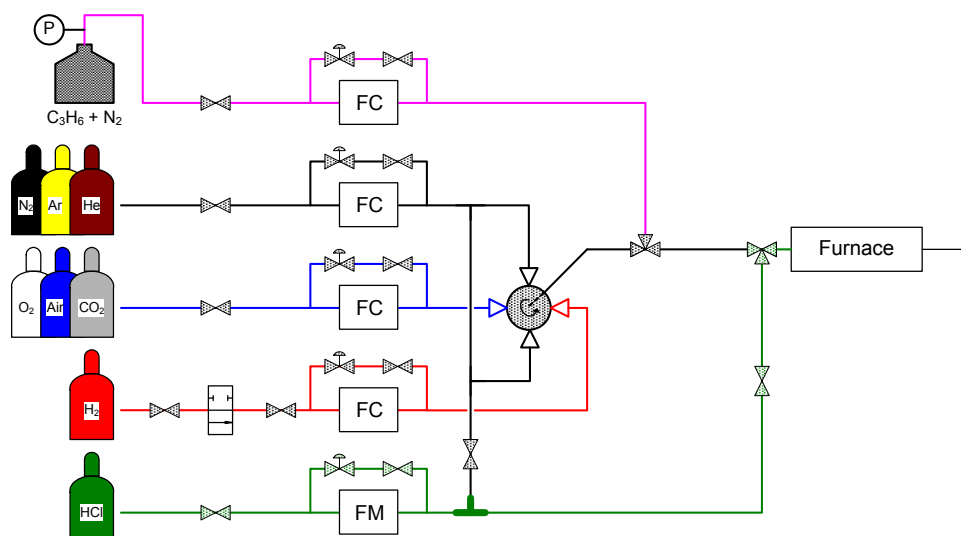

Figure B.1 – Schematic representation of the control panel of the furnace's feed gases.
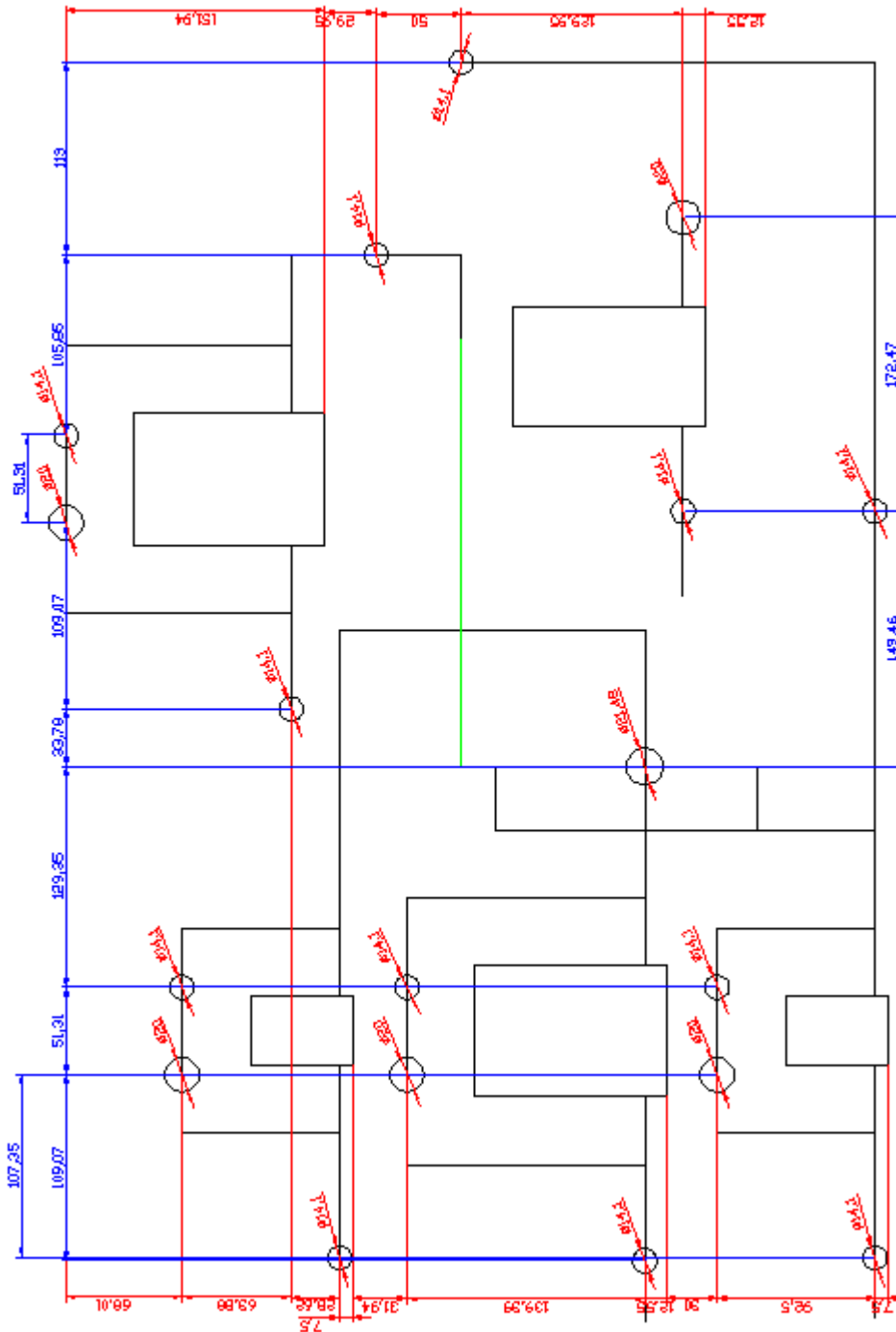
Figure B.2 – AutoCAD sketch of the control panel of the oven's feed gases.

Figure B.3 and Figure B.4 provide an overview of the set-up assembled in the lab.
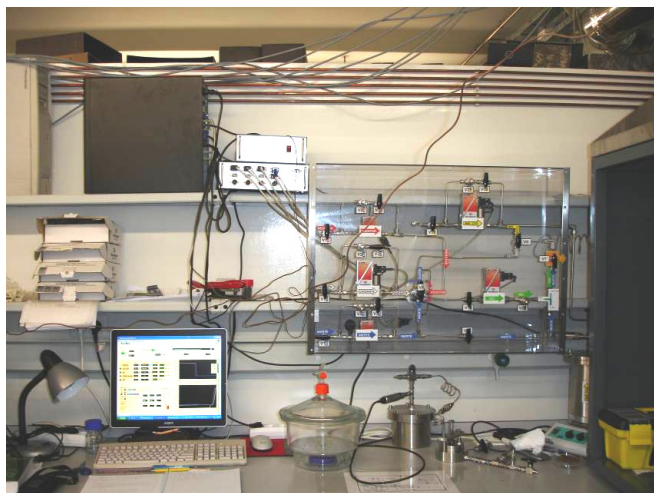

Figure B.3 – Control panel of the oven's feed gases.

Figure B.4 – Global view of the CMSM pyrolysis set-up.

B.1.2. Data acquisition program – based on LabView

The data acquisition and monitoring was performed using a LabView programming interface specifically developed to this system. This program is able to control the furnace and the feeding gases. Figure B.5 illustrates the program developed.
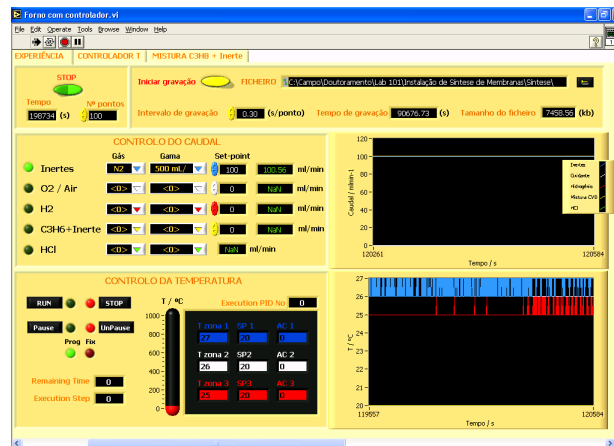
Figure B.5 – Program developed for controlling the furnace and feeding gases.

The settings of the temperature controller (Shimaden, MR13) can be manually modified and activated but it would be undoubtedly easier and worthy to control the furnace exclusively with the computer, via the RS232 port in the controller. The controller of the furnace allows storing in memory the PID parameters for three different temperatures, making possible to have in the same temperature history the most recommended PID values. The program was improved for simplifying procedures and saving time (Figure B.6).

Figure B.6– Program developed for controlling the furnace - PID parameters input.

B.1.3. Preliminary experiments

B.1.3.1. Study of the flow pattern on the quartz tube – O_2 breakthrough experiments

The synthesis set-up is prepared to operate under several different atmospheres, i.e. nitrogen, oxygen, hydrogen and others. Therefore, strict safety procedures are required when dealing with hydrogen and oxygen. The upper explosive limit for hydrogen is 74.8 % in air, which means that the tube has to be cleaned by an inert gas down to a residual concentration of 5.5 % in oxygen. However, in order to decrease the risk of any accident, this value will be decreased down to 0.5 %. In practical terms these conditions will be assured by controlling the flowrate and feeding time of the inert gas to the tube.

Another important issue is the effect of oxygen during pyrolysis. Thus, this residence time is also important to assure that no undesired reactions occur between oxygen and the substrate.

Step perturbation tracer experiments have been performed at 300 ºC and an axially dispersed plug flow model [1] was found to successfully fit to the experimental data. The following equation represents the referred model.

$$\frac{C}{C_0} = 1 - \int_0^t \frac{\sqrt{\tau Pe}}{2\sqrt{\pi t^3}} e^{-\frac{Pe(\tau-t)^2}{4\tau t}} dt \qquad \text{(B.1)}$$

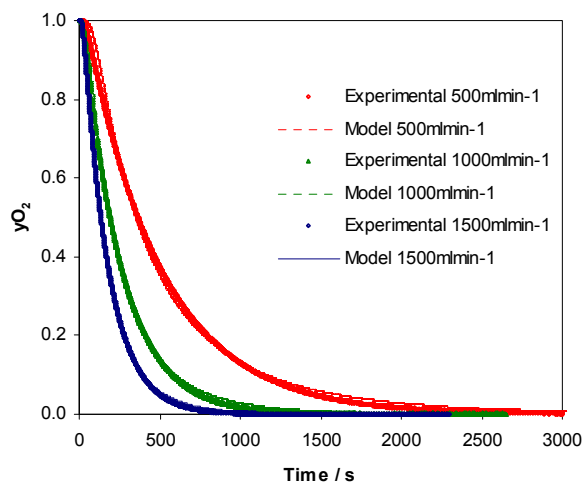Figure B.3 represents graphically the experimental breakthrough curves.

Figure B.7 – Oxygen mole fraction history to a step perturbation of nitrogen to the quartz tube at 300 °C.

Fitting the model to the experimental results, Peclet number, Pe, and mean residence time, τ, were determined and presented in Table B.1.

Table B.1 - Model parameters.

Q (mL$_N$ min^{-1})	Pe	τ (s)
500	1.9	533
1000	2.0	276
1500	2.2	188

A very high axial dispersion was observed, indicating a flow pattern approaching the perfectly mixed behavior. This means that there should be no stagnant areas where e.g. oxygen may accumulate. From the model and for a 1 L$_N$/min feed flowrate, the cleaning time should be 40 min at 300 °C.

B.1.3.2. Evaluation of the temperature profiles in the quartz tube

The furnace has three heating elements, each one with an independent control action. Three thermocouples placed in each heating element measure the temperature, $T_{furnace}$, which is forced to reach the desired set-point. These thermocouples are located near the heating element, outside the quartz tube. For low temperatures, around room temperature, radiation phenomena are not very relevant and for that reason the temperature inside the quartz tube, T_{real}, is not very different from the temperature indicated near the heating elements. However, as the temperature increases, radiation becomes more significant leading to an increase of the temperature inside the quartz tube. So, as the pyrolysis occurs inside the quartz tube, T_{real}, is the variable of the process that has to be controlled. Though, a priori calibration of the temperature was done. For this, a clean K type thermocouple was introduced inside the quartz tube, as shown in Figure B.8, measuring the real temperature which corresponded to several set-points imposed from room

temperature up to 600 ºC. A linear regression was found relating $T_{furnace}$ and T_{real} and is represented by Eq. (B.2):

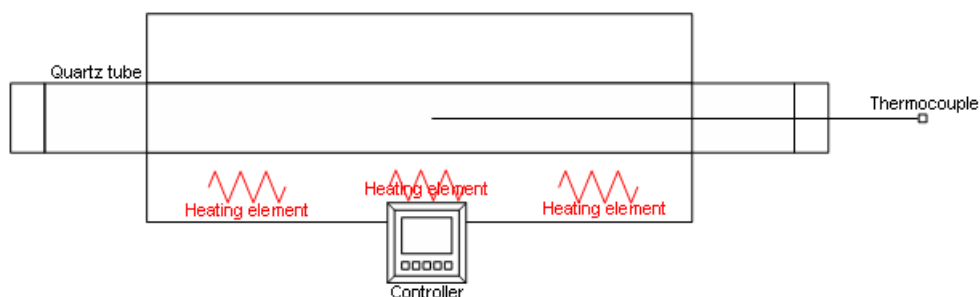$$T_{\text{furnace}} = 0.928 T_{\text{real}} - 24.674 \qquad\qquad (B.2)$$

Figure B.8– Scheme of the furnace with three independent heating zones and the probing thermoucouple.

B.1.3.3. Evaluation of the best tray

At first a quartz tray made has been used to introduce the precursors inside the quartz tube to pyrolyse them. A quartz tray is inert and for this reason should provide a good support. Disks of P84 films brought from MTG (Twente University, The Netherlands) were introduced inside the quartz tube placed over this quartz tray. Unfortunately, all the attempts failed – the resulting carbon membranes broke in many ways, because of their extreme brittleness. The same conditions used at MTG's furnace were used in the set-up at LEPAE, except for the tray, which was originally a stainless steel grid, instead of a dense quartz tray. So, perhaps the quartz tray was in the origin of this increase in brittleness that was not observed before with a grid. In fact with a dense tray made of quartz, the heat transmitted to the membrane occurs by convection at the top and by conduction at the bottom of it. As the quartz has a high thermal conductivity, this may originate a temperature gradient in the membrane and cause internal tensions leading to a higher brittleness. As referred elsewhere, [2] a grid of stainless steel was chosen and better results were achieved, in terms of brittleness.

B.2. Permeation set-up

B.2.1. Pseudo-steady state – pressure increment method

A new setup for measuring the permeability of the membranes towards water vapor was designed assembled and tested. This set-up up was used to characterize the cellophane-based carbon membranes presented in the second part of Chapter III.
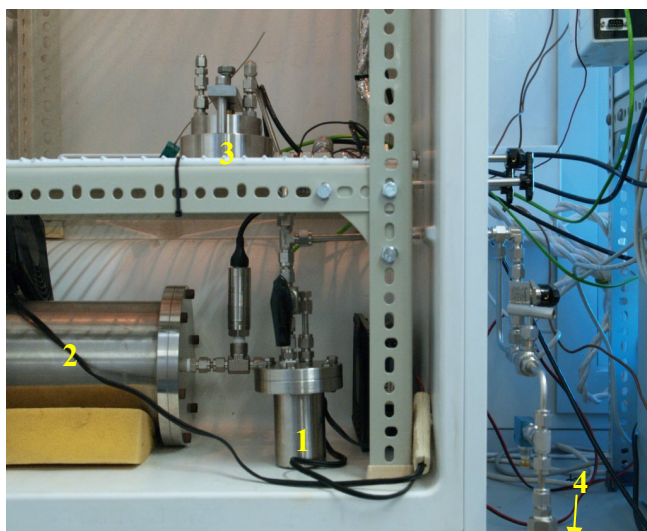
Legend:

1 – Vessel with liquid water.
2 – Vessel with water vapor.
3 – Permeation cell.
4 – Vacuum pump.

Figure B.9 – Picture of the pressure increment method setup.

As the temperature controls the water vapor pressure it is necessary a temperature control system. Also the valves' system was designed to be handled without opening the thermostatic cabinet in order to avoid condensation.
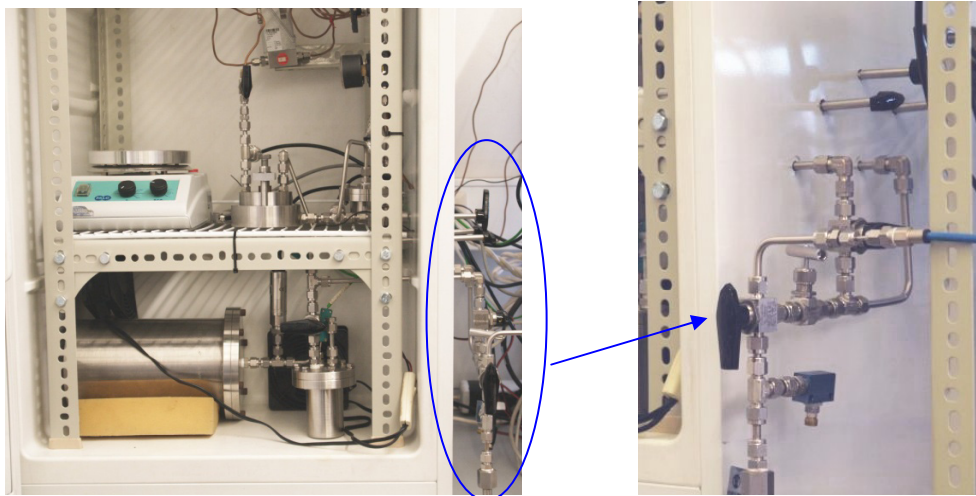
Figure B.10 – Pressure increment method set-up – valves system.

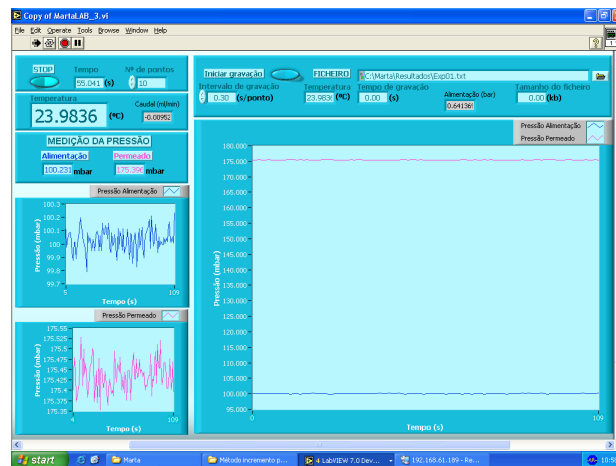A program for data acquisition was developed as illustrated in Figure B.11.

Figure B.11 – Software for data acquisition in LabView programming.

The data acquisition is done using a LabView program specially developed for this set-up.

B.2.2. Steady state – flowrate method

B.2.2.1. Carbon flat sheet membranes

The experimental set-up was placed in a thermostatic cabinet, also in-house assembled, and based on a domestic freezer, as shown in Figure B.12.
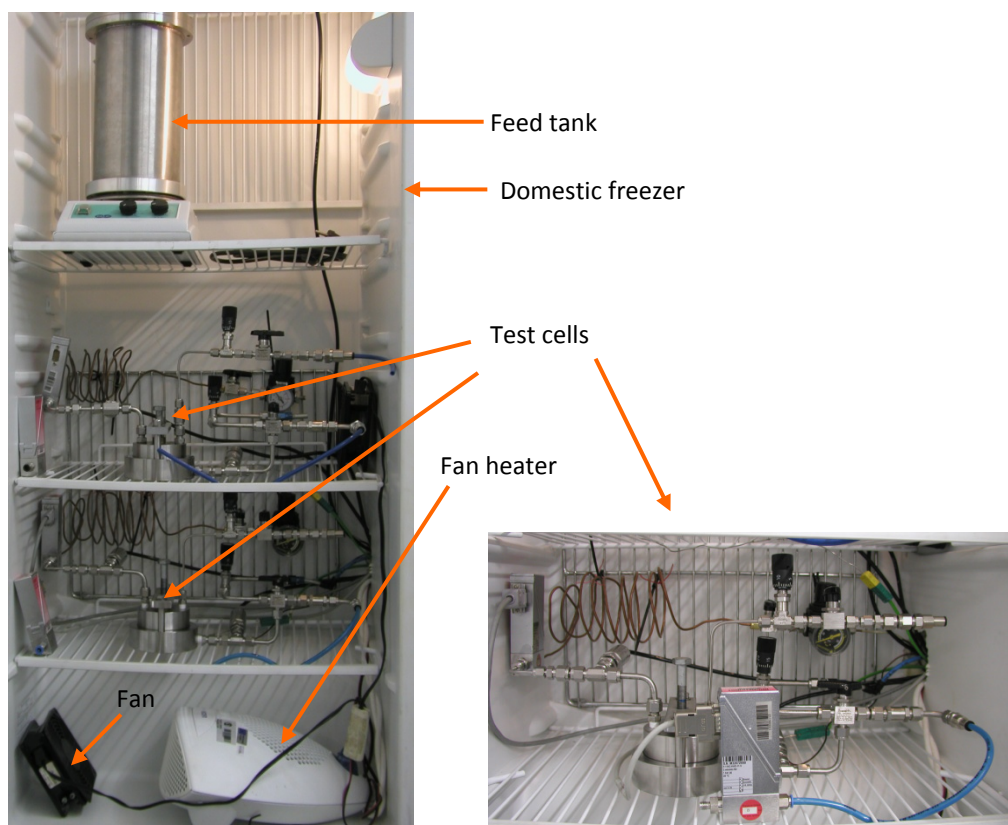

Figure B.12 – Steady state, flowrate method set-up.

A data acquisition program was also developed based in LabView language - Figure B.13. The pressure and the flow rate values are read by this program.
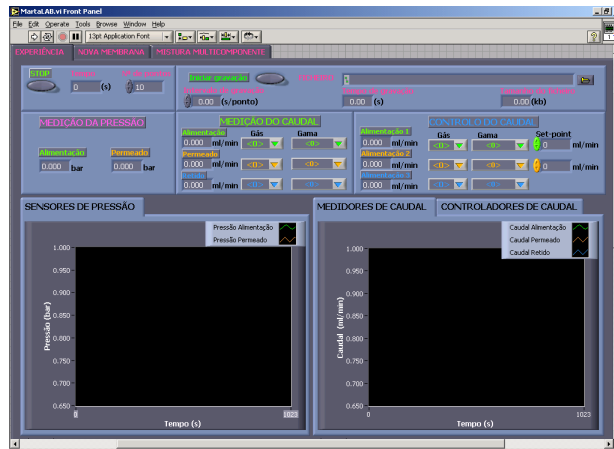
Figure B.13 – Data acquisition program (LabView).

B.2.2.2. Carbon membrane monoliths

The company Blue Membranes provided monolithic like membrane modules as shown in Figure B.14. These were ceramic supports coated with a selective carbon layer.

Figure B.14 – Monolith sent by Blue Membranes, Germany, on the left; top view of the monolith glued very each row. The blue line represents feed going in.

The effective membrane permeation area for the suggested flow configuration is 1 m^2/dm^3, and the module should work according to Figure B.15. The attempts to assemble the monolith into a membrane module for permeation experiments can be followed in the sequence of Figure B.16.
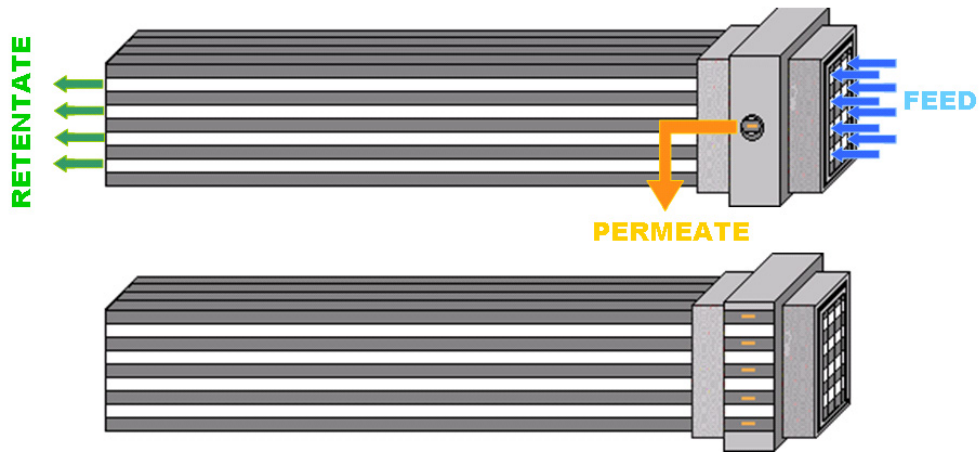
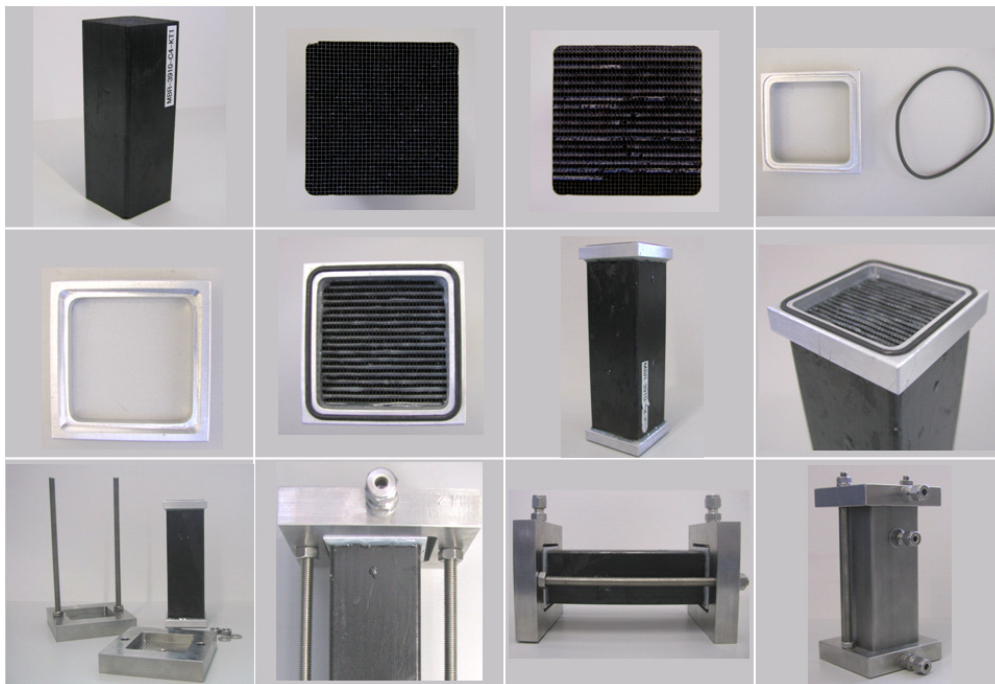Figure B.15 – Flow configuration for the monoliths.

Figure B.16 – Sequence of steps to assemble the monolith module.

In the final stage of the sequence, the module was introduced in the permeation set-up provided in the previous sub-section, replacing the cell for flat sheet membrane. However, the modules were defective and highly permeable to SF6, and thus not selective.

B.3. Adsorption set-up – gravimetric method

B.3.1. Modification and enhancement of the magnetic suspension balance set-up

The adsorption studies were conducted in a magnetic suspension balance already assembled for sorption studies with permanent gases, with a pressure sensor in the range of 0-7 bar. However, it was adapted by the author, namely a second pressure sensor in the range of 0-350 mbar was installed, for obtaining the water vapor isotherms and uptake curves.

Legend:

1 – Tank with water
2 – tank with vapor
3 – 0-350 mbar pressure sensor
4 – heating plate
5 – vacuum pump

Figure B.10 – Picture of the magnetic suspension balance adapted for operation with water vapor.

B.4. References

[1]   A. Mendes, Laboratórios de Engenharia Química. Reactores em Fase Homogénea, Reactores Catalíticos, Separações não Convencionais e Tecnologia dos Sólidos Divididos, 1 ed., FEUP edições, Porto, 2002.

[2]   J. Barsema, Carbon Membranes - Precursor, preparation and functionalization, Enschede, PhD Thesis, 2004

Appendix C

Appendix C - Supports for CMSM

C.1. Cellulose composite support

To attain carbon membranes with increased mechanical strength, cellulose based supports are trying to be developed. Thus, inorganic fibers were incorporated in two types of cellulose pulp at Gescartão SGPS, SA (see samples in Figure C.1).

One type was based only in a pulp of virgin fibers and the other based on a mix of treated fibers. Also three different densities of final paper were prepared. In each category different amounts of inorganic fibers were incorporated. Table C.1 psummarizes all the membrane supports prepared.

Table C.1 – Membrane supports made of kraft paper with inorganic fibers.

% Inorganic fibers	Pulp of virgin fibers			Pulp of treated fibers		
	60 (g cm^{-3})	120 (g cm^{-3})	300 (g cm^{-3})	60 (g cm^{-3})	120 (g cm^{-3})	300 (g cm^{-3})
10	x	x	x	x	x	x
20	x	x	x	x	x	x
30	x	x	x	x	x	x
40	x	x	x	x	x	x
50	x	x	x	x	x	x

Figure C.1 – Example of supports made of cellulose+50 % inorganic fibers: pulp of virgin fibers (F.V.) and of treated fibers (F.M.); 1, 2 and 3 correspond to 60, 120 and 300 g cm^{-3} paper densities.